

Investigating the effects of model position and orientation
on parts manufactured using the selective laser sintering
process

Hansi Strobel

Bachelor's Thesis
Lapland University of Applied Sciences
Mechanical Engineering
Bachelor of Engineering

2021

Lapland UAS
Mechanical Engineering
Bachelor of Engineering

Author	Hansi Strobel	Year	2021
Supervisor	Ari Pikkarainen M.Sc. (tech.)		
Commissioned by	Ari Pikkarainen M.Sc. (tech.)		
Title of Thesis	Investigating the effects of model position and orientation on parts manufactured using the selective laser sintering process		
Number of pages	82 + 16		

This work aims to explore the influence of part position and orientation within the build volume of selective laser sintering machines on visual part quality and tensile properties. This is done in an attempt to optimize both machine time and manufacturing costs. Furthermore, students and staff at the Lapland University of Applied Sciences are introduced to the workflow around the novel selective laser sintering machine found in the Lapland University of Applied Sciences 3D printing laboratory.

In a first set of experiments, it was discovered that the position and orientation of parts within the build volume of selective laser sintering machines plays a crucial role in the success of a manufacturing run. Incorrect positioning may lead to warping or severe alteration of part geometry.

Further experiments revealed that tensile specimens manufactured in different positions and orientations show similar behaviour in the elastic region but differ in their behaviour in the plastic region. Significant anisotropy between specimen orientations was discovered. Specimens manufactured perpendicularly to the build direction show a 50 % reduction in elongation at break and 25 % reduction in ultimate tensile strength compared to specimens manufactured parallel to the build direction.

Moreover, it was discovered that high model densities and fast layer times lead to local hot spots, resulting in part growth due to amplified secondary sintering effects. Increased part growth was observed in the first layers as a result of increased temperatures caused by the employed method of build volume heating. Furthermore, specimens which experienced overheating during the build stage showed a significant improvement in their tensile properties.

Key words: selective laser sintering, tensile property, part position, anisotropy, polyamide-12

CONTENTS

1	INTRODUCTION	7
1.1	Objective.....	8
1.2	Scope.....	8
1.3	Method.....	9
2	ADDITIVE MANUFACTURING.....	10
2.1	Steps in the additive manufacturing process chain.....	11
2.2	Powder Bed Fusion (PBF)	13
2.3	Selective Laser Sintering (SLS)	14
2.3.1	Process steps.....	15
2.3.2	Process mechanisms	16
2.3.3	Process parameters	17
2.3.4	Materials.....	21
2.3.5	Post-processing.....	22
2.3.6	Powder recycling	23
2.3.7	Design guidelines and considerations	24
3	SLS SETUP AT LAPLAND UAS.....	27
3.1	Safety.....	27
3.2	SLS workspace and equipment	29
3.2.1	SLS printing room.....	29
3.2.2	Sinterit LISA PRO.....	30
3.2.3	Sinterit Powder Sieve	32
3.2.4	Sinterit Sandblaster	33
3.2.5	Sinterit ATEX Vacuum Cleaner and Sinterit Powder Separator	34
3.3	Workflow	35
3.3.1	Model acquisition and slicing.....	36
3.3.2	Preparation.....	37
3.3.3	Part removal and cleaning.....	41
3.3.4	Powder refreshing	43
3.3.5	Post-processing.....	44
3.3.6	Printing different materials.....	46
4	INVESTIGATION OF PART POSITIONING AND ORIENTATION	47
4.1	Limitations of LISA PRO	48
4.1.1	Methodology.....	48

4.1.2	Results and discussion.....	50
4.2	Investigation of part quality and material properties.....	53
4.2.1	Methodology.....	53
4.2.2	Visual quality and geometrical accuracy	56
4.2.3	Tensile material properties	63
5	CONCLUSION.....	73
6	REVIEW AND OUTLOOK	75
7	LIST OF TABLES	76
8	LIST OF FIGURES	77
9	BIBLIOGRAPHY	80
	APPENDICES.....	83

FOREWORD

This thesis is the culmination of my story of achieving Bachelor's degrees in both, renewable energy technologies, as well as mechanical engineering. I first started my university career in 2014 with a mechanical engineering degree at the University of Stuttgart, and later switching study programs to renewable energy in 2015. However, a lack of motivation led me to an early exit in my academic career. After spending some time on trying to find other ways of fulfilment in the professional world, my search ultimately led me back to the University of Applied Sciences Technikum Wien. In Vienna, I started my Bachelor's studies in urban renewable energy technologies in 2018. While mostly enjoying my time in Vienna, the main spark of my joy being my favourite flatmates: Jacob and Marcus, I soon got offered the opportunity to partake in a Double Degree Program at the Lapland University of Applied Sciences in Kemi. As this would allow me to not only finish my Bachelor's degree in urban renewable energy technologies, but also pursue a degree in mechanical engineering, I immediately took the opportunity. Through my studies at Lapland UAS, I got introduced to the novel technology of additive manufacturing, which ultimately led to the creation of this thesis. Furthermore, the experiences at Lapland UAS showed me that there is more to the field of engineering than only solar panels and ventilation systems. This now leads me to look forward into a future in which I see myself as more than just a guy at a desk, giving people advice on how they shall install their solar panels. I rather see myself as an aspiring engineer, looking to find a suitable Master's Degree in another field of engineering.

Finally, I want to express my thanks to my amazing supervisor, Ari Pikkarainen. Thank you, Ari, for giving me this opportunity to redeem myself and achieve both Bachelor's degrees I started earlier in my life. Also, shoutout to Peter Franz for making the Double Degree Program in cooperation with Lapland UAS happen. Furthermore, I want to thank my favourite hairdresser and frog-across-street-carrier, Nicole. Also, shoutout to Markus and Zsombor for inspiring a lot of my dumb ideas when it comes developing my own CNC plotter. Keep changin' those nozzles, boiii! Finally, shoutout to both of my families and the best tutor in the world for keeping me company during these extraordinary times in Kemi.

SYMBOLS AND ABBREVIATIONS

3D	Three-Dimensional
3MF	3D Manufacturing Format
AM	Additive Manufacturing
AMF	Additive Manufacturing File Format
ATEX	Atmosphere Explosible
CAD	Computer Aided Design
EB	Elongation at Break
HEPA	High-Efficiency Particulate Air
IPA	Isopropyl Alcohol
IR	Infrared
OYS	Offset Yield Strength
PA	Polyamide
PAEK	Polyaryletherketones
PBF	Powder Bed Fusion
PP	Polypropylene
PS	Polystyrene
SLS	Selective Laser Sintering
STL	Standard Triangle Language/Standard Tessellation Language
TPE	Thermoplastic Elastomers
TPU	Thermoplastic Polyurethane
UAS	University of Applied Sciences
UTS	Ultimate Tensile Strength
VP	VAT Polymerization
YM	Young's Modulus

1 INTRODUCTION

With a major decrease in equipment costs during the recent years, the Selective Laser Sintering (SLS) additive manufacturing process has become more easily accessible to large parts of the additive manufacturing community. With several manufacturers offering low-cost alternatives to capital intensive industrial machines, the educational sector, and especially the private sector may soon experience broad exposure to this technology (Formlabs 2021; Sinterit 2021b; Sintratec 2021). For this reason, the spread of knowledge and education around the SLS manufacturing workflow and the intricacies of SLS manufacturing is crucial. Especially when it comes to handling the microparticles involved in the SLS process, awareness of safety and health risks is critical in order to prevent accidents and long-term consequences when it comes to the health of operating personnel.

In 2020, Lapland University of Applied Sciences (Lapland UAS) expanded the capabilities of its 3D printing laboratory with an SLS machine in order to enable its students to learn about SLS manufacturing. As this addition introduces a novel technology to the laboratory, a safe and coherent workflow around SLS manufacturing is yet to be defined. Establishing a proper workflow is crucial in order to guarantee efficient manufacturing cycles and maximize machine time, which directly translate into reduced manufacturing costs. Moreover, by manufacturing multiple parts simultaneously the machine time of SLS machines can be decreased. Therefore, maximizing the usage of these simultaneity effects by optimizing the space utilization within the build volume is highly desirable. However, part position must be thoroughly considered during the preparation of a manufacturing run. On one hand, part position directly affects the temperature profile and cooling rate of the part during the process, which may lead to undesired part deformation (Zhao, Wudy & Dietmar 2018). On the other hand, the orientation of parts may have an influence on their characteristics due to the anisotropic nature of layer-based manufacturing processes, like SLS (Diegel, Nordin & Motte 2019, 93).

Consequently, in order to optimize space utilization within the build volume, and, as a result of that, the manufacturing time and cost, the effect of part position and orientation within the build volume must be examined.

1.1 Objective

The objective of this thesis is split into two major parts. In the first section, the aim is to introduce future users to the basic principles that define the SLS process, as well as acquaint them with the new SLS setup found in the Lapland UAS 3D printing laboratory. Furthermore, a safe and efficient workflow shall be established. The workflow will include all the steps necessary to convert a virtual 3D model into a finished part. A particular focus will be on issuing guidelines for safe powder handling and general safety in the working environment.

The second part of the thesis focuses on investigating the impact of part position and orientation within the build volume of the SLS machine on the quality of the resulting part. While the focus of the investigation will primarily be on the change in the tensile properties of the material, samples manufactured for material testing will also be judged upon their visual quality and geometrical accuracy.

1.2 Scope

The results of this thesis will serve multiple purposes. On one hand, the students and staff at Lapland UAS will receive a comprehensive description of the SLS workflow in the Lapland UAS 3D printing laboratory. Additionally, new personnel will more easily be able to understand the general working principle, as well as the intricacies of SLS manufacturing. On the other hand, the results of the material testing will help optimize space utilization within the build volume of SLS machines, increasing machine time and decreasing manufacturing cost. Furthermore, future users of the SLS printer at Lapland UAS will be able to make a more educated decision when choosing the position of a part within the build volume in accordance with the desired material properties, visual quality, and geometrical accuracy.

1.3 Method

To work with machine that employs a novel technology, first, a basic understanding of the machine, its components, and the mechanisms involved in the manufacturing process was acquired. To do so, comprehensive literature research on the subjects of additive manufacturing, and more specifically the SLS process was done. Using the theoretical knowledge and practical experience acquired while working with the setup in the Lapland UAS 3D printing laboratory, a workflow around the SLS process was established.

Following that, a range of test specimens was manufactured that serve to help evaluate the tensile properties of parts manufactured using the SLS process in dependency of their position and orientation within the build volume. Tensile properties were tested by the means of tensile tests according to the standard for determining the tensile properties of plastics, ISO 527-2. Furthermore, the visual quality and dimensional accuracy of the specimens was evaluated. The specimens were manufactured using the SLS setup at the Lapland UAS 3D printing laboratory and tested at the Lapland UAS material testing facility. The results of these tests were analyzed and discussed. In the end, a conclusion of the findings of this thesis were given.

2 ADDITIVE MANUFACTURING

Additive Manufacturing (AM) is an umbrella term used for a range of technologies that utilize the principle of part creation by stacking layers of material on top of each other each layer representing a thin slice of the model, until a part is finished. AM is also often referred to as “3D printing”, and for that reason the two terms will from now on be used interchangeably. Historically, AM processes were referred to as Rapid Prototyping (RP) as most processes found application in the manufacturing of concept models and pre-production prototypes. However, due to improvements in the quality of the output of AM machines, nowadays even final parts are directly manufactured using the AM process. One of the major advantages of AM technologies over traditional additive (injection molding, casting, etc.) and subtractive processes (boring, turning, etc.), is that there is no need for part-specific tooling, which means that any part can be created by an AM machine without a requirement for changes to the hardware configuration. Furthermore, most AM processes enable the user to manufacture parts without any prior knowledge of the inner workings of the AM machine or manufacturing skills required. Therefore, this removes the need for highly skilled machine operators, resulting in reduced operating costs when compared to more traditional manufacturing processes like turning, milling, CNC machining, etc. However, one cannot assume that a part manufactured using an AM process is always cheaper than the same part created by conventional manufacturing methods. As a matter of fact, due to the relatively slow and expensive technologies used for AM, its often more expensive to use AM to create a part than if a means of traditional manufacturing would have been employed. (Gibson, Rosen, Stucker & Khorasani 2021, 1, 2; Diegel, Nordin & Motte 2019, 1-4; Kumar 2020, 1, 2.)

AM technologies are generally divided into seven overarching categories: vat photopolymerization, material extrusion, material jetting, binder jetting, powder bed fusion, direct energy deposition, and sheet lamination (3D Hubs 2021a; Pazhamannil 2021). Within these categories, certain commercial terms have developed which divide the technologies further according to the specific process or material used in part creation. A graphic overview of these technologies can

be seen in appendix 1. For reasons of relevancy, the only AM technology which this work will explore in further detail is the PBF process. More information on other AM processes can be obtained through other literature sources, for example through the book “A Practical Guide to Design for Additive Manufacturing” by Diegel et al. (2019).

The materials which can be used in the wide range of AM processes range from thermoplastics like ABS, PLA and PET, to different metals, paper, wax, or even different kinds of food. (Diegel et al. 2019, 19-37.)

2.1 Steps in the additive manufacturing process chain

The AM process typically starts with a model created in a three-dimensional Computer Aided Design (3D CAD) software. While creating the model, it is of high importance that the design guidelines for additive manufacturing are taken into consideration, as this will smoothen out the additive manufacturing process and prevent major mishaps and surprises during the whole process. Other options for model creation employ reverse engineering techniques to digitize a physical component, an example for reverse engineering is laser and optical scanning. (Gibson et al. 2021, 3, 4; Kumar 2020, 4.)

Next, the model is exported using a suitable additive manufacturing file format which primarily contains information about the three-dimensional surface geometry of the model. The most popular file format used is the STL (Standard Triangle Language or Standard Tessellation Language) format. The STL format turns the model into a mesh of interconnected triangles which tries to accurately replicate the model geometry. However, in case of curvatures in the model geometry, the representation through the triangle mesh will not be exact and therefore cause the manufactured part to slightly deviate from the original model. As an attempt to rectify this issue, the resolution of the STL file can be increased, which means a decrease in the triangle size and therefore more accurate representation of the model. Though, the underlying problem of using triangles to recreate round shapes cannot be ultimately solved but only lessened by these means. Unlike the older STL format which is somewhat dated, newer additive manufacturing file formats like AMF (Additive Manufacturing File Format) or 3MF

(3D Manufacturing Format) have the additional ability to convey information on colour, materials, lattices, textures, constellations and metadata of the model. (European Committee for Standardization 2017, 33; Kumar 2020, 4; Diegel, Nordin & Motte 2019, 4, 5.)

Following that, the file containing the model geometry is transformed into an assortment of horizontal layers by intersecting the model with horizontal planes that have a predefined spacing, also called the layer-height. This process is often referred to as “slicing” the model and is done in a piece of software called the “slicer”. The height of these layers typically ranges from 25 to 250 microns, or even greater in some special cases and applications. After dividing the model into layers, the software creates a tool path for every layer which the AM machine can interpret and understand. This tool path is called the machine code, often referred to as g-code. Besides the layer-height, the slicer gives the additional option to change other process parameters like part position/orientation, temperatures, speeds, accelerations, etc. However, these parameters are often very specific to the AM technology applied. (Kumar 2020, 4, 5; Gibson et al. 2021, 5.)

After generating the machine code, the code must be transferred to the AM machine. Traditionally, this is done using a portable flash storage device like a USB stick, SD card, or TF card. However, in newer machines and especially in industrial applications, files are often transferred to the AM machine over the network. Having transferred the file, the AM machine must now be set up and prepared for the building process. Depending on the technology, this can be achieved within a couple minutes and it is as easy as cleaning the build surface and loading the desired material into the device, like in the case of most material extrusion machines. However, in other cases like power bed fusion (PBF) machines, this process may incorporate multiple hours of manual labor between loading new material, preparing the print volume, preheating for the build process, and cleaning several machine elements involved in the build process. Having completed the setup and preparation of the machine, the build process can start. Nowadays, most machines have a highly automated build process and require little to no manual input during the build process. Merely occasional monitoring of

the process should be done in case of errors which might arise due to software glitches, mechanical failures, or running out of material. (Gibson et al. 2021, 5.)

Following the completion of the build process, the part must be removed from the AM machine. Again, in the case of material extrusion machines, this can be as simple as removing the final part from the build platform with bare hands. Though with other technologies like vat polymerization (VP) or PBF this process is not quite as simple, because the part might be covered in potentially harmful substances and therefore require additional care and safety procedures during removal. After the successful extraction of the part and depending on the technology, post-processing might be necessary in order to achieve the desired result. In special cases, like some material extrusion parts, no post-processing might be necessary at all. However, in other cases like VP or PBF parts, more extensive post-processing might be required. These post-processing tasks can range from removing support structures from a material extrusion part using some pliers, to sand blasting a PBF part, or post-curing a VP part. Parts manufactured using direct energy deposition (DED) technology might even require secondary machining to achieve the desired surface finish or to implement certain features like threads, which cannot be manufactured by the AM machine due to limitations in manufacturing accuracy and tolerance. (Gibson et al. 2021, 6; Diegel et al. 2019, 6.)

2.2 Powder Bed Fusion (PBF)

As some of the earliest and most versatile AM processes, PBF processes were some of the first processes to be commercialized (Gibson et al. 2021, 125). The basic principle of all PBF processes revolves around lowering a powder bed by a certain height according to the desired layer-height of the model, spreading a thin layer of material with a roller, and fusing selected parts of that layer together using a heat source. One of the reasons why PBF processes are so popular in the commercial world is that they are relatively isotropic in terms of their behaviour in the X, Y, and Z directions. Because of that, PBF processes can produce high strength, production ready parts (Diegel et al. 2019, 33). Furthermore, PBF processes can utilize a wide range of materials to create parts from. Examples

include polymers, metals, ceramics, and all sorts of composites based on these materials (Gibson et al. 2021, 127-130).

Generally, PBF processes can be divided into beam based and non-beam-based processes (Figure 1). Beam based processes, like the name suggests, rely on high-energy beams to direct the heat to a certain area of the build layer, while non-beam-based processes use other heat sources such as heaters, lamps, and microwave. Furthermore, beam based processes can be divided into laser beam based and electron beam based processes. Laser beam-based processes, also called laser powder bed fusion, can be further differentiated by the main driving mechanism of the processes and the materials used. When processing polymers, the mechanism which drives the process is partial melting, while in the case of metals, the main driving mechanism is full melting of the material. In the commercial world, this kind of polymer processing using AM is usually referred to as Selective Laser Sintering (SLS), whereas metal processing using PBF is typically referred to as Selective Laser Melting (SLM). (Kumar 2020, 42, 43.)

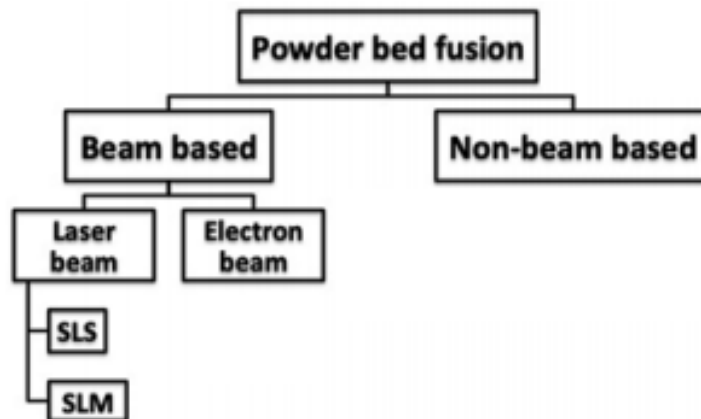


Figure 1. Overview of powder bed fusion (PBF) processes (Kumar 2020, 42) (modified)

2.3 Selective Laser Sintering (SLS)

As the investigations in this thesis are based around the Sinterit LISA PRO, the focus will be set on the PBF process which is used in this AM machine. Sinterit LISA PRO uses the SLS process. The process steps involved in manufacturing

an SLS part, the mechanisms at work, the process parameters, and the available materials for SLS machines will be covered in the following chapters.

2.3.1 Process steps

As depicted earlier, SLS is based on the same principle as most PBF processes. The main build process revolves around three steps which are repeated until the part is done. Again, these three steps are: lowering the build volume by one layer, spreading a thin layer of material using a roller, and applying heat in areas where powder is supposed to be fused together. However, for the build process to start, some preparation is necessary. First, the adequate amount of material (powder) has to be loaded into the powder container(s). The powder container is suspended on a piston head, which enables the machine to transport the material upwards towards the roller. The roller is often called recoater, which better describes its primary function of recoating the build volume with a new layer of material. After loading the material into the machine, the machine starts to preheat itself right up to a few degrees below the melting point of the material (Gu, Bashir & Yang 2019, 194). This is done in order to decrease the amount of laser-energy required to partially melt and fuse the powder on one side, and to minimize temperature gradients within the build volume which could cause the part to deform and warp. Preheating is usually by infrared or resistance heaters. Following the completion of the preheating process, the machine will start with the actual build process, spreading layers of material and fusing them together. As depicted earlier, the heat source responsible for the partial melting of the powder in SLS machines is a focused laser beam. The laser scans the entire area of the active layer which is supposed to be fused together. Depending on the type of SLS machine, the laser is either directed by a mirror which is actuated by two galvanometers in the x- and y-axis, or mounted on an xy-gantry which is moved by a set of motors. Additionally, depending on the material, the entire process can be run in a non-oxidative environment by filling the machine volume with nitrogen or argon gas. A schematic diagram of the SLS process and the main components involved in the process can be seen in Figure 2. (Diegel et al. 2019, 33-35; Gu et al. 2019, 194; Gibson et al. 2021, 125-127; Kumar 2020, 45, 46.)

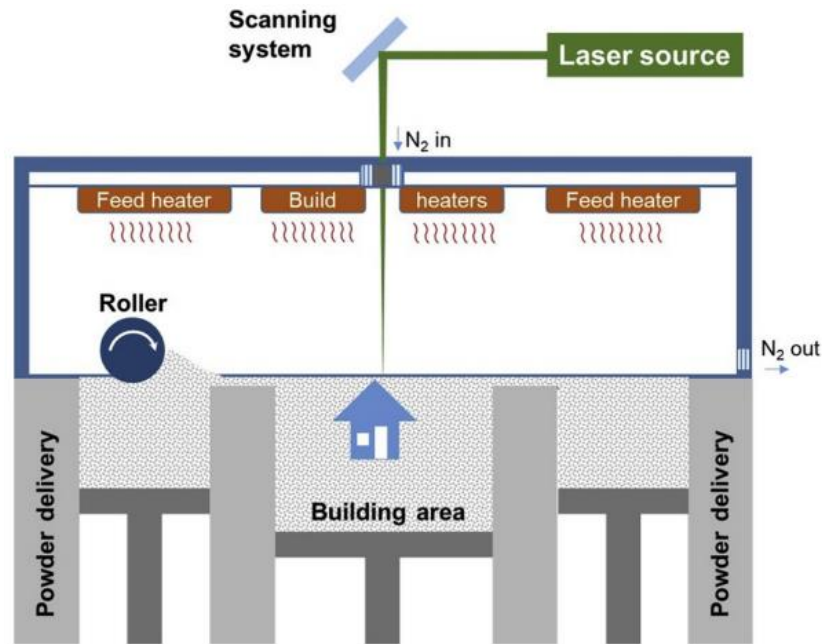


Figure 2. Schematic diagram of the selective laser sintering (SLS) process (Gu, Bashir & Yang 2019, 195)

Following the completion of the build process, the cooldown stage starts. During the cooldown, the part and the surrounding powder which has not been used during the build process, the so-called "part cake". In this stage, the part starts the actual solidification process where it crystallizes. It must be added that in the initial phase of the build process, the build area is coated with a couple layers of powder to create a heat insulating layer around the part. The same procedure is repeated after completing the last layer of the part. This is done in order to guarantee an even cooldown process of the finished part and prevent uneven crystallization and therefore part warpage. (Wudy & Drummer 2019, 4; Soldner et al. 2021, 1.)

2.3.2 Process mechanisms

The name selective laser sintering suggests that the main mechanism used in SLS is sintering. However, contrary to its name, the main mechanism used in SLS technology is not sintering, because it never actually takes place during the actual laser scanning process. The mechanism which enables SLS to work is partial melting, often referred to as liquid-phase sintering. For sintering to take place hours of time are required while the scanning of a layer is done within a

couple of seconds or minutes. This partial melting process refers to melting of parts of the powder while other parts remain as a solid. The melted material then acts as a glue, combining the solid parts of the material. However, during the SLS process, some form of sintering can still take place if the part is either big enough that the scanning duration is very high, or the part is not removed from the hot machine for hours. This sintering can have a multitude of effects on the part cake and the part itself. On one side, the particles in the part cake can start to sinter to one another, which results in an increase of the average particle size of the powder. This size increase is considered a negative effect, as this causes a change in the spreading and melt characteristics of the powder. Furthermore, one of the side effects when scanning the desired bed area is heating up of the surrounding powder. This can lead to the surrounding powder sintering to the actual part and therefore causing a skin-layer to build up around the part itself. There are ways to compensate this behaviour, but in general this form of sintering is undesirable when trying to create a consistent output from the machine. (Gibson et al. 2021, 131-134; Kumar 2020, 44, 45.)

2.3.3 Process parameters

To manufacture a part using SLS technology, first a couple of considerations must be made concerning the parameters of the process. These parameters encompass laser-related, scan-related, powder-related, and temperature-related parameters. It must be noted that most process parameters are interdependent which means that changing one parameter will have an influence on others, therefore making the balance of all parameters the key challenge in SLS manufacturing (Gibson et al. 2021, 143). In the following, all critical process parameters and their influence of part quality will be discussed.

As alluded to earlier, in the SLS process fusion occurs due to a laser passing over the powder in a desired location and partially melting it. This scanning of the powder surface is not done at random, but rather according to a certain predefined pattern. This pattern can vary depending on the material, but generally start with a scan of the layer contour. This ensures a certain level of accuracy and surface finish quality. The remaining layer is then scanned using a fill pattern.

Fill patterns can be as simple as scanning a raster of the entire layer from one side to another by the laser sweeping back and forth in one axis and slowly stepping from one end of the layer towards the other in the other. Other fill patterns divide the area into stripes or squares and scan these one after another while rotating the scan angle with every scanned layer. Stripe and square fill patterns are usually used for metals, while raster patterns are often used to process low-temperature materials like polymers. As the development of residual stresses in the part must be considered, scan pattern selection should be done very carefully. Sometimes randomized scan patterns are applied to reduce the problem of residual stresses. (Gibson et al. 2021, 43, 44.)

When scanning the pattern, the laser speed, beam diameter, and hatch spacing of the laser must be set accordingly. The laser speed, as the name suggests, is the travel speed the laser. The beam diameter, or spot size, is the diameter of the projected area of the laser beam on the powder surface. The hatch spacing, often referred to as scan spacing or hatch distance, is the distance between the center points of two laser passes. Figure 3 illustrates the interplay of hatch spacing, beam diameter and beam overlap. The beam overlap results from the beam diameter being greater than the hatch spacing. A certain degree of beam overlap is necessary due to the nature of the laser beam. As a typical Gaussian beam profile, the laser power in the center is the highest, while it is reduced towards the boundaries, therefore requiring a certain degree of beam overlap in order to provide an even distribution of heat on the powder surface. (Kumar 2020, 48; Gibson et al. 2021, 143, 144.)

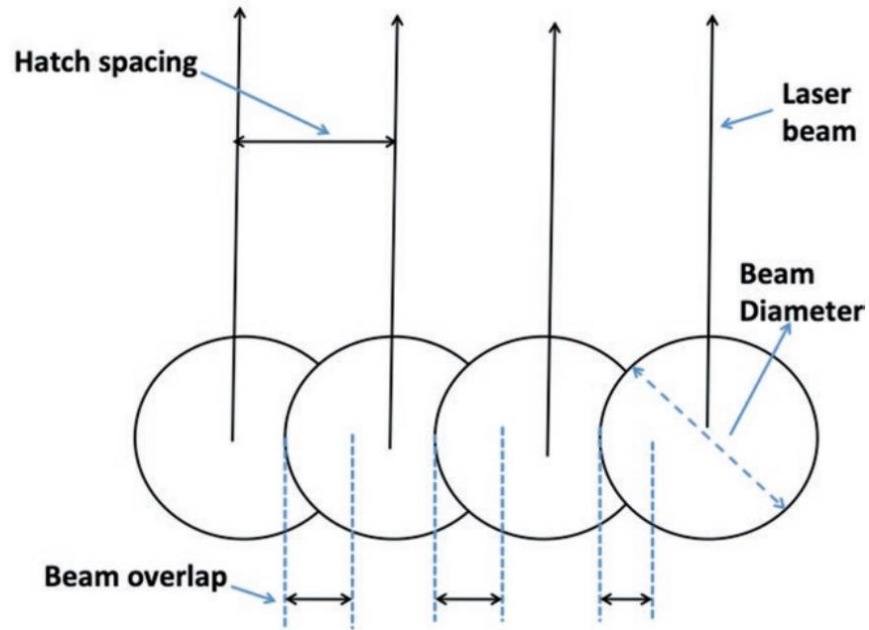


Figure 3. Illustration of hatch spacing, beam diameter, and beam overlap (Kumar 2020, 47)

The laser speed, also called the scan speed, is a parameter that strongly influences the production speed. With higher scan speed comes higher production speed, therefore resulting in faster machine cycles and lower production cost. However, the scan speed is inversely proportional to the laser energy density, as can be seen in equation 1. This means that with an increase in scan speed, the laser energy density decreases, resulting in less heat transmission which causes the material melting capability of the laser to diminish. To counteract this, the laser power could be increased. However, an increase in laser power can cause other unwanted side effects like part growth, poor recyclability of the part cake, and further complication of post-processing. (Gibson et al. 2021, 144; Kumar 2020, 48.)

Layer thickness is another critical parameter in the SLS process. The layer thickness determines the height of the powder layer the recoater applies on top of the build volume after finishing a slice of the model. Like the scan speed, an increase in layer height causes a decrease in production time. Though, with a decrease in layer height, greater precision can be achieved. This precision difference can be clearly noticed when trying to construct fillets or other round features in z-axis direction. At larger layer heights, a clear stair-stepping effect

can be observed in the final part, while a decrease in layer height lessens this effect. However, stair-stepping will still be noticeable, even at small layer heights. Smaller layer heights have the additional benefit of lower surface roughness and less part shrinkage, which results in greater dimensional accuracy. Though, as depicted earlier, this will increase production time and cost. The layer thickness, like the scan speed, is inversely proportional to the laser energy density, as can be seen in (1). (Kumar 2020, 49, 50; Gibson et al. 2021, 144.)

$$E_v = \frac{P}{L_t \cdot V_s} \cdot \left[\frac{(2 \cdot S_d - S_s)}{S_d^2} \right] \quad (1)$$

where

E_v	is	laser energy density [J/mm ³]
P	is	laser power [W]
S_d	is	spot size [mm]
V_s	is	scan speed [mm/s]
L_t	is	layer thickness [mm]
S_s	is	scan spacing [mm]

The properties of the powder material are another major factor that impact the result. For example, the maximum particle size is limited by the layer height. The minimum particle size is not as clearly defined but limited by inter-particle forces reducing its flowability. The size, shape, and colour of the powder also influences its laser absorption characteristics and thermal conductivity. The smaller the particle size, the greater the surface area of the powder bed, therefore increasing the heat absorption capability of the powder bed. This results in a less powerful laser being required to process the powder, reducing other side effects mentioned earlier. Another important parameter of the powder is its molecular weight, which directly influences the powders viscosity and flowability. Furthermore, in the case of polymers, a homogeneous molecular weight distribution across the entire powder batch is desirable to minimize fluctuations of the melting point. On the topic of melting temperature, the temperature inside the build chamber should also be kept at a constant and slightly below the melting point of the material. Keeping the temperature slightly below the melting point allows for a less powerful laser to be used, therefore causing local temperature spikes in areas where powder is being sintered to be lessened. This ultimately results in better

part quality and improved warpage behaviour. (Kumar 2020, 49; Gibson et al. 2021, 144, 145.)

It can be seen that the SLS process and the resulting part is influenced by a whole range of factors. To achieve good, repeatable results, close monitoring of process parameters during the build stage is essential. There is always a trade-off between the different parameters. To change one parameter, many other parameters need adjustment in order to restore a proper balance and guarantee a good output. Especially when it comes to production speed, trade-offs must be made. Tuning any parameter towards greater production speed typically results in a worse part quality. An example would be laser scanning speed. If the scanning speed is increased, the energy density is reduced, as can be seen in equation 1. However, this reduction in laser energy density must now be compensated for in another way in order to provide sufficient energy and temperature levels to melt the powder material. One possibility of achieving this is changing other parameters which directly influence laser energy density, like laser power, layer height, scan spacing, or spot size. Another option is lowering the laser energy density requirement of the process. This can be accomplished by increasing the powder bed temperature or reducing the layer height. Now, after successfully increasing the scan speed, by changing either of the parameters listed above, you may still end up with an equivalent or lower production speed, as decreasing, for example the layer height decreases the production speed. The same problem occurs when decreasing the laser spot size and scan spacing. In contrast to that, increasing the powder bed temperature may realistically increase the overall production speed. Though, closing the gap between powder bed temperature and the melting point of the powder increases the probability of undesired sintering of the part cake, ultimately resulting in worse part quality and part cake recyclability. (Gibson et al. 2021, 144.)

2.3.4 Materials

Common commercially available materials used in SLS processes include, but are not limited to: polyamides (PA), polystyrene (PS), polypropylene (PP), thermoplastic elastomers (TPE), polyaryletherketones (PAEK), and thermoplastic

polyurethane (TPU) (EOS GmbH 2021; Sinterit 2021; 3D Systems 2021; Gibson et al. 2021, 393, 394). However, with a 90 % share, polyamides are the most used material by far. Especially polyamide 12 (PA12) is the most used polymer with the highest value in the market (Wudy & Drummer 2019, 2; Amado Becker 2016, 23). Polyamides come in a whole range of different variations such as PA12, PA11, and PA6, where the number indicates the number of carbon atoms that are provided by one of the monomers which are reacted during the production of polyamides. Furthermore, polyamides, as well as other plastics are available as composite materials which improves certain material properties such as their stiffness or tensile strength. Examples are the addition of small glass beads, aluminium particles, or carbon fibers. (Gibson et al. 2021, 5, 393). It must be noted that some materials require specific atmospheric conditions provided through a chemically inert shielding gas during the manufacturing process. An example would be PA11. This material requires the build chamber to be filled with nitrogen gas during the manufacturing process to prevent the material from reacting with gases present in air (e.g., oxygen and water vapor) (Sinterit 2021c).

2.3.5 Post-processing

Before a part produced using SLS can be implemented in its final use, the part must undergo certain post-processing steps. These post-processing steps can range from removing the part cake or improving the surface finish, to enhancing the mechanical properties of a part. An unavoidable step in polymer based SLS manufacturing is the removal of the supporting powder around the part, the part cake. Typically, this is done by first using a brush or scraper to remove the bulk of excess powder and later blasting the part with sand, glass beads, or polymer powder in order to remove more persistent powder residue. When using an abrasive like sand, care must be taken when treating the part, because the treatment may lead to a loss in dimensional accuracy or the resolution of certain features. This issue can be rectified by blasting the part with the same polymer powder the part is made of. However, this results in significantly higher post-processing times. (Gibson et al. 2021, 458, 459; Diegel et al. 2019, 184.)

Sand blasting the part does not only help in excess material removal, but it can also be used to improve the surface finish of the part. Other popular methods employed to improve the surface finish of SLS parts are tumbling, vibro polishing, or sanding. One of the main objectives when treating the surface of AM parts is the removal of visible layer lines. However, as AM parts are also commonly used for aesthetic purposes, altering the outside appearance of a part is another frequent post-processing step. This alteration can be done either by painting, dyeing, wrapping, using hydrographics, or metalizing the part. (Gibson et al. 2021, 462, 463; Diegel et al. 2019, 194-199.)

2.3.6 Powder recycling

With material cost being a large contributor to the overall cost of an SLS part, reducing the amount of fresh material required to manufacture a part through recycling of the part cake is highly desirable. However, due to material aging induced by the material being exposed to high temperatures in the build chamber over a prolonged period of time, the reusability of the powder is somewhat limited. Holding polymer materials at temperatures so close to their melting point for an extended duration will increase their molecular weight, as well as the average particle size of the powder. On one side, the higher molecular weight will result in changes to the melt characteristics, while on the other side larger particle sizes will increase the dimensional deviation of the process. Furthermore, it has been discovered that material aging leads to changes in the thermal properties of the powder, as well as to changes in the resulting part crystallinity and characteristics. (Wudy & Drummer 2019, 8, 9; Gibson et al. 2021, 152, 153, 393.)

To improve the overall characteristics of recycled powder, it is very common to mix used powder with fresh virgin powder. Typically, 30-50 % virgin powder is mixed with the used powder in order to restore the material properties to a point where the part result will be acceptable. The ratio of virgin powder to used powder is called the “refresh ratio”. The powder mix is then processed using a particle sorting method, most commonly a vibrating sieve, which ensures a certain particle size for the following manufacturing cycle by breaking up powder

conglomerates and sorting out larger particles. (Gibson et al. 2021, 152, 153, 393.)

2.3.7 Design guidelines and considerations

One of the main advantages of SLS manufacturing is the high degree of freedom in the design stage. As designed parts usually do not need additional support structures due to the unfused powder acting as a support structure all around the part, even compared to other AM technologies like material extrusion, SLS provides even greater freedom in part design. However, the freedom in complexity of SLS parts does not come without its cost. Before making the decision on manufacturing a part using SLS, or any other AM method for that matter, the designer must decide if the part complexity and production volume justifies using SLS to manufacture the part. Especially with lower complexity parts or at very high production volumes, more traditional manufacturing methods are often more suitable for the job when regarding production time and cost. (Kumar 2020, 9-11; Diegel et al. 2019, 110.)

If the decision on the manufacturing method for a part has fallen onto SLS, the designer must now follow certain guidelines when it comes to the design. First of all, the accuracy and tolerances of the SLS machine must be identified. As these are different for every machine, one must design every part in line with the limitations of the specific machine which will be used in the manufacturing of that part. When it comes to the designing different features, the design rules shown in Figure 4 can be taken as a general design guideline. One of the distinctive features in SLS part design are escape holes. Escape holes are necessary in order to remove any excess powder from within the part. Therefore, when designing a part for SLS, the designer must take the addition of such escape holes into consideration to prevent unfused powder from getting trapped inside the part itself. Reasons for doing this are mainly to save on material and to remove the added weight of unfused powder inside the part. (Diegel et al. 2019, 110-115.)

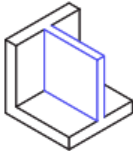
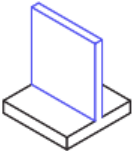
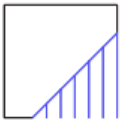
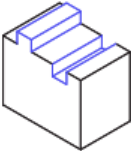

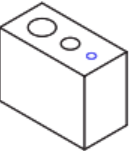
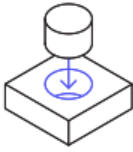
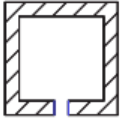
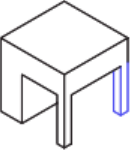
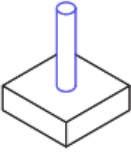
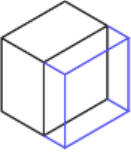
Supported walls	Unsupported walls	Support & overhangs	Embossed & engraved details	Horizontal bridges	Holes
Walls that are connected to the rest of the print on at least two sides.	Unsupported walls are connected to the rest of the print on less than two sides.	The maximum angle a wall can be printed at without requiring support.	Features on the model that are raised or recessed below the model surface.	The span a technology can print without the need for support.	The minimum diameter a technology can successfully print a hole.
					
0.7 mm			1 mm wide & high		Ø1.5 mm
Connecting /moving parts	Escape holes	Minimum features	Pin diameter	Tolerance	
The recommended clearance between two moving or connecting parts.	The minimum diameter of escape holes to allow for the removal of build material.	The recommended minimum size of a feature to ensure it will not fail to print.	The minimum diameter a pin can be printed at.	The expected tolerance (dimensional accuracy) of a specific technology.	
					
0.3 mm for moving parts & 0.1 mm for connections	5 mm	0.8 mm	0.8 mm	±0.3% (lower limit ±0.3 mm)	

Figure 4. Selective Laser Sintering (SLS) design guidelines (3D Hubs 2021b) (modified)

Another important detail in the design for AM is the anisotropic nature of parts manufactured by layer-based manufacturing methods. Anisotropy means that the mechanical properties of a part are not identical in all directions. For most SLS machines, this anisotropy applies in the z direction as the adhesion between layers is generally weaker and therefore the part can withstand less stress if loaded in the z direction opposed to being loaded in the x, or y direction. When comparing SLS parts to other parts produced using other AM processes, SLS

parts are generally considered as less anisotropic due to the relatively high adhesion between the individual layers. (Diegel et al. 2019, 93, 94.)

3 SLS SETUP AT LAPLAND UAS

In this chapter, an introduction of the SLS setup as it is currently found at the Lapland UAS 3D printing laboratory will be given. To begin with, safety in the SLS working environment will be discussed, with special emphasis put on microparticle handling. Furthermore, an overview of the SLS machine, as well as several components used in the preparation and post-processing stages of a manufacturing cycle will be given. To conclude, a recommendation for the SLS workflow in the 3D printing laboratory will be given.

3.1 Safety

When working with polyamide powder, certain safety guidelines must be followed, and precautions must be taken to ensure a safe working environment for the operating personnel and to lower the chance of incidents. As the PA12 powder with an average particle size of 30 to 50 μm qualifies as a microparticle, the manufacturer advises users to wear appropriate eye protection when handling the powder. Furthermore, in case of prolonged or frequent skin contact, suitable protective gloves should be worn by the user. In case there is a risk of further skin contact besides hand contact; suitable protective clothing should be worn to prevent skin irritation. If the powder is handled correctly under normal conditions, there is no need for respiratory protection. However, if the user is exceeding the exposure limit values, the working environment is insufficiently ventilated, or there is an increased chance for the formation of dust, appropriate respiratory protection should be worn. (Sinterit 2021c, 3, 4.)

If an employee encounters an accident with the powder, certain first aid steps should be followed depending on the type of contact:

- In case of powder inhalation, the casualty should be taken to a fresh air environment and kept at rest.
- In case of skin contact, gently wash the affected part with water and soap.

- If an employee gets their eyes in contact with the powder, the affected eye(s) should be rinsed cautiously with water for several minutes.
- In case of ingestion, the mouth should be rinsed, and water should be taken in in little sips to create a dilution effect. Inducing the casualty to vomit is not advised. (Sinterit 2021c, 2.)

In case any of the above-named incidents cause more severe symptoms or the irritations persist, it is advised to consult a physician and seek medical treatment. (Sinterit 2021c, 2.)

Besides getting in direct contact with the powder material, dust explosions are another potential threat that must be accounted for. When handling powder materials with small particle sizes, these particles have the tendency to become airborne and float. Especially in confined spaces, this may lead to a significant buildup of particles within the working environment. With a decrease in size, the reactivity of said particles increases as a result of the increasing surface to volume ratio. Because of that, the risk of ignition in the presence of an atmosphere containing oxygen increases significantly. As a result, small sparks, friction, or electrostatic discharge can lead the dust particles to ignite and create an explosion. For that reason, any equipment intended for use in potentially explosive environments which is to be sold on the European market must be ATEX certified. (European Parliament & Council of the European Union 2014.)

Dust explosions present a threat to the SLS operation in two ways. On one side, dust explosions may be an issue within the surrounding SLS facility as a result of improper powder handling by personnel. On the other hand, dust explosions problem may occur inside the SLS device itself, due to material being airborne by the powder handling system during the recoating procedure. To mitigate the risk of dust explosions inside the SLS device, the manufacturer must design the machine in a way where no significant level of dust buildup is possible. Furthermore, airborne dust might settle on critical components inside the machine (i.e., laser optics, sensors), therefore, the formation of floating dust should be avoided in the first place. If dust formation cannot be avoided, the manufacturer may use an inert gas inside the build chamber in order to prevent

the dust from reacting with oxygen inside the atmosphere. To prevent dust explosion from occurring in the AM facility, personnel must receive sufficient training in powder handling to prevent dust formation. Furthermore, any ignition sources present in the direct vicinity of the powder handling area must be eliminated. (Gibson et al. 2021, 150.)

3.2 SLS workspace and equipment

The following chapter will give an introduction of the SLS workspace and the equipment which is involved in the 3D printing laboratory SLS workflow. This introduction serves as an overview of the setup for future personnel and gives information on the properties of the dedicated workspace and the characteristics, features, and limitations of the equipment.

3.2.1 SLS printing room

To ensure a clean and safe workspace, a dedicated SLS printing room was constructed inside the Lapland UAS 3D printing laboratory (Figure 5). This room serves as an area which houses the equipment involved in the SLS process, including preparation, manufacturing, and post-processing tasks. As handling powder materials will inevitably result in some degree of powder spillage, containing said spillage inside this dedicated area serves to protect other sensitive AM equipment inside the laboratory, as well as other personnel working inside the laboratory. The SLS printing room is operated at negative pressure to further reduce the probability of powder escaping from inside the room, contaminating the surrounding environment. The negative pressure operation additionally serves to contain fumes and bad odors that may be present while the SLS machine is running. Moreover, the back wall of the room was treated with an anti-static liquid which aims to reduce the likeliness of dust particles adhering to the perimeter walls. The anti-static properties also lower the probability of dust particles igniting by the means of static electricity arcs and therefore reducing the risk of dust explosions. Furthermore, the floor of the SLS printing room is covered with porous rubber mats that serve to capture any powder spilled on the floor

during powder handling, further reducing the chance of powder escaping from the SLS printing room and contaminating the surroundings.



Figure 5. Lapland UAS SLS printing room

3.2.2 Sinterit LISA PRO

Currently, Lapland UAS is in possession of one AM machine capable of the SLS process. This machine is of the model “LISA PRO” by the manufacturer Sinterit and can be seen in Figure 6a.

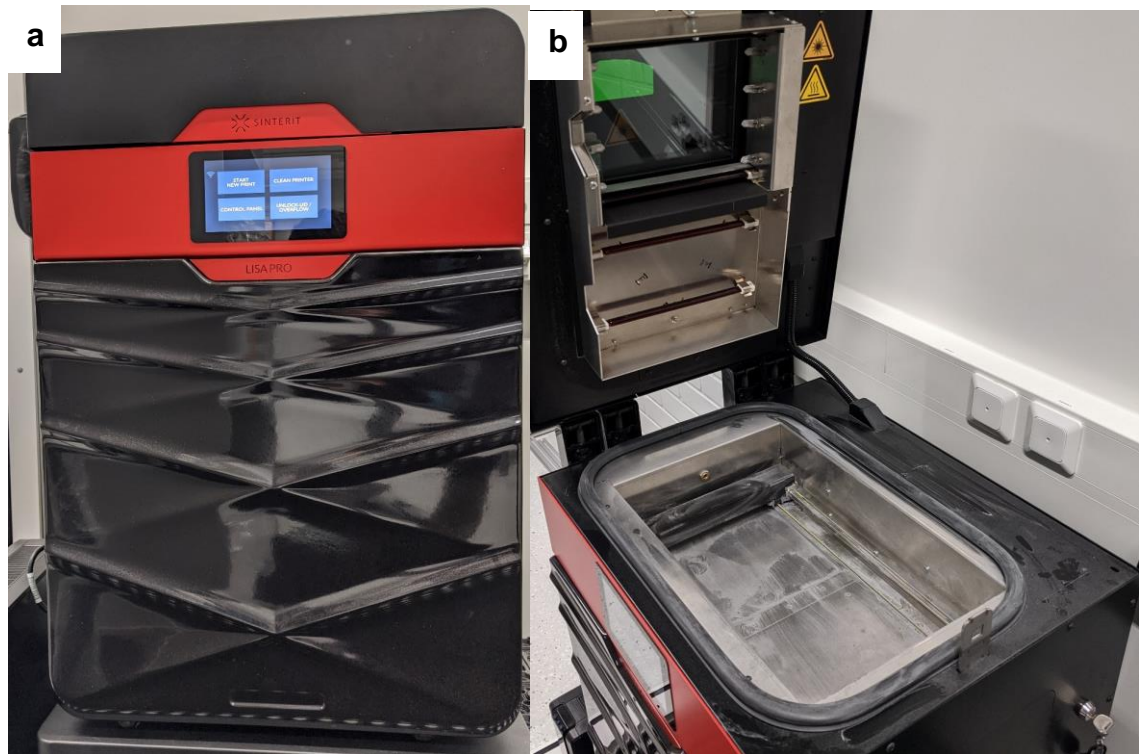


Figure 6. Front view of the Sinterit LISA PRO (a) and view of the open hatch, revealing the build chamber (b)

Opening up the hatch of the LISA PRO reveals the build chamber in the lower part, as well as the laser and its optics assembly in the top part of the device (Figure 6b). The LISA PRO employs a 5 W IR diode laser with a wavelength of 808 nm to process the powder. The build chamber temperature can reach up to 200 °C, with an independent heating system for the pistons and cylinders of the lifting mechanism, as well as for the feed and print bed. Thanks to its built-in nitrogen chamber and temperature capabilities, the LISA PRO is capable of processing a range of materials, including: PA12, PA11, TPE, and TPU (Sinterit 2021j). Additionally, the LISA PRO not only supports first-party powders provided by the manufacturer, but also allows for the use of third-party powders. The build volume inside the device is 150 x 200 x 260 mm, with a maximum diagonal part size of 308 mm. However, for TPU/TPE and PA materials, the manufacturer guarantees high accuracy parts only within a build volume of 110 x 150 x 245 mm and 90 x 130 x 230 mm, respectively. Furthermore, the manufacturer advertises the process to have an XY-accuracy of 50 μm , a minimum wall thickness of 0.4 mm, minimum detail size of 0.1 mm, minimum hole diameter of 0.5 mm, and a moving part clearance of 0.2 mm. The layer height can be varied from 0.075 to

0.175 mm. Basic interfacing with the machine happens through the built-in touchscreen (Figure 6a). Files can be transferred to LISA PRO using either its USB-interface, seen in Figure 7b, or the built-in WIFI-module. Besides the USB-interface, the right-hand side of the device features an ignition key to start the device, an emergency stop button, and an overflow bin. The overflow bin is used to catch any excess powder accumulated by the recoater during powder bed preparation and the build process. The nitrogen gas for the nitrogen chamber of the device is supplied through a pneumatic quick coupling located on the left-hand side of the device (Figure 7a). (Sinterit 2021a; Sinterit 2021f.)

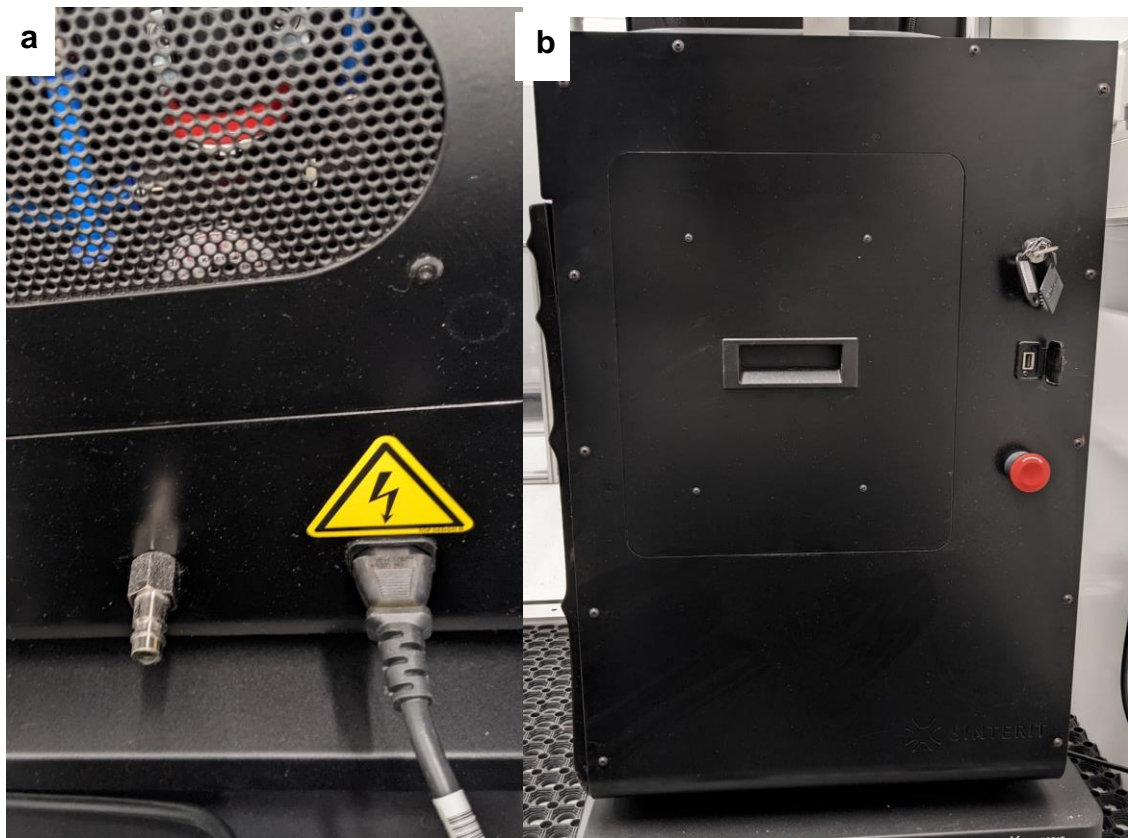


Figure 7. Left side (a) and right side (b) of the Sinterit LISA PRO featuring: nitrogen quick coupling, power plug, USB-interface, emergency stop button, ignition key, and overflow bin

3.2.3 Sinterit Powder Sieve

To process the powder after having undergone a manufacturing cycle, Lapland UAS has invested in a Sinterit Powder Sieve (Figure 8). This sieve allows the user to automatically sift the used powder, breaking up powder agglomerates

and removing any contaminants which might have remained in the powder. Moreover, this device can be used to refresh the part cake with virgin powder by mixing the two in the sieving chamber. The Sinterit Powder Sieve has a powder capacity of 5 L, and according to the manufacturer a sieving cycle takes 18 min. After completing the cycle, the refreshed powder can be retrieved by taking out the collection bucket in the bottom part of the device. (Sinterit 2021d; Sinterit 2021f.)

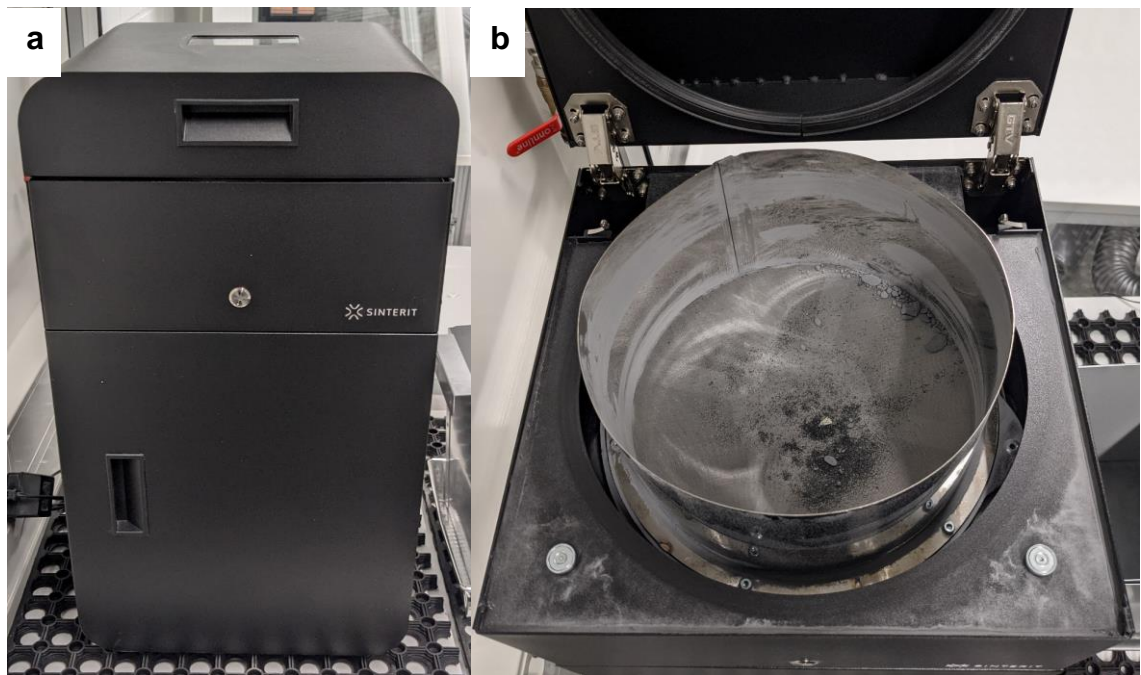


Figure 8. Front view of the Sinterit Powder Sieve (a) and a look inside the sieving chamber (b)

3.2.4 Sinterit Sandblaster

In order to post-process the part surfaces and free the parts from unwanted powder, a sandblaster is used. The sandblaster found in the SLS setup is of the model “Sandblaster” by Sinterit and can be seen in Figure 9.

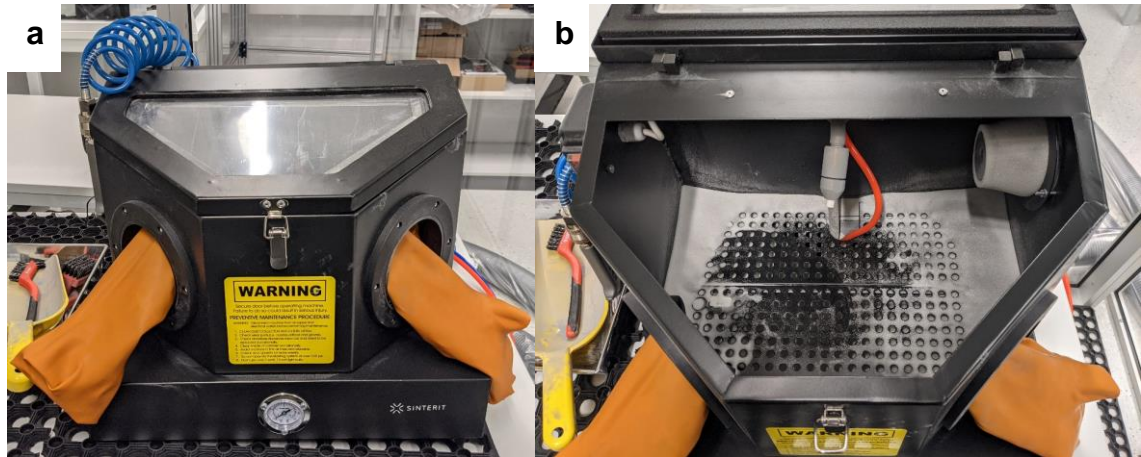


Figure 9. Sinterit Sandblaster as seen in the Lapland UAS 3D printing laboratory. Front view (a) and top view with open hatch (b)

The sandblaster uses 200 μm glass balls with an abrasive capacity of up to 4.5 kg to blast the parts. The working area of the device is 410 x 310 x 200 mm. The sandblaster must be supplied with compressed air at a pressure of 8.62 bar and has an air consumption of 290 L/min. (Sinterit 2021h.)

3.2.5 Sinterit ATEX Vacuum Cleaner and Sinterit Powder Separator

To ensure safety during powder handling and speed up the workflow, Sinterit sells an ATEX certified vacuum cleaner. As alluded to earlier, the ATEX directives force the manufacturer to certify any equipment which is meant for use in potentially explosive environments. Therefore, especially vacuum cleaners, which are driven using electricity and make powder airborne by design, must be certified to work with low graduation powder. (Sinterit 2021a; European Parliament & Council of the European Union 2014.)

The vacuum cleaner enables the user to remove any unsintered powder from the SLS machine as well as powder and dust from the workplace. By using the complementing Sinterit Powder Separator, the user is able to separate the powder from any dust and debris, making powder recycling easier. The ATEX certification is critical when working with microparticles, as dust explosions always pose a threat in these situations, as depicted in Chapter 3.1. Aside from the ATEX certification, the vacuum cleaner features an absolute HEPA filtration and an M class star filter. Before using the Sinterit ATEX vacuum cleaner, the

user must ensure that the grounding wire clamps of both the vacuum cleaner and powder separator are attached to the grounding pin located on the back wall of the SLS printing room. Both the Sinterit ATEX Vacuum Cleaner and Sinterit Powder Separator can be seen in Figure 10. (Sinterit 2021a; Sinterit 2021k.)



Figure 10. Sinterit ATEX Vacuum Cleaner and Sinterit Powder Separator

3.3 Workflow

In the following chapter, the workflow around the SLS setup at Lapland UAS will be explained. This includes all steps required to complete a successful manufacturing cycle using LISA PRO. A schematic illustration of the SLS workflow can be seen in Figure 11.

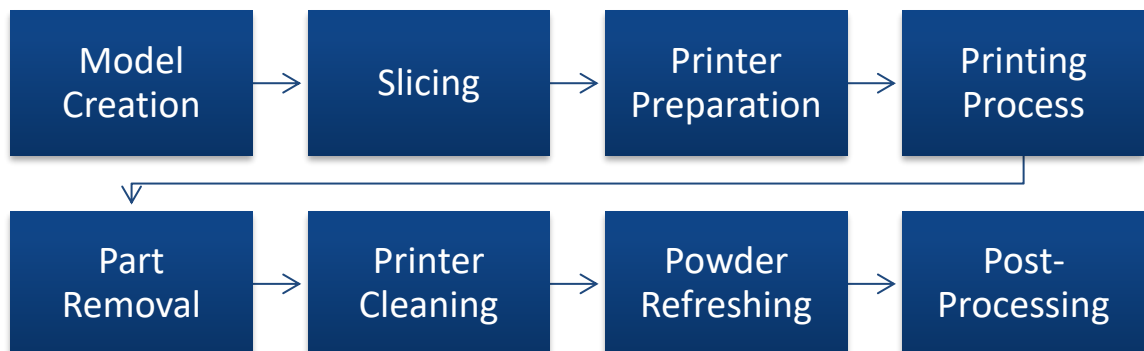


Figure 11. SLS workflow schematic

As shown in Figure 11, the SLS process starts at the model creation, followed by the slicing of the model using the software included with LISA PRO, “Sinterit Studio”. After that, LISA PRO must be prepared for the print and the printing process must be started. Following completion of the manufacturing cycle, the parts must be removed, the machine must be cleaned, and the powder must be refreshed. After all of that is done, the manufactured parts may be post-processed. All of the mentioned steps will be elaborated on in further detail in the following.

3.3.1 Model acquisition and slicing

The first step in the SLS process chain is acquiring a model which is suitable for SLS manufacturing. This mainly involves following the design guidelines presented in Chapter 2.3.7. The model can now be imported into the dedicated slicer software “Sinterit Studio”. When opening Sinterit Studio the user is first presented with the “Preset” tab (appendix 2). In this tab the device model (Printer Model), powder type, and layer height can be adjusted. The device at Lapland UAS is of the model “Lisa Pro rev.A”. Moreover, the user may connect to the 3D printing laboratory WIFI network in order to connect to the device in a later step. Once the WIFI connection has been established, the model of the printer can also be detected using the “Detect” button in the user interface (UI). Powder type and layer height shall be chosen according to the part requirements. The “Advanced Options” dropdown allows for further tuning of process parameters. However, adjustment of these parameters should only be necessary in special cases outside of typical use.

The next step is importing the model(s) into the software using the “Models” tab. The imported model will be displayed and its position can be adjusted using the 3D UI (appendix 2). When positioning a model, the user must make sure the model is as close to the center as possible, as this will guarantee the best possible manufacturing result. Positioning the part in the zone indicated in red leads to alteration of part geometry, and in the worst case to a loss of the manufacturing cycle due to warped parts obstructing the path of the recoater, causing it to crash.

After all models have been positioned within the build volume, the next step is to slice the models. In the “Slice” tab (appendix 2) the user may choose a printer software version and has the option to generate a report. The former should be set to “Newest”, but this may vary in special cases. Generating is recommended, as this allows the user to review process parameters, manufacturing time, and powder volumes. Pressing the “Slice” button prompts the user to choose a name and location for the proprietary scode file that will be generated for LISA PRO to interpret. After slicing is complete, a short list of key process data is displayed. The user may choose to expand said list to display additional information on the process. The generated scode file can now be viewed in the “Preview” tab (appendix 2). Alternatively, other scode files can be loaded and viewed.

Finally, the scode file must be transferred to LISA PRO. This can either be done by loading the file onto an USB flash drive and transferring it that way or using the previously acquired network connection to the device. Transferring the file using the network is done by using the “Printers” tab (appendix 2). Besides allowing the user to send scode files to the internal storage of the device, the Printers tab also enables remote monitoring of the device using either the print status indicator or the integrated camera. It may be noted that the device must be powered on in order for it to be detected and accessed over the network.

3.3.2 Preparation

After the scode file has been transferred successfully using either an USB flash drive or the network, device preparation can start. When working on anything within the SLS workflow which involves powder handling, the manufacturer recommends wearing eye, skin, and respiratory protection. In case of uncertainties regarding safe powder handling, refer to Chapter 3.1. Before starting the preparation procedure, the user should get certain appliances and consumables ready. These include:

- print-ready powder material
- powder scoop
- powder compactor

- brush
- plastic scraper
- cotton cloth
- isopropyl alcohol (IPA)
- silicone oil

To start the preparation sequence, press “Start New Print” on the printer interface. The device will now guide the user through all the necessary preparation steps automatically. Therefore, this part of the workflow will only briefly touch on key events in the sequence and point out important details of this otherwise fairly automated sequence.

In the first step, the LISA PRO will ask the user to open the lid. This can be done by pressing “UNLOCK LID” on the touchscreen, lightly pressing down the lid itself until an audible click can be heard, and then lifting the lid up. It is to note that the lid cannot be opened if the temperature inside LISA PRO is above 50 °C.

The next step is selecting the scode file which has been previously transferred. After selecting the file, LISA PRO will display the expected manufacturing time, as well as the previously selected material. Using the right material is key in achieving a good result as the process parameters vary greatly between different materials. Following the scode selection, LISA PRO will ask the user if the last batch of parts (printout) has been removed. If not, press “REMOVE PRINTOUT” and refer to Chapter 3.3.3, else press “SKIP”.

Next, the device will ask the user to clean the laser protective glass. This is done by removing the split pin from the heating module, lowering the heating module, and unscrewing both nuts holding the protective glass in place (Figure 12). Great care must be taken when lowering the heating module as the hinge mechanism holding the module in place is fragile and might get damaged or break if the module is lowered too quickly.



Figure 12. Heating module split pin and laser protective glass nuts

The protective glass shall now be cleaned on both sides using a cotton cloth soaked in IPA. Afterwards, the glass shall be wiped down using a dry piece of cotton cloth and put back in its place.

LISA PRO will now ask the user if the feed volume (feed bed) and build volume (print bed) have been cleaned. If so, hit “SKIP” on both requests, if not, refer to Chapter 3.3.3.

Next, all tools must be removed from within the build chamber and the path of the recoater must be checked for any obstructions. If there is nothing obstructing the recoater or the beds, the user must confirm it by hitting “DONE” on the touchscreen. Subsequently, LISA PRO will start homing and leveling the feed bed, print bed, and recoater position. After the leveling is done, LISA PRO will prompt the user to fill the feed bed with compacted powder. To do this, the user shall add powder from the steel container labeled “PRINTREADY MIX” to the feed bed using the powder scoop. Every third of the way to filling the bed, the powder should be compacted by using the compactor to press down on the powder until light resistance can be felt (Figure 13a). After having filled the bed with compacted powder, the bed should be topped up with additional powder.

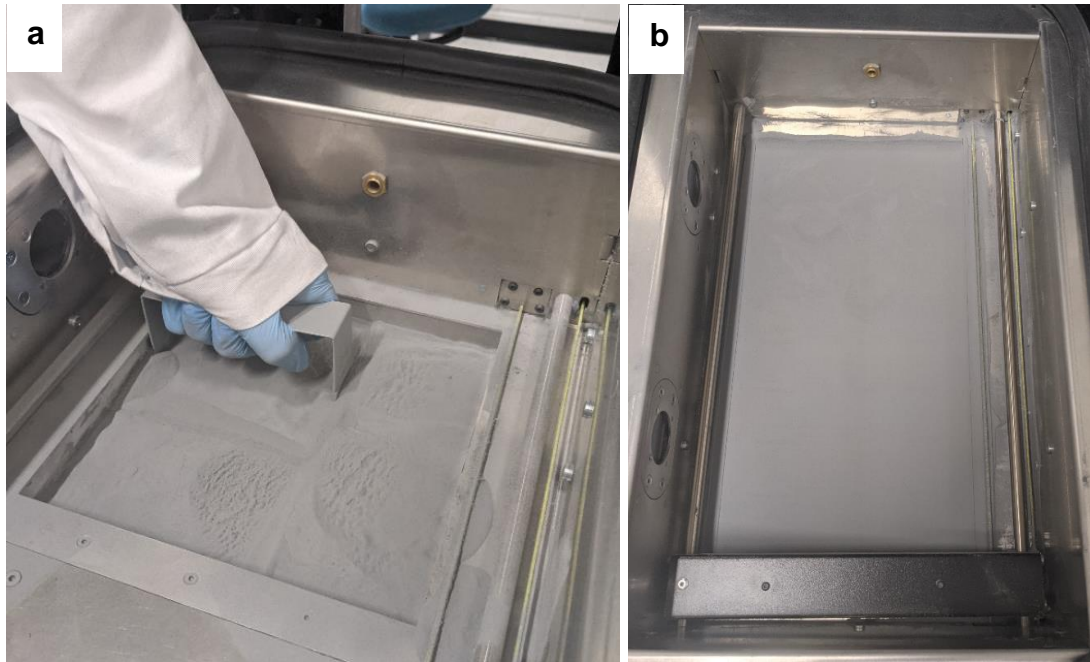


Figure 13. Powder compacting (a) and desired powder surface after successful powder bed leveling (b)

The plastic scraper can now be used to move any powder spillage around the bed back into the feed bed. Once the bed is filled to an adequate level, the user shall confirm this by hitting “DONE” on the touchscreen.

LISA PRO will now start leveling the powder beds. The user may assist LISA PRO during this process by moving any powder from the edges of the build chamber towards the beds. However, this must be done with care as touching any of the powder on the beds with the scraper may result in further leveling being necessary. Upon reaching adequate powder leveling (Figure 13b), the user may stop the leveling process manually by hitting “LEVELING DONE” on the touchscreen. If the result of the leveling is insufficient, the process may be repeated.

In the next step, LISA PRO prompts the user to clean the glass in front of the camera and pyrometers. The glass should be cleaned by first using cotton cloth soaked in IPA, and dry cotton cloth later (Figure 14).



Figure 14. Camera and pyrometer windows

Following the cleaning procedure of the camera and pyrometer windows, the guide rails of the recoater must be cleaned using dry cotton cloth. After cleaning it, a couple drops of silicon oil should be applied to the guide rails to lubricate the recoater.

After completing all of these steps successfully, the lid can now be closed, and the manufacturing cycle will start after the user gives confirmation to the machine by hitting “START PRINTING” on the touchscreen. LISA PRO will now start preheating the build chamber until it reaches the manufacturing temperature specific to the material. During this stage, and all subsequent stages (build stage, cool down stage), LISA PRO shall not be turned off or interfered with in any way.

3.3.3 Part removal and cleaning

After the cooldown stage, the parts and part cake may now be removed from the machine. Under normal circumstances, part removal should take place within 30 minutes of the completion of the cooldown stage. A delay of the part removal should be avoided as the unsintered powder may start absorbing moisture from the surrounding air which may impact its manufacturability and decreases the overall quality of the powder. For the removal procedure, the following tools will be required:

- part carriage plates
- powder tray
- ATEX vacuum cleaner
- brush

In order to start the part removal, the lid must be opened using the interface of LISA PRO. Again, after pressing the button, the user must first lightly press down on the lid and lift it to open it. After making sure that nothing is obstructing the recoater, the user must hit “REMOVE PRINT”, “REMOVE PRINTOUT”, and “DONE” to start the automated part removal procedure. LISA PRO will now lift the part cake out of the build volume. The part cake may now be removed from the machine using the part carriage plates (see Figure 15a). After capturing the part cake, it shall be moved onto the tray.

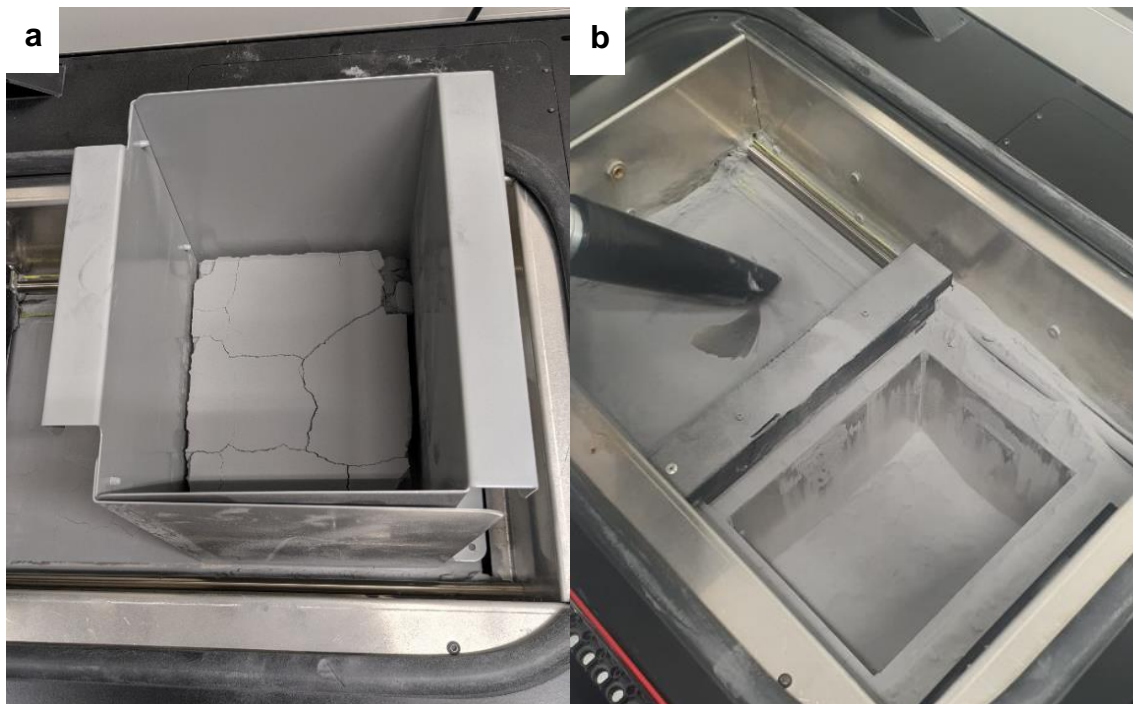


Figure 15. Part cake removal using part carriage plates (a) and build chamber cleaning using ATEX vacuum cleaner (b)

LISA PRO will now ask to empty the overflow bin. However, this will be done in a later step after cleaning the build chamber. Following that, LISA PRO will continue by asking the user to clean the laser protective glass. Since the LISA PRO at Lapland UAS will be used by many different users, this step will be done in the beginning of a manufacturing cycle, so every user can make sure the laser protective glass is cleaned properly ahead of a cycle. This will ensure that the user must not rely on the proper cleaning of others in order to get a good result. In the next step, LISA PRO will ask to clean the feed bed. Again, it must be made sure that nothing is obstructing the path of the recoater. The recoater will move

to one side of the build chamber, while the feed bed and print bed will position themselves ready to be cleaned. After the positioning is done, the build chamber may be cleaned from any unsintered powder using the ATEX vacuum cleaner and a brush (see Figure 15b).

LISA PRO will then ask the user to clean the print bed, which will move the recoater to the other side of the build chamber and move the print bed upwards. Any remaining powder may now be removed by using the brush and ATEX vacuum cleaner. After completing all these steps, the overflow bin must now be removed and emptied into the powder sieve. After returning the overflow bin back to its place and confirming it by hitting "DONE", the cleaning sequence is complete.

3.3.4 Powder refreshing

After successful part separation, the part cake must be moved to the powder sieve. In the powder sieve, the part cake will be mixed with the powder from the overflow bin, the powder captured by the cyclone of the ATEX vacuum cleaner, as well as fresh powder. The exact amount of fresh powder can be obtained either from the instructions of LISA PRO during part removal or in the report generated during the slicing of the model(s) in the Sinterit Studio software. It must be noted that not all materials require powder refreshing. At Lapland UAS, only PA12 and TPU powders are in use at this moment in time, of which only PA12 requires a powder refresh. When refreshing PA12, the correct powder must be used since there are two types of powder containers. One contains powder labeled "FRESH", while the other one contains powder labeled "PRINT READY" (Figure 16a). As these containers look very similar, one might confuse one for the other, which would result in a decrease of powder quality. For the purpose of powder refreshing, "FRESH" powder must be used. The powder labeled "PRINT READY" will only be used if there is no powder left over from previous manufacturing cycles. Fresh powder is usually stored in the humidity-controlled material cabinet in the 3D printing laboratory. If there is no already opened fresh powder container, or the amount of powder inside the open container does not suffice, new, vacuum-sealed powder containers can be found on the shelf inside the SLS

printing room. Before dumping the powder mix into the sieve, one must remove any residue of old powder left inside the sieve. Furthermore, the user must check and ensure that a powder container with sufficient capacity is placed in the lower part of the sieve (Figure 16b). After making sure the sieve is clean, the powder mix may be added to the upper part of the powder sieve and the sieving process may be started via the button on the sieve.

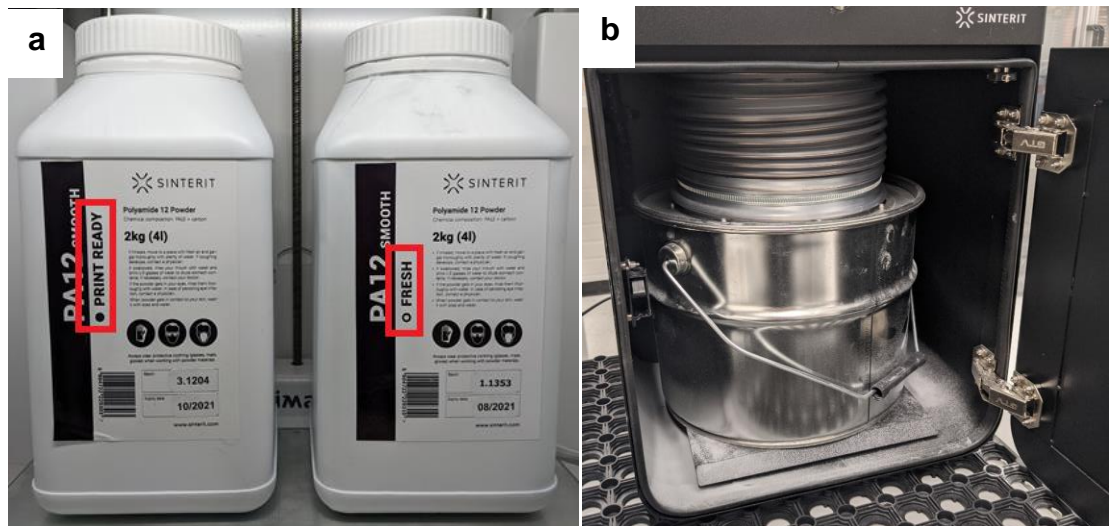


Figure 16. "FRESH" and "PRINT READY" powder containers (a) and properly inserted powder capture container (b)

The mixed powder may now be taken from the container in the lower part of the sieve and poured back into the steel container labeled: "PRINTREADY MIX".

3.3.5 Post-processing

Before starting the post-processing stage, the user must put on adequate respiratory, and skin protection. Furthermore, the user shall ready the tools which will be used during the process. The tools and appliances used for the post-processing of printed parts may vary depending on the desired type of post-processing. Therefore, these tools and appliances may include:

- brushes (flat, brass, steel)
- prying tools
- sanding paper
- Sinterit Sandblaster

Also, as powder refreshing must take place following the removal of all printed parts from the part cake, the fresh powder container must be placed in the SLS room before starting any powder handling. This is done in order to prevent the user from having to leave the SLS room during post-processing and powder refreshing, which further reduces the chance of powder contamination of the 3D printing laboratory, and especially the humidity-controlled material cabinet which the fresh powder is stored in. After successful removal of the printout, the printout is placed on the tray using the part carriage plates. The part carriage plates may now be taken away from the tray, exposing the printout. Prior to part carriage plate removal, it must be made sure that there is no risk of unnecessary powder spillage due to large printout size. If there is a risk of powder being excessively spilled while removing the plates, the part removal must be done with the plates still in place until a sufficient portion of the printout has been taken away and the risk of powder spillage has been nullified. After the removal of the part carriage plates, the user may start to carefully remove the part cake using their hands. As both the part cake and the parts may still be quite hot after the cooldown stage, especially towards the center of the printout, care must be taken while removing the powder. The part cake might be slightly sintered, causing it to stick together in chunks. However, these chunks may be broken apart by hand during part seeking. If a part has been found in the printout, any excess powder stuck to the part must be removed using one of the brushes. After sufficient cleaning, the part may be moved aside for further post-processing later. It is important that all the parts are removed from the printout and cleaned from any excess powder.

After successfully separating the parts and the part cake, the part cake must be moved to the Sinterit Powder Sieve and refreshed. It is of utmost importance that this step is done prior to any further post-processing of parts, as leaving the powder exposed to air and moisture will result in a degradation of powder quality. If the powder has been refreshed and stored away safely, the user may proceed with further post-processing steps. Depending on the desired result, this may include a range of processes. An overview of the different types of SLS post-processing can be seen in Chapter 2.3.5.

At Lapland UAS, post-processing of parts mainly includes improving the surface finish, using either sanding paper (by hand, or using the disc and belt sander), or the Sinterit Sandblaster. To process a part using the Sinterit Sandblaster, the part must first be placed in the sandblasting chamber. After it has been made sure that the chamber is safely locked, the user may turn on the compressed air supply to the Sinterit Sandblaster. The user may now proceed by blasting the part, using the foot-pedal to control airflow. If the desired surface finish has been achieved, the compressed air supply must be turned off and any excess air remaining in the pressured air lines of the Sinterit Sandblaster must be removed using the foot-pedal. The chamber may now be opened, and the part can be removed for further inspection. If the result does not meet the desired standards, the process may be repeated until it does. If a model contains more delicate features like small holes or gaps between moving parts, post-processing the part using small prying tools or similar may be necessary in order to achieve the desired freedom of movement.

3.3.6 Printing different materials

When working with different types of materials inside LISA PRO, one must be mindful about the different melting points of the materials. For example, PA12 material has a melting point of 180 °C, while TPU material has a melting point of 160 °C. Now, if the build chamber was not properly cleaned after a TPU manufacturing cycle, using PA12 in the next manufacturing cycle may lead to unwanted melting of leftover TPU powder due to increased build chamber temperatures, which, in the worst case, may result in system failure. To combat this, the build chamber must be thoroughly cleaned ahead of a material change. Furthermore, a lab supervisor should be informed if a material change is planned, as they can then inform other users that a material change has taken place, further diminishing any risk of possible machine malfunction or failure due to build chamber contamination.

4 INVESTIGATION OF PART POSITIONING AND ORIENTATION

The determination of part quality, both in terms of visual quality and material properties, is key in judging the viability of different part positioning inside the build volume. Therefore, testing will be done which aims to determine the material properties of printed parts dependent on their position by the means of a tensile test. Test samples for the tensile tests will be manufactured using the LISA PRO SLS machine at the Lapland UAS 3D printing laboratory. Test sample geometry and test conditions for the tensile tests are given by the standard for plastics tensile testing, ISO 527-2. Besides that, specimens will be judged upon their visual quality and geometrical accuracy.

Even though the 3D printing laboratory is equipped with two different materials, namely "Sinterit PA12 Smooth v1" (PA12), and "Sinterit Flexa Grey" (TPU), due to resource limitations, and because the instructors of the Lapland UAS 3D printing laboratory plan on mainly using PA12, only the material properties of PA12 will be investigated. PA12 Smooth v1 is a PA material, commonly known as nylon, which represents the large majority in SLS material market share. PA12 materials mainly find application in structural or mechanical parts, which makes the investigation of its material properties all the more important (Sinterit 2021d; Sinterit 2021l). Table 1 shows some of the key material properties of PA12 as advertised by its manufacturer Sinterit.

Table 1. Sinterit PA12 Smooth v1 material properties (Sinterit 2021d)

Material	PA12 Smooth v1
Granulation	38 μ m
Colour	Navy Grey
Refresh Ratio	30 %
Ultimate Tensile Strength	40.1 MPa
Young's Modulus	1020.4 MPa
Elongation at Break	13 %
Charpy – Impact Strength	15 - 20 kJ/m ²
Melting Point	180 \pm 2 $^{\circ}$ C

As depicted earlier, PA12 represents a stiff material used for structural components. This can also be seen in its Young's modulus and elongation at

break, as according to Sinterit, the Young's modulus of their PA12 material is 1020.4 MPa, and the elongation at break is rather low at 13 %. As the material properties seen in Table 1 are claims made by the manufacturer, the results of the tensile tests done within the scope of this thesis will be compared to these claims in order to look into their reproducibility in a realistic setting.

As the manufacturer advises against positioning parts within the red, outer perimeter of the xy plane of the build volume, but the exact behaviour of parts placed in these regions is not yet documented, investigations on said behaviour will be done. The results of these preemptive tests will later be used to develop a suitable methodology for the investigation of the visual quality, geometrical accuracy, and tensile properties of PA12.

4.1 Limitations of LISA PRO

As depicted in Chapter 3.2.2, LISA PRO's manufacturer only guarantees high accuracy parts within a certain boundary of the build volume. Depending on the material, this boundary is either 90 x 130 x 230 mm in the case of PA, or 110 x 150 x 245 mm for both TPU and TPE. However, as this severely restricts the usable build volume, testing shall be done concerning the impact of part positioning on dimensional accuracy and visual quality. Testing the dimensional accuracy of the machine will serve to investigate the printer's ability to manufacture specimens that fulfill the strict tolerances required for the ensuing tensile tests.

4.1.1 Methodology

To investigate part manufacturability within different areas of the xy plane, and especially within the red zone, a test case was developed in which a range of test samples was placed in different positions within the build volume. Samples used for this investigation were a generic tolerance test sample with the aim of investigating the manufacturability of small features (see appendix 3), as well as test samples which will later be used for tensile tests done within the scope this thesis, as well as Charpy-impact tests of future theses. Positioning of the test

samples for this test can be seen in Figure 17. It must be noted that all parts seen in Figure 17 were manufactured in the same manufacturing cycle (Figure 17d). However, for the sake of improving visibility, the schematic preview was split into multiple images (Figure 17a-c).

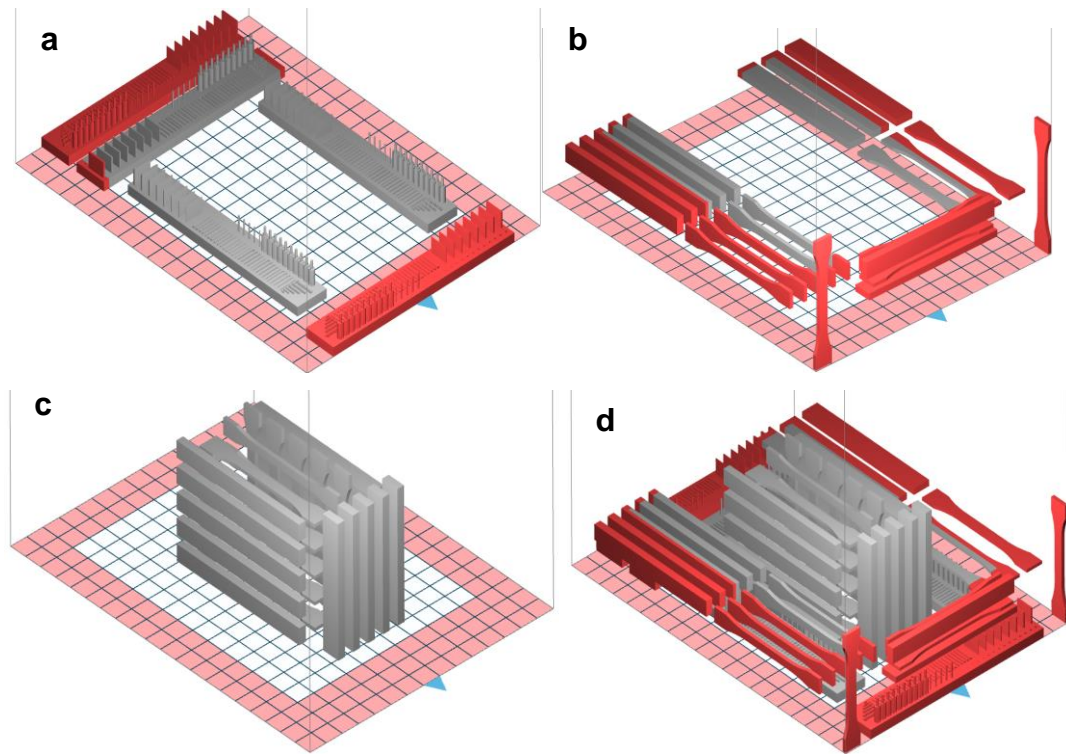


Figure 17. Preview of test sample positioning with (a) tolerance test samples, (b) outer tensile/Charpy-impact test samples, (c) center tensile/Charpy-impact test samples, and total preview (d)

As seen in Figure 17a, two tolerance test samples were intentionally positioned bordering the build volume perimeter walls. Additionally, three more tolerance test samples were placed within the manufacturer's recommended area to allow for a comparison between parts manufactured within the recommended area, and parts manufactured in areas the manufacturer advises against.

To evaluate the manufacturability of dimensionally accurate samples for tensile- and Charpy-impact testing, samples were placed in different orientations and positions near the perimeter walls, as can be seen in Figure 17b. Furthermore, another batch of samples was placed in the center area of the build volume (Figure 17c). This was done to investigate if it is at all possible to manufacture

adequate test samples for the planned material tests using the manufacturer's recommended positioning inside the build chamber of LISA PRO.

The samples were manufactured using PA12 Smooth powder at a layer height of 0.2 mm. PA12 Smooth was chosen for this test due to its more heavily restricted recommended build volume. Therefore, sensitivity of PA12 towards temperature gradients within the build volume should be greater than the sensitivity of Flexa Grey material. The layer height of 0.2 mm was chosen in order to investigate the visibility of layer lines in manufactured parts. This is especially important for investigating the manufacturability of the radii present in tensile test samples. All other machine parameters were left unchanged and on the default setting.

4.1.2 Results and discussion

The machine encountered a crash during the build stage, which led to a forced cancellation of the test. However, even though the test was aborted, the test still produced some results which may be interpreted in order to set guidelines for future testing. The crash most likely occurred at a layer shortly after the tolerance test samples were complete. This can be derived from the fact that all of the tolerance test samples, as well as five tensile, and three Charpy-impact test samples were completed successfully. Since there are no witnesses of the moment the machine crashed, the exact cause of the crash can only be speculated. The manufacturer suggests that the z-axis cross section of a solid model shall be minimized as large cross sections cause an accumulation of heat which results in part curling and warpage (Sinterit 2019, 19). Therefore, the most likely cause of the crash is a part which had warped and got caught on the recoater. This caused the recoater to drag the warped part around the build chamber, ultimately building up a large pile of unsintered or partly sintered powder. Images of the crash can be seen in appendix 4. As the tolerance test samples have the greatest cross section relative to the z-axis, it could be suggested that these were the parts which caused the crash. However, all of the tolerance test samples were completed successfully, which means that the part which caused the crash was one of the tensile or Charpy-impact test samples. Looking at all part orientations, the samples with the largest surface area

perpendicular to the z-axis are the ones with their flat side parallel to the xy-plane, as seen in the samples in the top right of Figure 17b. The manufacturer further suggests that flat and thin surfaces may experience a lot of internal strain and shrinking, causing the model to deform (Sinterit 2019, 19). Therefore, it can be assumed that one of the tensile samples with their thickness of only 2 mm, at a width-to-height-ratio of 5:1, was the one which caused the crash to occur.

As this manufacturing run had to be interrupted due to the recoater crashing, the cooldown of the parts occurred under non-nominal conditions. Therefore, the results of this run will not be judged upon their visual quality or geometrical accuracy. However, using the results of this test, a couple of assumptions for future manufacturing runs and the methodology used in the following investigations can be made. Regarding the tolerance test samples, it can be seen that both samples placed within the recommended perimeter returned the best results (Figure 18).

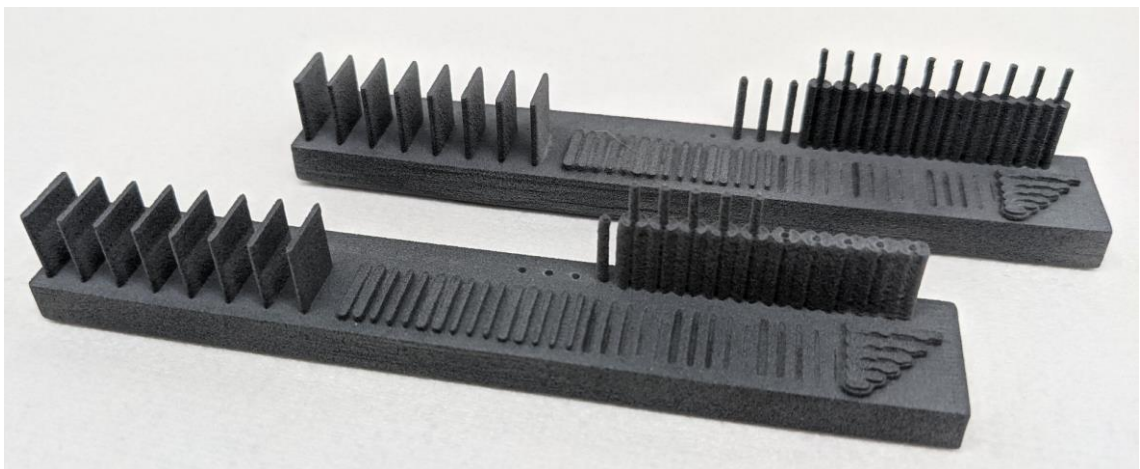


Figure 18. Result of tolerance test samples manufactured within the recommended build perimeter

In contrast to the samples that were placed within the recommended build perimeter, the two tolerance samples placed adjacent to the build perimeter walls experienced severe deformation (Figure 19).

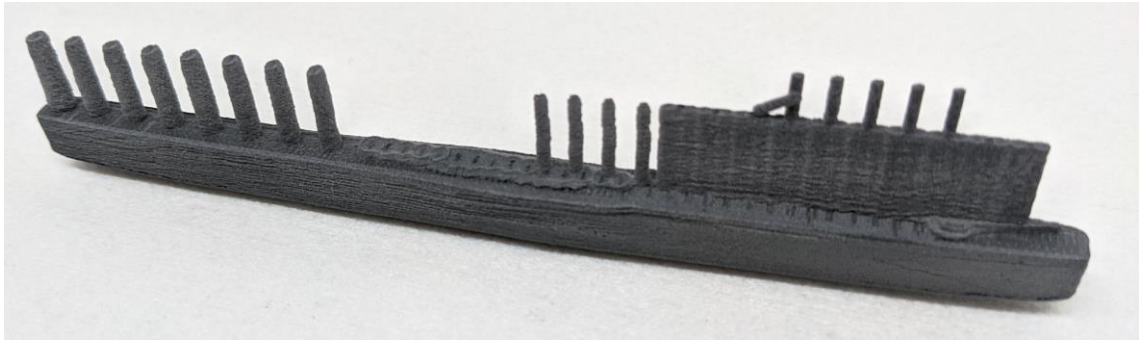


Figure 19. Result of tolerance test sample placed adjacent to the build perimeter walls

As Figure 19 shows, half of the specimen's footprint is missing entirely. Moreover, the features of the missing half were sintered onto the other half of the part, resulting in severe part deformation. The reason for this behaviour is most likely a software issue, as Sinterit Studio allows the user to place parts in these areas of the build volume but alters their geometry during the slicing process without notifying the user, resulting in severe alteration of part geometry.

Concerning the chosen layer-height of 0.2 mm, the tensile specimens manufactured horizontally with its flat side up show clearly visible layer-lines in their upskin surface radii, making this layer-height not suitable for manufacturing test samples that require tight manufacturing tolerances (see Figure 20a).

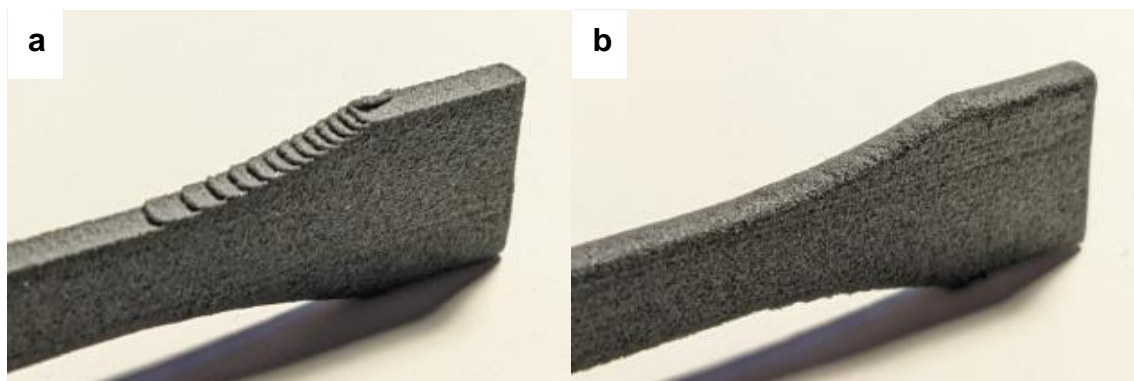


Figure 20. Layer line visibility of horizontally manufactured tensile test specimen showing the upskin (a), and downskin surface (b)

However, these layer lines are only visible on the upskin surface of the specimens. In contrast to that, no visible layer lines can be seen on the downskin surface of the specimens (Figure 20b).

From this preliminary test, the following guidelines can be derived for future testing. On one hand, if placed within 10 mm from the perimeter walls, samples either will not be detected by the software at all, or if detected, experience severe deformation. Additionally, tensile samples, and possibly Charpy-impact samples, run into severe manufacturability issues when orientating their flat side is parallel to the xy-plane. Finally, a layer-height less than 0.2 mm is recommended to decrease layer-line visibility and improve part accuracy.

4.2 Investigation of part quality and material properties

Using the knowledge gained on the limitations of the build volume and the manufacturability model geometries through the earlier test results (Chapter 4.1), an adequate testing methodology for the tensile tests can be drafted. As seen in the earlier results, orienting thin parts perpendicular to the z-axis leads to a high probability of crashing the machine during the build process, ultimately causing the test run to fail. For both time as well as machine availability reasons, crashes and the repeat of manufacturing runs must be prevented wherever possible. Therefore, in order to minimize the chance and severity of an unexpected event, such as a recoater crash, a test specimen layout which is less susceptible to warping will be attempted.

4.2.1 Methodology

As explained earlier, the tensile tests will be carried out in line with the standard for determining the tensile properties of plastics, ISO 527-2. For the ensuing tensile tests, test specimens of Type 1A will be used (Figure 21).

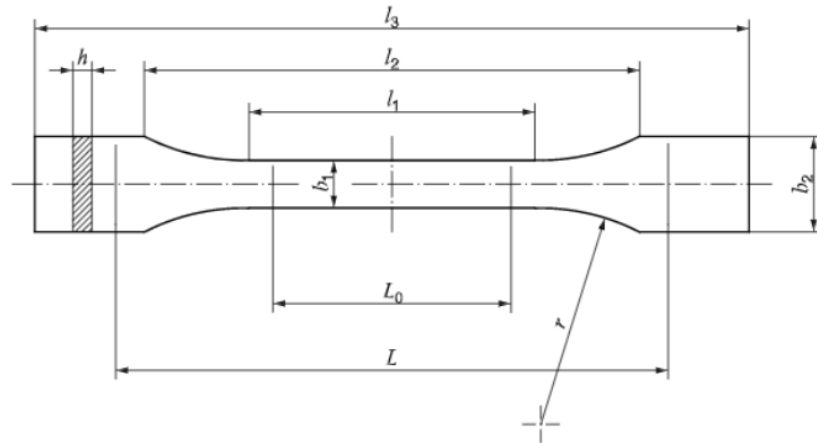


Figure 21. ISO 527-2 tensile test type 1A specimen geometry (Austrian Standards Institute 2012, 4)

The overall length of the tensile specimen (l_3) is 170 mm, the height (b_2) is 20 mm, and the thickness (h) is 4 mm. The narrow part of the specimen is 10 mm wide (b_1). More detailed information on the dimensions of the test specimen can be found in appendix 3.

In order to investigate the influence of the parts positioning within the xy-, and xz-plane, specimens were positioned at a varying distance to the perimeter walls. Both planes were divided using a 5x5 matrix. Using this grid, 25 tensile test specimens were positioned vertically along the xz-plane, with another 25 specimens positioned horizontally along the xy-plane. The layouts and naming schemes used for the test specimens can be seen in Figure 22.

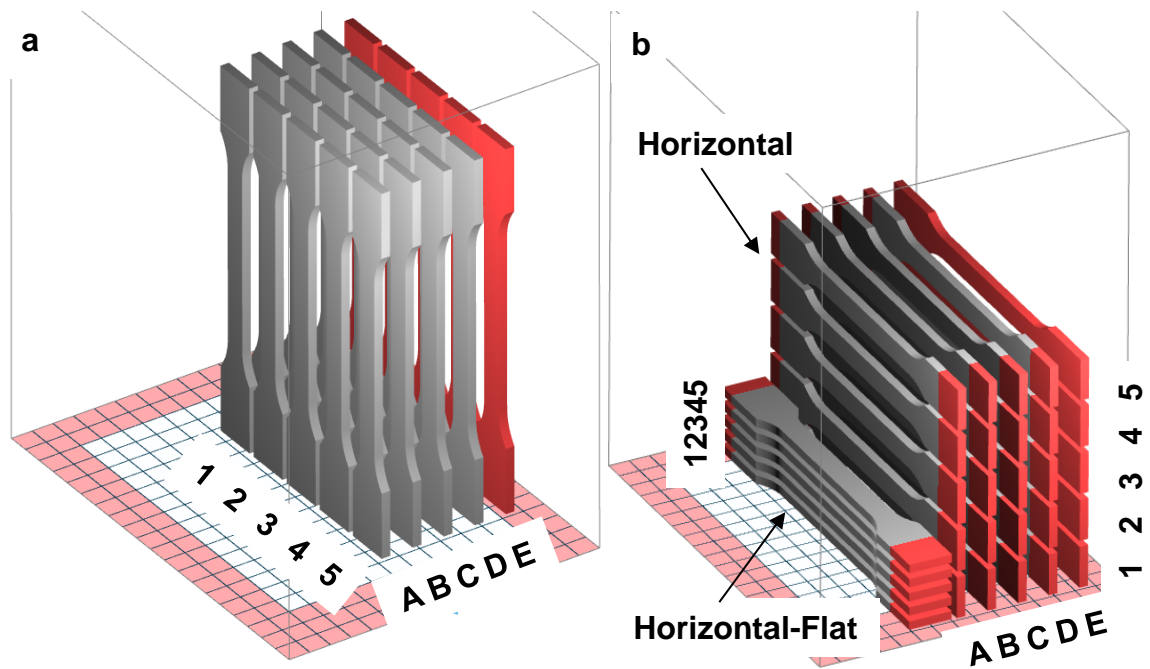


Figure 22. Vertical (a), and horizontal (b) 5x5 tensile specimen matrix, with an additional five horizontal specimens placed flat

The specimen will be named in line with their orientation, as well as position within the build volume. Therefore, a specimen oriented vertically (V), and positioned at the location A1, will be referred to as V-A1. The same naming scheme will be used for horizontal (H), and horizontal flat (HF) specimens. Placing the test specimens in a matrix pattern enables the investigation of the tensile properties in a number of different positions within the xy-, and xz-plane. While this matrix does not cover the entire build volume, this was deemed a good compromise of result resolution versus time and required manufacturing cycles. Moreover, the matrix was planned out in a way where the outermost specimens were placed with a minimum distance of 10 mm to any of the perimeter walls. This should ensure a successful print of all test specimens with no significant anomalies in the machine operation, as well as a reduced chance for severe part deformation, as has been observed during earlier testing. While the specimens in position A were x-axis centered, further specimens (B-E) were positioned at 15 mm increments, relative to the x-axis. Regarding the y-axis position (vertical specimens), and z-axis position (horizontal specimens), the specimens were spaced 3 mm apart from each other, which is the minimum model spacing, as suggested by the manufacturer of LISA PRO. For the ensuing tests, a layer-height of 0.15 mm was chosen. When compared to the previous test, this should

lead to less noticeable layer-lines and therefore result in greater geometrical accuracy. Furthermore, five tensile specimens were printed lying flat in the xz-plane (Figure 22b) to allow for an investigation of the impact of part orientation on the degree of anisotropy in SLS printed parts. The build chamber in both manufacturing cycles was filled with other parts aside from the tensile specimens in order to decrease manufacturing costs and allow for a more efficient use of powder. The documentation of the exact layout used in both prints can be found in appendix 5.

After the manufacturing run was complete, the specimens were taken out of LISA PRO and marked according to their position within the build volume. Post-processing of the specimens was held to a minimum and merely involved removing excess powder using a brush. This was done to preserve the geometry of the specimens, as printed. After that, the specimens went through a visual inspection and the measurements for the ensuing tensile tests were taken. The tensile testing was done using a ZwickRoell Z250 universal testing machine. The specimens were tested at a temperature of 20.8 °C. The test speed was 5 mm/min, and the specimen clamping pressure was 1.5 MPa.

4.2.2 Visual quality and geometrical accuracy

During the manufacturing of the specimens no major issues were encountered and both manufacturing runs were completed successfully. Illustrations of all tested specimens can be found in appendix 6. To begin with, the visual quality and geometrical accuracy of the specimens will be evaluated. While the specimens printed in vertical orientation showed no major defects in their geometry, specimens printed horizontally experienced some sort of part warpage. While the narrow section of the specimens is mostly intact, the ends of the specimens experienced the most noticeable warpage, as can be seen in Figure 23.

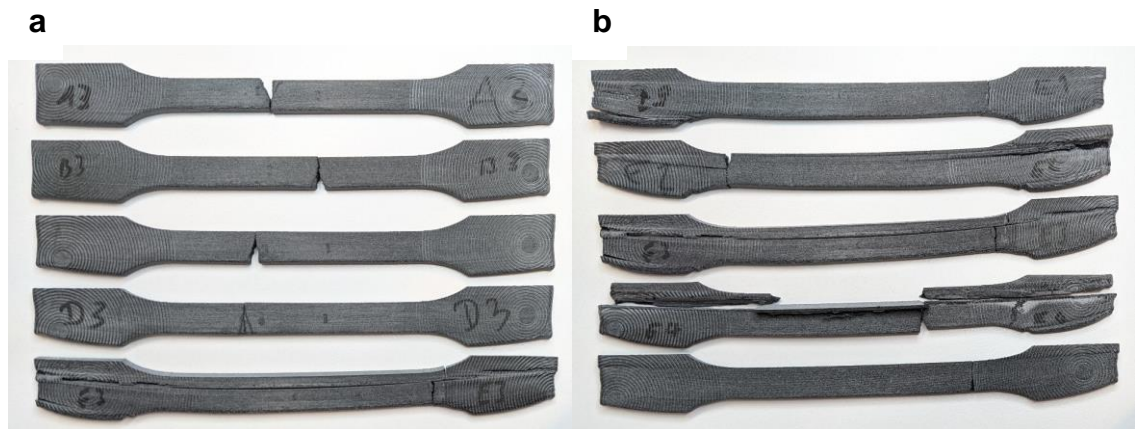


Figure 23. Tensile test specimens H-A3 - H-E3 (a), and H-E1 - H-E5 (b)

As Figure 23a shows, the curling of the ends of the specimens intensifies the closer the specimens were positioned towards the perimeter wall. While the curling seen in sample H-A3 is rather weak, samples H-B3 - H-E3 show more significant curling. Furthermore, unlike specimens H-A3 - H-D3, specimen H-E3 also experienced warpage of its narrow section, which can also be seen in other specimens printed within the same column (H-E1 - H-E5), as can be seen in Figure 23b. Besides significant warping and curling artifacts, specimens H-E1 - H-E5 also experienced layer shifting during the build stage, which caused severe alteration of the sample geometry. These layer shifting artifacts are most noticeable in the specimens H-E3 and H-E4, as these are split along their entire length. The layer shifts were most likely caused by the curled ends of the specimens sticking up from the powder bed and intersecting with the path of the recoater. This caused the recoater to move the specimens slightly, resulting in shifted layers. Due to the severe alteration in the geometry of specimens H-E1 - H-E5, these specimens and their testing results will be excluded from the subsequent comparison study. The horizontal-flat specimens showed slight warping, though not as severe, as those specimens were positioned close to the center of the build volume, analogous to the specimens H-A1 - H-A5. As part warpage is a result of material contracting at varying rates due to temperature gradients, it can be derived that these gradients are more severe towards the edges of the build perimeter. Though, the highest severity was experienced in the corners of the build volume, as part warpage in the corners was so significant that it caused the curled ends of specimens H-E1 - H-E5 to intersect the recoater path.

Besides the aforementioned warping and curling artifacts observed in some of the specimens, the downskin surface consistently showed rounding artifacts throughout all printed specimens, as can be seen in Figure 24a-c. Upskin surfaces show minor curling in the corners, most noticeable in the horizontal-flat specimens (Figure 24b). Most side surfaces were printed with no visible artifacts, although an exception to this rule are the side surfaces on the ends of the horizontal and horizontal-flat specimens, which show slight rounding and a small protrusion on the lower corner.

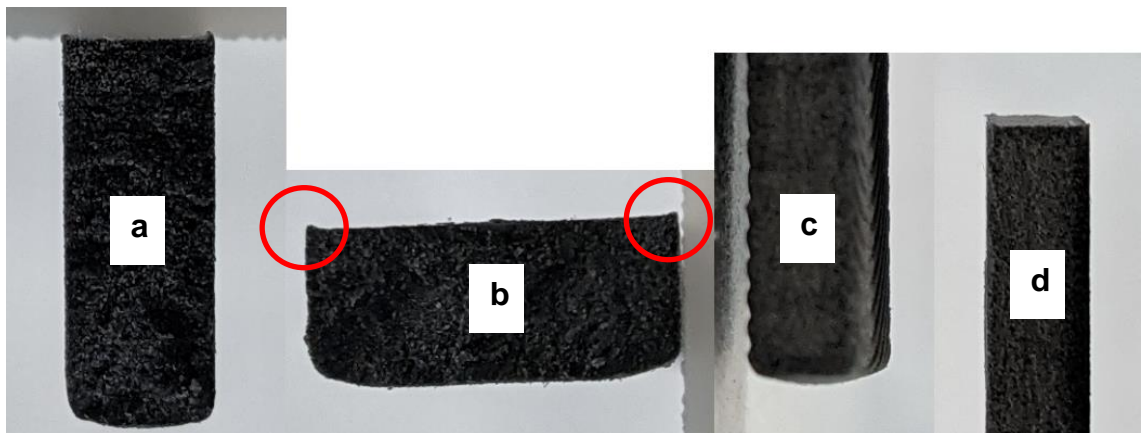


Figure 24. Cross-section view of horizontal (a), and horizontal-flat (b) specimens, as well as side view of vertical specimen, with bottom facing end (c), and top facing end (d)

Since the rounding artifacts mainly occurred on the downskin surfaces, this leads to believe that the cause for the rounding is the first layer of the part being insufficiently supported only by layers of loose powder, which results in slight sagging and rounding of the downskin surface. This suspicion is further supported by the fact that similar rounding and sagging behaviour can also be observed in parts that feature unsupported overhangs. Another possible cause for this behaviour could be the upskin and downskin effect, which is a result of the layer-by-layer nature of SLS manufacturing. This effect causes additional powder layers to adhere to the upskin and downskin surfaces of a part due to transmission of laser powder beyond the sintered layers. This effect is further amplified by the fact that as a result of the chosen layer-height of 0.15 mm, an increased laser power density is required in order to sinter the powder layers. (Benedetti, Brulé, Decreamer, Evans & Ghita 2019, 6.)

The impact of these rounding artifacts can also be seen in the specimen dimensions. As can be seen, depending on the part orientation, a certain degree of part growth can be observed. As seen in Figure 25, when compared to other specimens, the horizontal specimens show a clear increase in average specimen width (Figure 25a), while horizontal-flat specimens show an increase in average specimen thickness (Figure 25b).

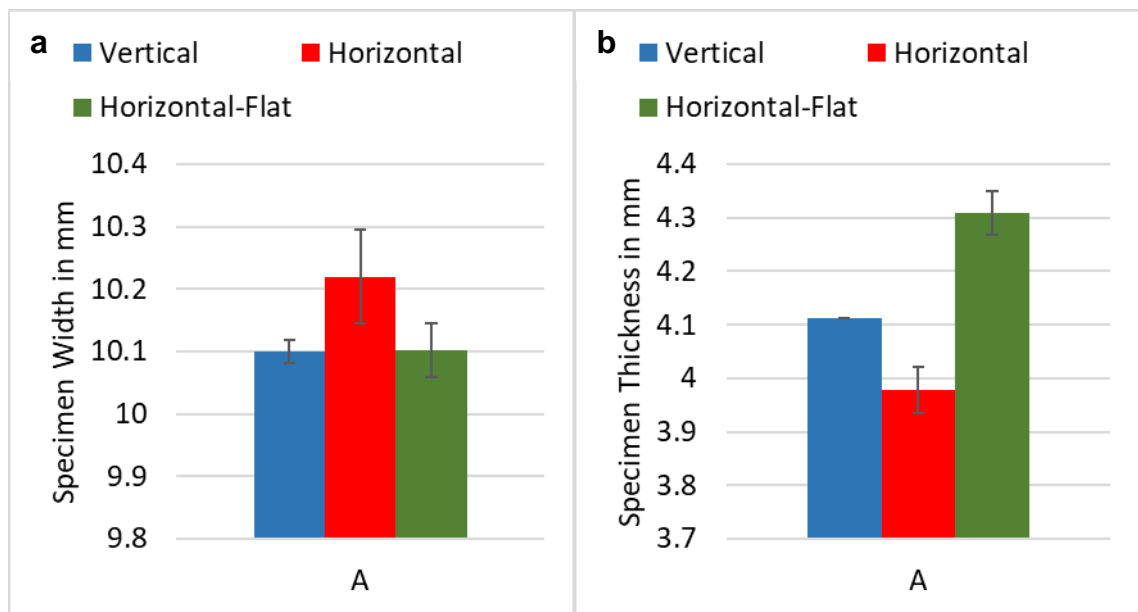


Figure 25. Measured average specimen width (a), and thickness (b) of specimens positioned in column A, by part orientation

This part growth is so severe that it renders all specimens printed in horizontal-flat orientation, as well as a large number of the horizontal specimens invalid for standardized tensile testing according to ISO 527, as the standard depicts a specimen thickness of 4.0 ± 0.2 mm, and a specimen width of 10.0 ± 0.2 mm. Only the specimens printed in vertical orientation fulfill the required tolerances across the board. However, both the rounding and curling artifacts introduce a certain measurement error as the width and thickness measurements were taken using calipers, which are not a high precision measurement tool. Furthermore, calipers are unable to accurately measure the cross-section of a workpiece with slightly rounded surfaces. For this reason, and because the dimension of the specimens which is not affected by the artifacts is consistently within the tolerances depicted by ISO 527, the results of the tensile tests of both the

horizontal, and horizontal-flat test specimens will be used as a basis for comparison but must not be used outside the scope of this thesis.

While one reason for the specimen part growth are the rounding artifacts alluded to earlier, another cause for the dimensional variation may be secondary sintering. This suspicion of secondary sintering is further validated when looking at the cross-sectional part growth seen in the vertical specimens (Figure 26). As the side surfaces of the vertical specimens are not affected by the rounding artifacts seen in horizontal and horizontal-flat specimens, but still show a substantial amount of part growth, secondary sintering can be identified as one of the main causes for the increase in the specimen cross-sectional area. As sintering is a function of both time and temperature, a closer investigation of the influence of specimen positioning on the degree of secondary sintering is necessary.

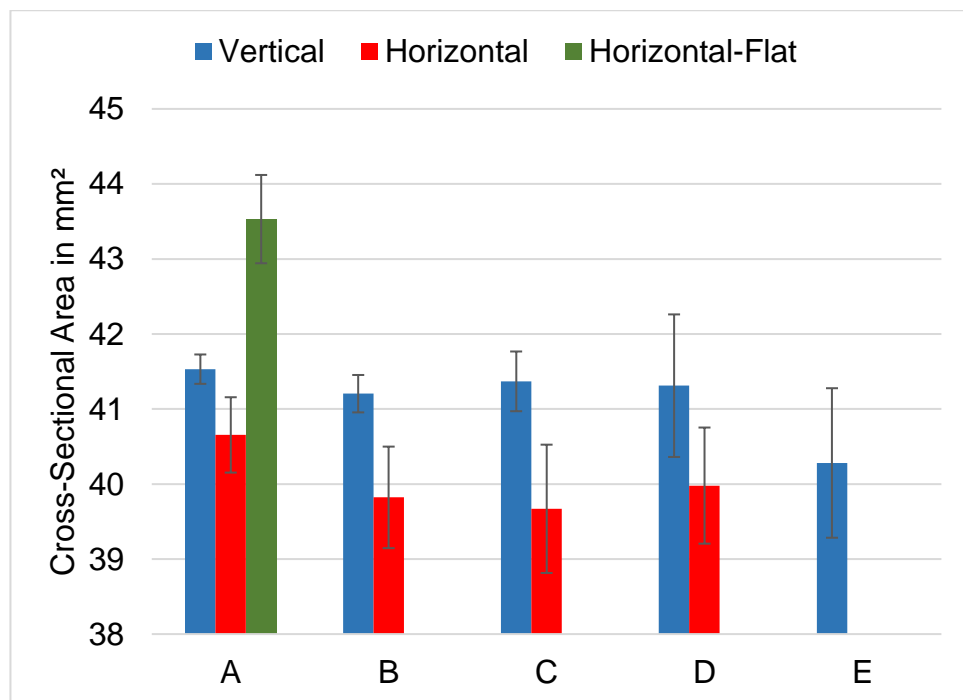


Figure 26. Tensile specimen cross-sectional area

As seen in Figure 26, the average part growth of the vertical specimens is fairly consistent across positions A-D, with a large drop-off in position E. In case of the horizontal specimens, this drop-off already occurs in position B, with positions B-D experiencing a low amount of average growth. However, the results of the

vertical specimens in positions D and E, as well as horizontal specimens in all positions show a substantial amount of deviation in cross-sectional area. Looking at the cross-sectional measurements of specimens V-D1 - VD-5 and V-E2 - V-E5 (appendix 7), it can be seen that the specimens positioned closer to the corners of the build volume experience only minor part growth, or even slight part shrinkage. In contrast to that, parts towards the middle of the build volume experience very noticeable part growth. Further looking at the part growth of the horizontal specimens in relation to their positioning within the build volume (Figure 27a), it can be seen that the most notable part growth can be observed in the bottom row (5), as well as in the top-left corner. A small increase of cross-sectional area can also be observed in specimen D2.

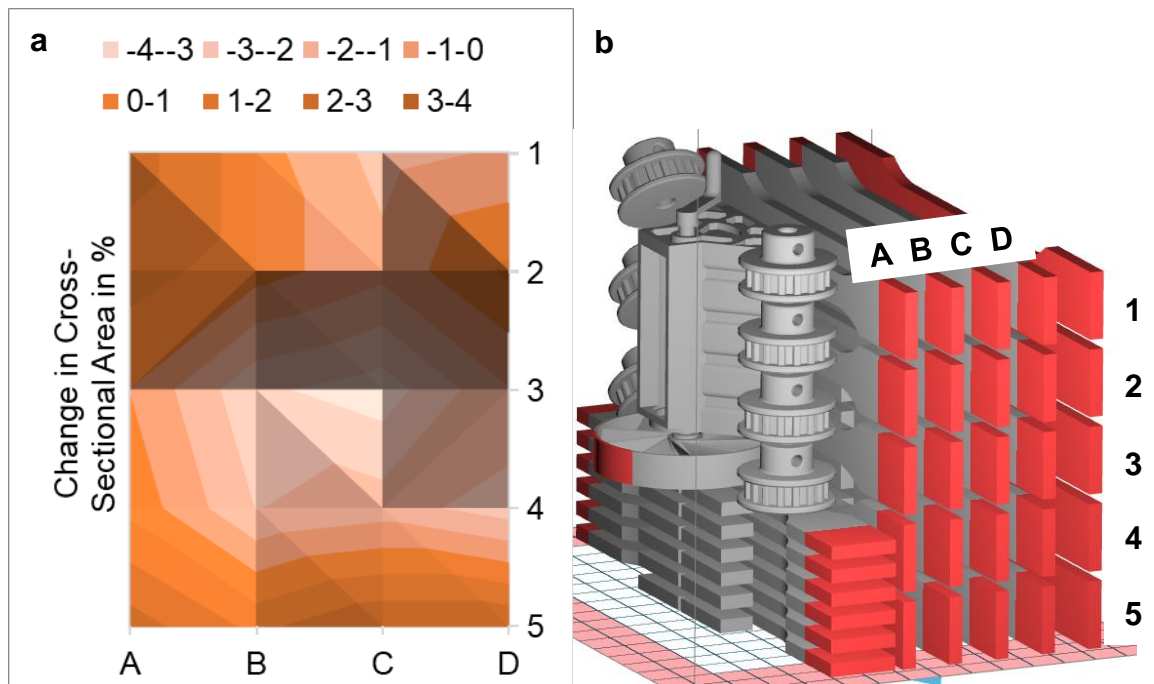


Figure 27. Change in cross-sectional area of horizontal tensile specimens relative to their positioning within the build volume (a), and print layout of the build chamber during horizontal specimen manufacturing (b)

As mentioned earlier, secondary sintering and subsequent part growth occurs in high temperature areas. Therefore, when looking at the print layout which has been used for the manufacturing of the horizontal specimens (Figure 27b), it can be seen that part growth is increasingly noticeable in areas that experience a higher amount of local heating due to higher part densities. Whereas areas of

lower part density experience less severe part growth, i.e., the center and top-right corner of the specimen matrix. Although, in contrast to that, the samples in the bottom row (5) also show substantial part growth of up to 3.5 %, even though the part density, especially around specimens C5 and D5, is comparatively low. A reason for this could be the heating system used in LISA PRO, as the build chamber is heated in different ways. While top-mounted infrared heaters are used to heat the surface of both the feed- and print bed, conductive cylinder and piston heaters are employed to heat the print- and feed beds from the sides and from below. As heat conduction requires a temperature gradient to be present, the outer powder layers must be kept at a higher temperature in order to keep the center of the build volume at the desired temperature. Therefore, the closer a powder layer is to the bottom of the build volume, the higher the temperature, and as a result of that, the more severe the effects of secondary sintering.

To further investigate part growth behaviour inside the build volume, the vertical tensile specimens must also be looked into. Figure 28a shows the relative change in the vertical specimen cross-sectional area along the z-axis.

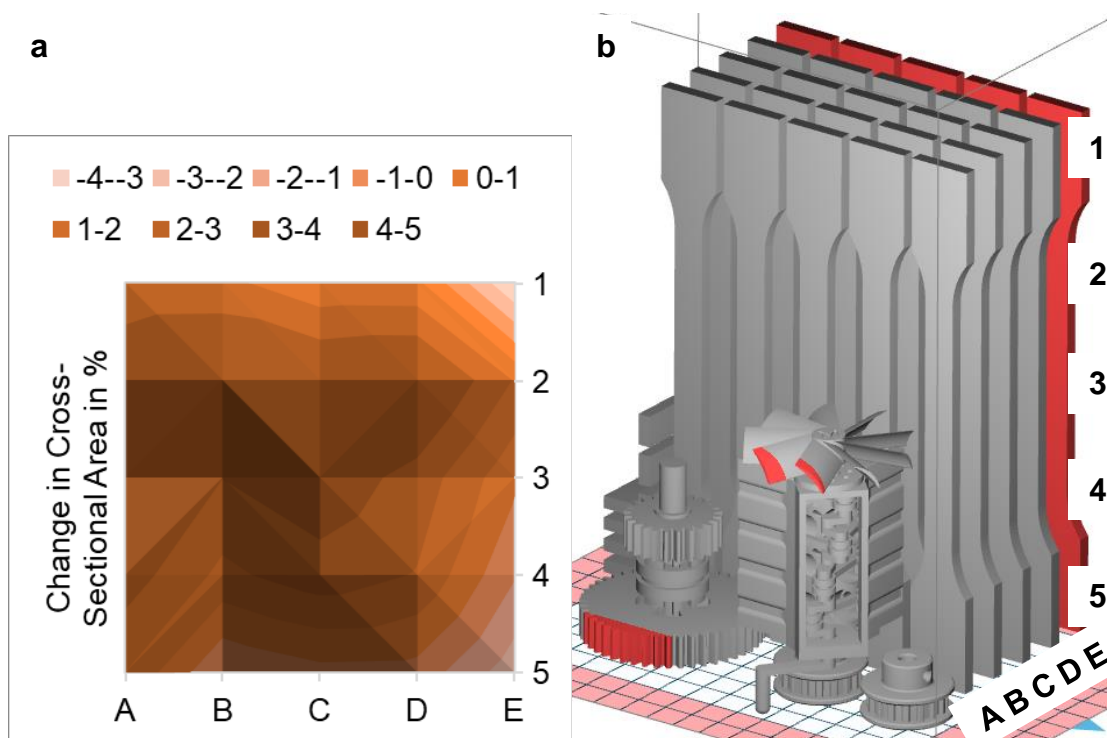


Figure 28. Change in cross-sectional area of vertical tensile specimens relative to z-axis (a), and print layout during vertical specimen manufacturing (b)

As can be seen in Figure 28a, analogous to the horizontal specimens, notable part growth in the range of 2 – 3 % can be observed in the lower layers of the build volume. Although, the secondary sintering effects do not see a reduction in the layers above (row 4) as has been seen in the horizontal specimens. One can also see that there is a sloping gradient in part growth towards the build perimeter border, with some specimens in column E even experiencing slight shrinkage in their cross-sectional area. Interestingly, a steep increase in part growth can be seen in row 2 and 3. This part growth reaches up to 4.5 % in the layers of row 2. Looking at the print layout (Figure 28b), it can be seen that at the point of row 3, foreign models have been completed and only the vertical tensile specimens are left. This means that layer times, which is the time it takes the SLS machine to scan a layer, decreases significantly after this point. The increase in part growth could therefore be reasoned by an elevated local temperature around the specimens due to the reduced cool down interval of the sintered parts in between laser passes. This also explains the reduced part growth in row 5, as layer times increase due to the larger cross-sectional area of the specimens at their end points. A similar behaviour can also be seen in the part growth behaviour of the horizontal specimens (Figure 27a), as layer times start to see a reduction after row 3, resulting in local heat accumulation and amplification of secondary sintering effects. Although, at a maximum of 2.5 %, the part growth in the horizontal specimens is less severe at than the growth of up to 4.5 % seen in the cross-sectional area of the vertical specimens.

4.2.3 Tensile material properties

The tensile tests were able to be completed for all specimens with the exception of specimens V-E1, and H-E1 - H-E4. The specimen V-E1 experienced failure during the clamping procedure, while the specimens H-E1 - H-E4 were unable to be tested, due to severe alteration of specimen geometry as a result of warpage and layer shifts. A detailed list of the tensile test results can be found in appendix 7.

Looking at the stress-strain diagram of specimens V-A3, H-A3, and HF-3 (Figure 29), it can be seen that no matter the specimen orientation, none of the

specimens show a clearly identifiable yield point. Therefore, in order to substitute the yield strength of the material, the offset yield strength at 1 % elongation will be used.

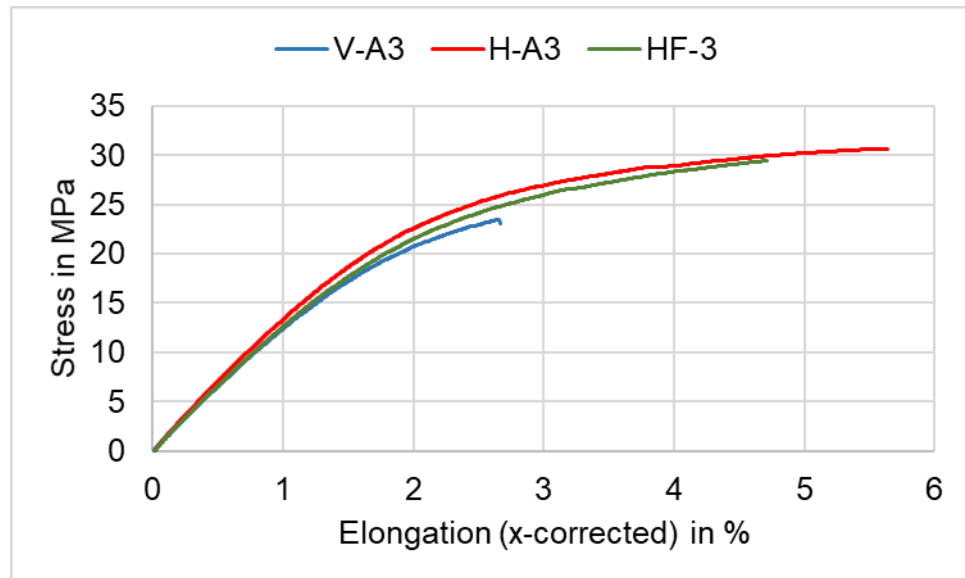


Figure 29. True stress-strain diagram of specimens V-A3, H-A3, and HF-3

As seen in Figure 29, while all specimen orientations show similar behaviour in the elastic region, distinctive differences in the behavior within the plastic region of the stress-strain diagram can be seen. To figure out what the most prominent differences are, the offset yield strength (OYS), ultimate tensile strength (UTS), Young's modulus (YM), and elongation at break (EB) of each specimen orientation, as well as each specimen position within the build volume will be investigated. Starting at the offset yield strength (Figure 30), it can be seen that overall, horizontal specimens performed the best out of all orientations at an average OYS of 15.58 MPa. Both vertical and horizontal-flat specimens showed similar results at 14.49 MPa and 14.06 MPa, respectively. Though, it can be seen that the influence of specimen orientation on the OYS of the specimens is rather weak, as the difference in average OYS does not exceed more than 1.6 MPa between orientations.

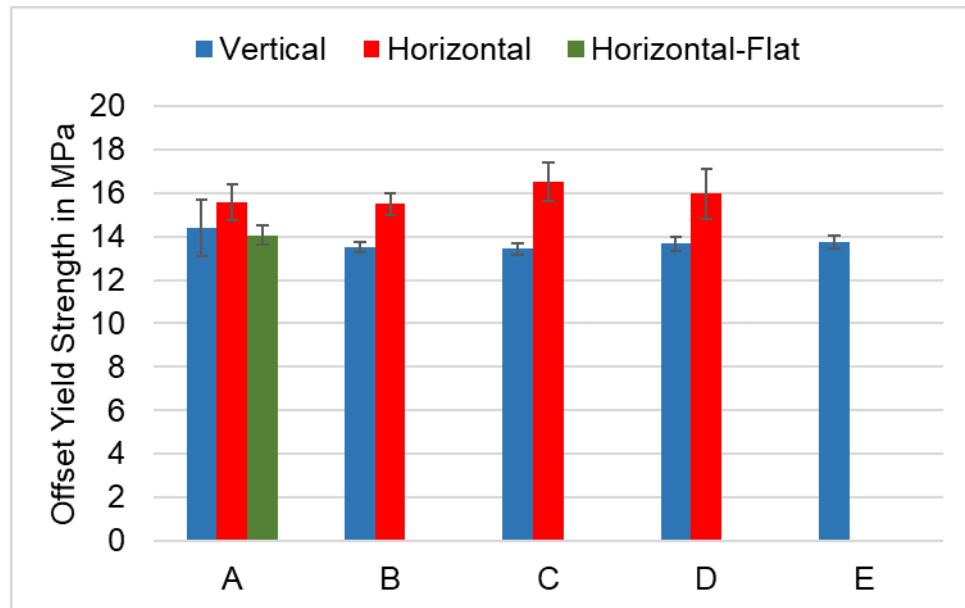


Figure 30. Offset yield strength results of tensile specimens

Moreover, regarding the influence of x-axis positioning, no major difference in the OYS, neither in case of the vertical, nor horizontal specimens can be observed. Merely a small increase in the OYS of the horizontal specimens for specimens positioned in column C can be seen. This small increase, however, results in a more pronounced gap between the OYS of horizontal and vertical specimens around position C and D of 3.1 MPa and 2.3 MPa, respectively. Looking at the vertical specimens in position A, it can be seen that specimen V-A2 performed significantly better than the other vertical specimens in position A at 16.5 MPa. Furthermore, one of the specimens positioned the closest to the perimeter walls, V-A5, shows a significantly lower OYS of 12.5 MPa. However, this anomaly is limited to this side of the print volume, as the opposing specimen, V-A1, does not show tendencies similar to specimen V-A5. Generally, with the exception of position A, vertical specimens show little deviation in their OYS, while horizontal specimens show more noticeable deviation, although not severe enough to justify further investigation.

Moving on to the Young's modulus, the results seen in Figure 31 show similar tendencies like the results of the OYS. Regarding the influence of specimen orientation, a small difference can be observed, again with horizontal specimens performing the best. Though, the YM of horizontal-flat specimens is slightly larger than the YM of the vertical specimens.

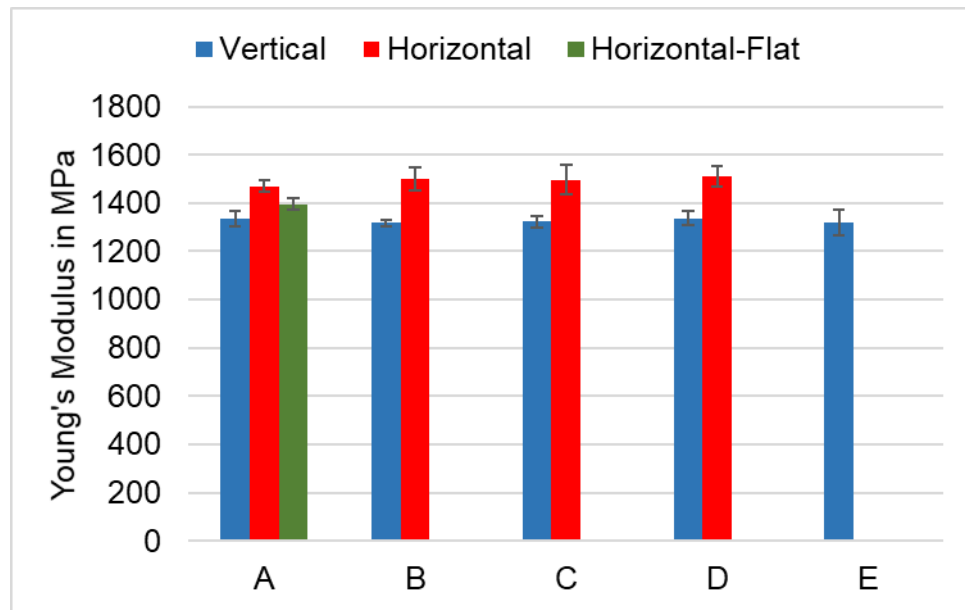


Figure 31. Young's modulus results of tensile specimens

Similar to the behaviour seen in the OYS, the YM of the horizontal specimens also sees a slight increase in specimens positioned further from the center of the build volume. This tendency cannot be seen in the vertical specimens, as these show a very consistent YM across the board with very little deviation.

Measurement results of the ultimate tensile strength are shown in Figure 32. As can be seen, depending on the specimen orientation, a significant difference in UTS can be noted. While horizontal and horizontal-flat specimens performed almost equally at 31.1 MPa and 29.9 MPa, respectively, vertical specimens show a clear deficiency at an UTS of 24.3 MPa. The reason for this behaviour can be reasoned by the more tensile load favorable layer orientation of horizontal and horizontal-flat specimens. Analogous to the OYS, at 29.7 MPa, specimen V-A2 outperformed all other specimens in position A by a significant amount. In addition to that, at 21.0 MPa, specimen V-A5 again clearly underperformed compared to the other specimens in position A. Although, this underperformance again is not mimicked by specimen V-A1.

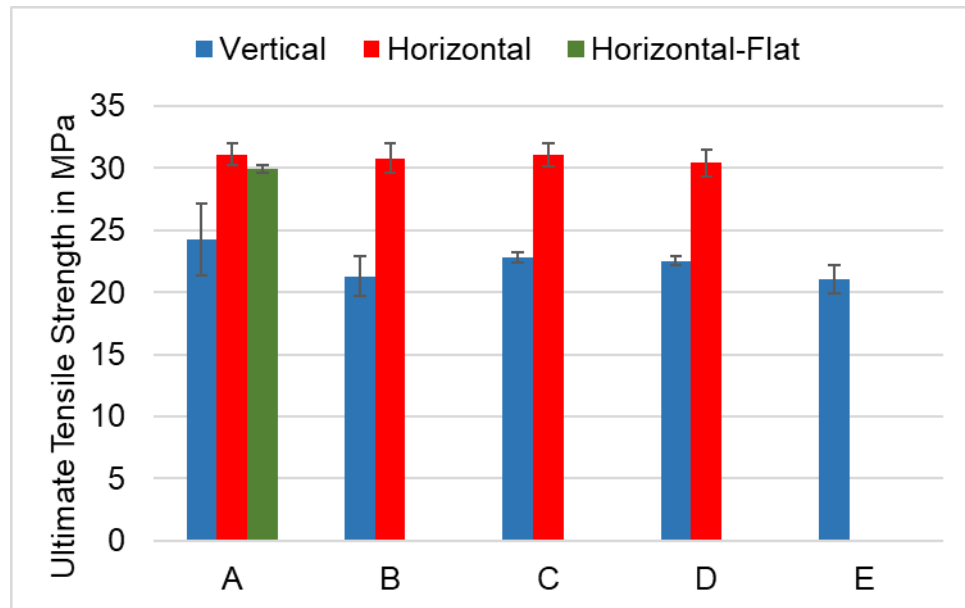


Figure 32. Ultimate tensile strength results of tensile specimens

Concerning the influence of specimen positioning, no considerable change in the UTS of the horizontal specimens can be seen in the test results. Vertical specimens show a remarkable maximum in position A, although other positions show no change in UTS worth investigating further.

At this point, the results of the vertical specimens have shown local maxima for both the OYS, as well as the UTS in specimen V-A2. Moreover, specimen V-A5 has shown local minima for both properties that are not mimicked by the opposing specimen. For that reason, a deeper investigation of the cause for this behaviour is necessary. As vertically oriented specimens show a clear deficiency in UTS compared to the other orientations, it can be assumed that one of the main factors which plays into this behaviour is the layer-based manufacturing used in the SLS process. Therefore, the stronger the interlayer bonding in an SLS part, the closer its UTS will be to a part manufactured in a more advantageous orientation. Research has proven that interlayer bonding and the UTS can be greatly improved by the means of additional heat being applied to specimens during the build stage (Yang, Jiang, Lalier, Bartolone & Chen 2020, 845, 846). Therefore, this leads to believe that the increase in UTS may be a result of local heat accumulation.

Examining the print layout during the manufacturing of the vertical specimens (Figure 28a), it can be seen that there are numerous objects positioned near specimens V-A1 - V-A5. These objects result in increased layer times, where specimens positioned further away from the non-specimen objects have a greater chance to cool down between laser passes than the specimens placed next to non-specimen objects, as these specimens are exposed to more heat conducted from the nearby objects. This local heat buildup was also noted while investigating the secondary sintering effect earlier, as an increase in part growth around the same specimen area was identified, as seen in Figure 28a.

Inspecting the point of failure of specimens V-A1 - V-A5 (Figure 33), it can be seen that specimens V-A1 - V-A4 saw fracture around the middle of the specimen, while V-A5 fractured at the lower end. This is in line with the findings concerning secondary sintering, as the point of failure indicates the weakest point of the specimen, which directly translates into the point with the smallest cross-sectional area. In contrast to specimens V-A1 - V-A5, the point of failure of the remaining vertical specimens is most often located close to the lower end, further confirming the findings of the part growth analysis (appendix 6).

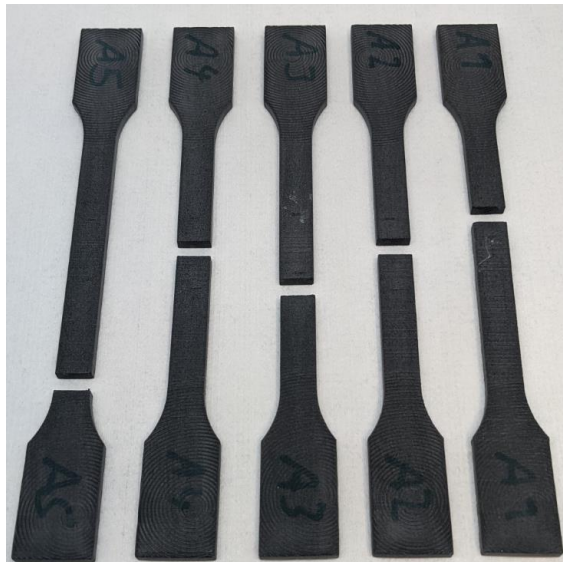


Figure 33. Fractured tensile specimens V-A1 - V-A5

While the point of failure of specimen V-A5 is in line with the cross-sectional area measurements, a higher UTS would be expected due to the specimen being positioned in close proximity to other objects within the build volume. Further

investigation of the cross-sectional area along the z-axis of specimens V-A1 - V-A5 shows specimen V-A5 as having the largest cross-sectional area at the lower specimen end. Therefore, it can be concluded that most local heating occurred in the lower part of the specimen, which is not relevant to improving the UTS of the narrow section. The specimen being positioned in close proximity to the perimeter wall may also have played a role in reducing the amount of local heat build-up.

Moving on to the elongation at break of the specimens, the results of which can be seen in Figure 34.

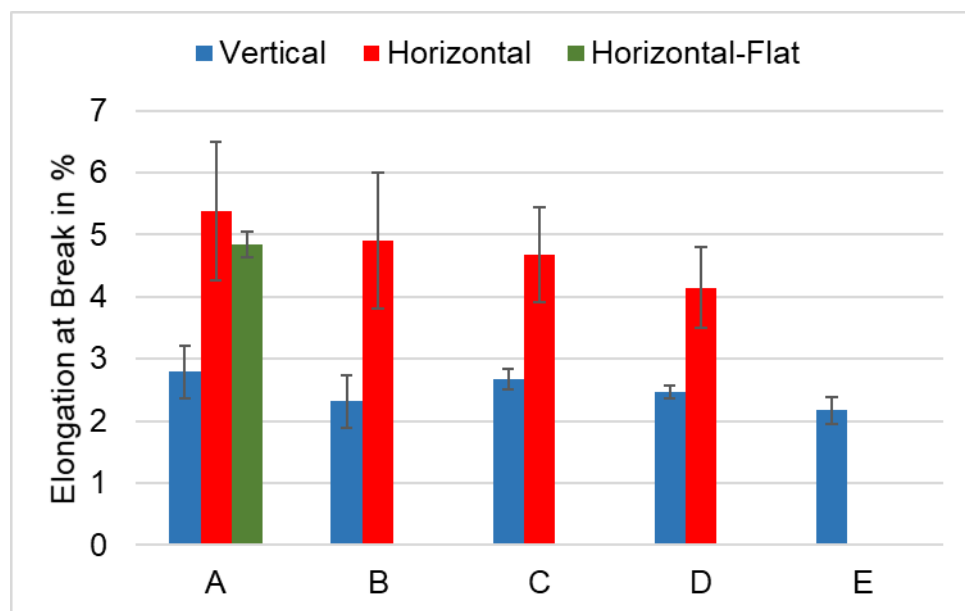


Figure 34. Elongation at break results of tensile specimens

As shown in Figure 34, a significant degree of anisotropy in the orientational behaviour of the material can be seen. While both horizontal and horizontal-flat specimens in position A perform similarly, with an EB of 5.37 % and 4.84 %, respectively, vertical specimens show a significantly reduced EB of 2.79 %. This anisotropy is a result of the layer-by-layer nature of SLS manufacturing. Whereas in horizontal and horizontal-flat specimens, tensile loads are distributed and taken up by a multitude of layers, vertical specimens depend on the strength of their individual interlayer bonds. This can also be seen in the type of fracture, as horizontal and horizontal-flat specimens show ductile fracture behaviour, whereas a typical brittle fracture can be seen in the vertical specimens. As seen

in Figure 35a, specimen H-C3 shows a higher degree of plastic deformation during tensile loading which culminates in a higher EB. This does not apply for specimen V-C3, as it shows very little plastic deformation, resulting in less favourable elongation behaviour due to an increased formation of stress concentrations as a result of micro cracks within the cross-section of the specimens.

Regarding the influence of specimen positioning on the x-axis, one can easily see an almost linear reduction in the amount of EB in horizontal specimens, with the EB of the vertical specimens being less affected. Though, still a slight reduction in the vertical specimens EB can be observed towards the outside perimeter wall. In addition to that, both vertical and horizontal specimens show noticeable deviation in their EB. While the EB of the vertical specimens mainly deviates around positions A and B, horizontal specimens show heavy deviation across the board. Taking a closer look at the individual horizontal specimens, the test results show that there is a strong correlation between the z-axis position of a specimen and its EB. As can be seen in Figure 35b, the further a specimen is positioned towards the top of the build volume, the higher the EB. Furthermore, a slight sloping gradient in the EB towards the edge of the build volume can be seen.

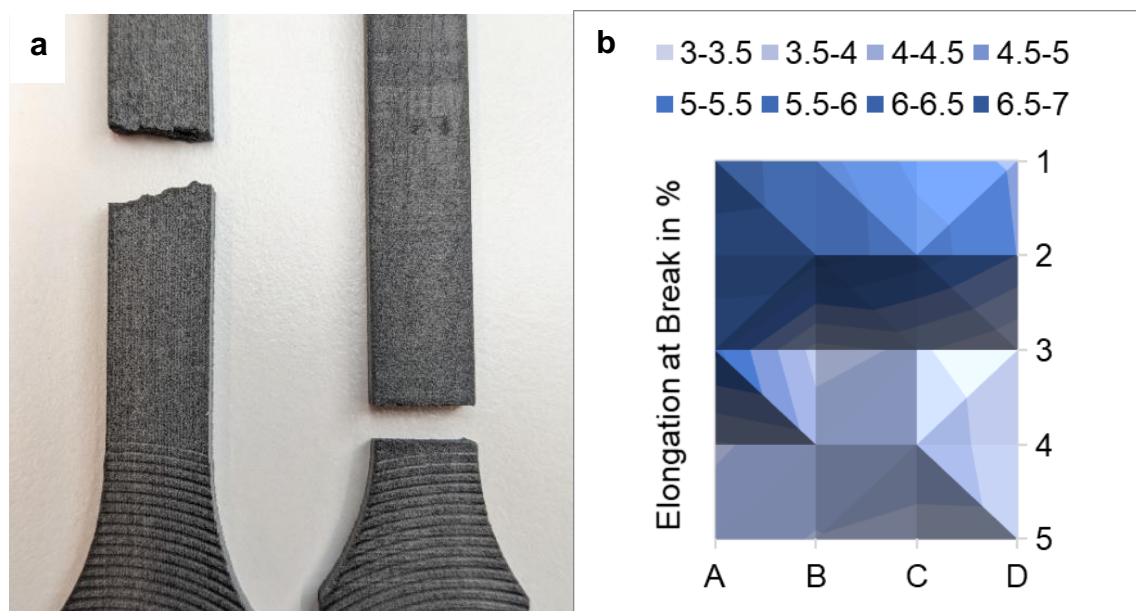


Figure 35. Detail of fracture of tensile specimens H-C3 and V-C3 (a), and elongation at break of horizontal specimens in relation to their position within the xz-plane (b)

While the sideways gradient towards the edge of the build volume is analogous to the gradient seen in the heat-induced secondary sintering effects of the horizontal specimens, the significantly reduced EB of specimens in row 5 does not coincide with these findings. Other works on the subject suggest that parts exposed to higher levels of heat see an increase of EB due to an increase in crystallinity, which in turn allows for a more favourable plastic deformation behaviour, resulting in an increased EB (Yang et al. 2020, 844, 845). However, this would suggest that the specimens of row 5 would not experience such low levels of EB. As this behaviour has been observed at a sample size of one, only a qualitative result may be presented, that is highly susceptible to volatility in the material's behaviour. As Figure 34 shows a substantial amount of result deviation, this suggests that at higher sample sizes results may differ significantly. To present a more quantitative result, further investigation of the positional dependency of the EB is required.

Comparing the test results to the material property claims made by the manufacturer (Table 1), it can be seen that the suggested UTS of 40.1 MPa was unable to be reached by any of the specimens. In fact, the highest average UTS was achieved in the horizontal specimens positioned in the center of the build volume, at 31.1 MPa. At only 77.6 % of the UTS suggested by the manufacturer, this property is significantly lower. The EB shows a similar tendency, as the manufacturer suggests an elongation at break of 13 %, though in the tests carried out within the scope of this thesis, the maximum average EB achieved was 5.37 % in horizontal specimens positioned in column A. Again, the material performed significantly worse at only 41.3 % of the suggested EB. In contrast to that, the YM of all tested samples consistently exceeds the suggestion of 1020.4 MPa. Especially the horizontal specimens with an overall average YM of 1488.2 MPa performed at 146 % of the manufacturer's claim. A possible reason for this behaviour may be found in the powder which has been used to manufacture the test specimens. It is unknown how many times and if the powder has been properly refreshed prior to it being used to manufacture the test specimens. Research on the influence of powder aging on material properties suggests that both the UTS and EB of aged PA12 material starts to noticeably

diminish after a certain number of material reuses as a result of reduced crystallinity. Moreover, the YM of recycled PA12 sees a remarkable increase compared to virgin PA12, for which parallels can be seen in the findings of this thesis. (Wudy & Drummer 2019, 5; Dadbakhsh et al. 2017a, 258.) While the UTS and YM seen in the findings of this thesis are comparable to the findings of other research done on the subject, the EB is significantly lower than the EB seen in the results of comparable research. While there of course is a difference in the exact PA12 blend used to manufacture the specimens, it has been found that even purposely aged PA12 shows a 2.5-times greater EB than the material used for the tests done in this thesis (Dadbakhsh et al. 2017a, 258).

Lastly, a special mention must be given to the results of specimen H-E5, as its OYS and UTS performance is exceptional compared to the other specimens, at 20.85 MPa and 37.23 MPa, respectively. The reason for these kinds of exceptional material properties can only be had by speculating. One reason that comes to mind is inhomogeneous mixing during the powder refresh procedure, resulting in an accumulation of fresh powder in the bottom layer. This fresh powder accumulation may also be one of the reasons for the anomaly observed in the EB behaviour towards the bottom of the build volume (Figure 35b), as research has shown that virgin powder performs worse in EB than recycled powder up to a certain number of reuses (Yang et al. 2020, 844). Although, the only way of achieving affirmation for this kind of behaviour is more extensive testing by the means of a future thesis on the subject.

5 CONCLUSION

In this work, a general understanding of the fundamentals of SLS manufacturing was given. Moreover, a safe and efficient workflow around the novel SLS setup found in the Lapland UAS 3D printing laboratory was established.

Furthermore, the influence of part position within the build volume on visual quality, geometrical accuracy, and material properties of SLS manufactured parts was investigated. On one hand, the results show that high part densities lead to localized part growth due to secondary sintering caused by local hotspots. On the other hand, specimens that experienced said local overheating show a significant improvement of up to 71.9 % in their elongation at break over specimens that did not experience overheating. Regarding build direction, a large distinction in material properties was seen in the ultimate tensile strength and elongation at break of the vertical specimens. Vertical specimens showed about 50 % worse elongation at break, and about 25 % worse ultimate tensile strength compared to horizontal and horizontal-flat specimens. Both horizontal and horizontal-flat specimens showed similar tensile test results.

Additionally, it was shown that there is a clear relationship between increased layer times and secondary sintering effects, as faster layer times reduce the cool down window in between laser passes, which enhances part growth as a result of increased local temperature levels. Increased temperature levels and stronger secondary sintering effects can also be observed in the first layers at the bottom of the build volume, with the print bed heating solution of LISA PRO being identified as a possible cause for said behaviour. It has also been discovered that parts positioned in close proximity to the perimeter walls, especially parts positioned in the corners of the build volume, experience remarkable amounts of part shrinkage.

Furthermore, it was found out that knowledge of the recycling history of the material used to manufacture parts is crucial when trying to optimize the mechanical properties of a part for a specific application, as the material properties of virgin PA12 notably differ from the properties of recycled PA12.

Concerning the capabilities of the LISA PRO SLS printer found in the Lapland UAS 3D printing laboratory, it was shown that the recommendations by the manufacturer concerning the manufacturability of parts depending on their orientation within the build volume are justified. However, investigations of the behaviour of parts placed within the boundary regions of the build volume showed severe alteration of part geometry due to issues related to the proprietary slicing software of LISA PRO, Sinterit Studio.

6 REVIEW AND OUTLOOK

Looking back at the work done within the scope of this thesis, large potential for further investigations of different areas within SLS manufacturing has been revealed. First of all, a substantial part of the findings of this thesis are based on the test results of a single specimen. Therefore, to prove the repeatability of these findings, the testing must be redone with a larger sample size. Moreover, as local overheating due to foreign objects within close proximity to test specimens has been proven to have a significant impact on material properties, the tests shall be repeated without foreign objects. This will help in deepening the understanding of the influence of part positioning on the material properties of parts manufactured using the SLS process. Future work in this area may focus on investigating the change in surface artifacting and part growth behaviour by varying different process parameters, such as layer-height or laser power.

7 LIST OF TABLES

Table 1. Sinterit PA12 Smooth v1 material properties (Sinterit 2021d)	47
Table 2. Vertical tensile specimens V-A1 - V-E5 measurement data.....	96
Table 3. Horizontal tensile specimens H-A1 - H-E5 measurement data	97
Table 4. Horizontal-flat tensile specimens HF-1 - HF-5 measurement data.....	98
Table 5. Vertical specimens V-A1 - V-E5 detailed cross-sectional area measurement data	98

8 LIST OF FIGURES

Figure 1. Overview of powder bed fusion processes (Kumar 2020, 42) (modified)	14
Figure 2. Schematic diagram of the selective laser sintering (SLS) process (Gu, Bashir & Yang 2019, 195)	16
Figure 3. Illustration of hatch spacing, beam diameter, and beam overlap (Kumar 2020, 47)	19
Figure 4. Selective Laser Sintering (SLS) design guidelines (3D Hubs 2021b) (modified)	25
Figure 5. Lapland UAS SLS printing room	30
Figure 6. Front view of the Sinterit LISA PRO (a) and view of the open hatch, revealing the build chamber (b)	31
Figure 7. Left side (a) and right side (b) of the Sinterit LISA PRO featuring: nitrogen quick coupling, power plug, USB-interface, emergency stop button, ignition key, and overflow bin	32
Figure 8. Front view of the Sinterit Powder Sieve (a) and a look inside the sieving chamber (b)	33
Figure 9. Sinterit Sandblaster as seen in the Lapland UAS 3D printing laboratory. Front view (a) and top view with open hatch (b)	34
Figure 10. Sinterit ATEX Vacuum Cleaner and Sinterit Powder Separator	35
Figure 11. SLS workflow schematic	35
Figure 12. Heating module split pin and laser protective glass nuts	39
Figure 13. Powder compacting (a) and desired powder surface after successful powder bed leveling (b)	40
Figure 14. Camera and pyrometer windows	41
Figure 15. Part cake removal using part carriage plates (a) and build chamber cleaning using ATEX vacuum cleaner (b)	42
Figure 16. "FRESH" and "PRINT READY" powder containers (a) and properly inserted powder capture container (b)	44
Figure 17. Preview of test sample positioning with (a) tolerance test samples, (b) outer tensile/Charpy-impact test samples, (c) center tensile/Charpy-impact test samples, and total preview (d)	49

Figure 18. Result of tolerance test samples manufactured within the recommended build perimeter	51
Figure 19. Result of tolerance test sample placed adjacent to the build perimeter walls.....	52
Figure 20. Layer line visibility of horizontally manufactured tensile test specimen showing the upskin (a), and downskin surface (b)	52
Figure 21. ISO 527-2 tensile test type 1A specimen geometry (Austrian Standards Institute 2012, 4)	54
Figure 22. Vertical (a), and horizontal (b) 5x5 tensile specimen matrix, with an additional five horizontal specimens placed flat	55
Figure 23. Tensile test specimens H-A3 - H-E3 (a), and H-E1 - H-E5 (b).....	57
Figure 24. Cross-section view of horizontal (a), and horizontal-flat (b) specimens, as well as side view of vertical specimen, with bottom facing end (c), and top facing end (d)	58
Figure 25. Measured average specimen width (a), and thickness (b) of specimens positioned in column A, by part orientation	59
Figure 26. Tensile specimen cross-sectional area	60
Figure 27. Change in cross-sectional area of horizontal tensile specimens relative to their positioning within the build volume (a), and print layout of the build chamber during horizontal specimen manufacturing (b)	61
Figure 28. Change in cross-sectional area of vertical tensile specimens relative to z-axis (a), and print layout during vertical specimen manufacturing (b)	62
Figure 29. True stress-strain diagram of specimens V-A3, H-A3, and HF-3	64
Figure 30. Offset yield strength results of tensile specimens	65
Figure 31. Young's modulus results of tensile specimens	66
Figure 32. Ultimate tensile strength results of tensile specimens	67
Figure 33. Fractured tensile specimens V-A1 - V-A5	68
Figure 34. Elongation at break results of tensile specimens	69
Figure 35. Detail of fracture of tensile specimens H-C3 and V-C3 (a), and elongation at break of horizontal specimens in relation to their position within the xz-plane (b)	70
Figure 36. Overview of commercially available additive manufacturing technologies (3D Hubs 2021a).....	84
Figure 37. Sinterit Studio: Preset tab	85

Figure 38. Sinterit Studio: Models tab	85
Figure 39. Sinterit Studio: Slice tab.....	86
Figure 40. Sinterit Studio: Preview tab.....	86
Figure 41. Sinterit Studio: Printers tab	87
Figure 42. Tensile test specimen Type 1A geometry and dimensions (Austrian Standards Institute 2012, 4, 5).....	88
Figure 43. Drawing of tolerance test sample.....	89
Figure 44. Recoater crash	90
Figure 45. Recoater crash, detail shot of the build volume	90
Figure 46. Recoater crash, detail shot of the recoater	91
Figure 47. Isometric view of print layout of horizontal and horizontal-flat specimens manufacturing	92
Figure 48. Top view of print layout of horizontal and horizontal-flat specimens manufacturing	92
Figure 49. Isometric view of print layout of vertical specimens manufacturing..	93
Figure 50. Top view of print layout of vertical specimens manufacturing	93
Figure 51. Illustration of fractured vertical tensile specimens V-A1 - V-E5.....	94
Figure 52. Illustration of fractured horizontal tensile specimens H-A1 – H-E5 and horizontal-flat tensile specimens HF-1 - HF-5.....	95

9 BIBLIOGRAPHY

3D Hubs 2021a. Additive manufacturing technologies: An overview. 3D Hubs. Accessed 3 February 2021 <https://www.3dhubs.com/knowledge-base/additive-manufacturing-technologies-overview/>.

3D Hubs 2021b. Key design considerations for 3D printing. 3D Hubs. Accessed 5 February 2021 <https://www.3dhubs.com/knowledge-base/key-design-considerations-3d-printing/>.

3D Systems 2021. Selective Laser Sintering. 3D Systems. Accessed 5 February 2021 <https://www.3dsystems.com/resources/information-guides/selective-laser-sintering/sls>.

Amado Becker, A.F. 2016. Characterization and prediction of SLS processability of polymer powders with respect to powder flow and part warpage

Austrian Standards Institute 2012. ÖNORM EN ISO 527-2:2012 05 15: Plastics - Determination of tensile properties - Part 2: Test conditions for moulding and extrusion plastics (ISO 527-2:2012).

Benedetti, L., Brulé, B., Decreamer, N., Evans, K.E. & Ghita, O. 2019. Shrinkage behaviour of semi-crystalline polymers in laser sintering: PEKK and PA12. *Materials & Design* Vol. 181, 107906.

Dadbakhsh, S., Verbelen, L., Verkinderen, O., Strobbe, D., Van Puyvelde, P. & Kruth, J.-P. 2017. Effect of PA12 powder reuse on coalescence behaviour and microstructure of SLS parts. *European Polymer Journal* Vol. 92, 250–262.

Diegel, O., Nordin, A. & Motte, D. 2019. *A Practical Guide to Design for Additive Manufacturing*. Singapore: Springer Singapore.

EOS GmbH 2021. Plastic 3D Printing Materials | EOS GmbH. . Accessed 5 February 2021 <https://www.eos.info/en/additive-manufacturing/3d-printing-plastic/sls-polymer-materials>.

European Committee for Standardization 2017. *Additive manufacturing - General principles - Terminology (ISO/ASTM 52900:2015)*.

European Parliament & Council of the European Union 2014. Directive 2014/34/EU of the European Parliament and of the Council of 26 February 2014 on the harmonisation of the laws of the Member States relating to equipment and protective systems intended for use in potentially explosive atmospheres (recast)Text with EEA relevance. , 48.

Formlabs 2021. Fuse 1: Benchtop Selective Laser Sintering (SLS) 3D Printer. Formlabs. Accessed 6 May 2021 <https://formlabs.com/eu/3d-printers/fuse-1/>.

Gibson, I., Rosen, D., Stucker, B. & Khorasani, M. 2021. *Additive Manufacturing Technologies*. Cham: Springer International Publishing.

Gu, H., Bashir, Z. & Yang, L. 2019. The re-usability of heat-exposed poly (ethylene terephthalate) powder for laser sintering. Additive Manufacturing Vol. 28, 194–204.

Kumar, S. 2020. Additive Manufacturing Processes. Cham: Springer International Publishing.

Pazhamannil, R.V. 2021. Current state and future scope of additive manufacturing technologies via vat photopolymerization. Materials Today, 7.

Sinterit 2021a. ATEX Vacuum Cleaner - Sinterit - Manufacturer of high quality desktop SLS 3D printers. Sinterit. Accessed 10 February 2021 <https://www.sinterit.com/atex-vacuum-cleaner/>.

Sinterit 2021b. Lisa Pro SLS 3D Printer - Sinterit - Manufacturer of high quality desktop SLS 3D printers. Sinterit. Accessed 10 February 2021 <https://www.sinterit.com/sinterit-lisa-pro/>.

Sinterit 2021c. PA11 Onyx - Sinterit - Manufacturer of high quality desktop SLS 3D printers. Sinterit. Accessed 9 February 2021 <https://www.sinterit.com/pa11-onyx/>.

Sinterit 2021d. PA12_SMOOTH. Accessed 8 February 2021 https://www.sinterit.com/wp-content/uploads/2014/05/PA12_SMOOTH.pdf.

Sinterit 2021e. Powder Sieve - Sinterit - Manufacturer of high quality desktop SLS 3D printers. Sinterit. Accessed 10 February 2021 <https://www.sinterit.com/powder-sieve/>.

Sinterit 2021f. Powders - Sinterit - Manufacturer of high quality desktop SLS 3D printers. Sinterit. Accessed 5 February 2021 <https://www.sinterit.com/powders/>.

Sinterit 2021g. POWDER-SIEVE_Specification. Accessed 10 February 2021 https://www.sinterit.com/wp-content/uploads/2020/05/POWDER-SIEVE_Specification.pdf.

Sinterit 2021h. Safety Data Sheet PA12 SMOOTH. Accessed 8 February 2021 https://www.sinterit.com/wp-content/uploads/2019/03/MSDS_PA12-SMOOTH.pdf.

Sinterit 2021j. Sinterit LISA PRO Product specification.

Sinterit 2021i. Sinterit SANDBLASTER. Accessed 10 February 2021 <https://www.sinterit.com/wp-content/uploads/2014/05/SANDBLASTER.pdf>.

Sinterit 2021k. Sinterit-Atex-Vacuum-cleaner-SPECIFICATION. Accessed 10 February 2021 <https://www.sinterit.com/wp-content/uploads/2020/04/Sinterit-Atex-Vacuum-cleaner-SPECIFICATION.pdf>.

Sinterit 2021l. Sinterit-Powders_Specification-Flexa-Grey. Accessed 16 February 2021 https://www.sinterit.com/wp-content/uploads/2020/12/Sinterit-Powders_Specification-Flexa-Grey.pdf.

Sinterit 2019. sinterit_studio_2019_manual. Accessed 28 January 2021 http://www.novabeans.com/sinterit/downloads/manuals/sinterit_studio_2019_manual.pdf.

Sintratec 2021. Sintratec Kit. Sintratec AG. Accessed 6 May 2021 <https://sintratec.com/product/sintratec-kit/>.

Soldner, D., Greiner, S., Burkhardt, C., Drummer, D., Steinmann, P. & Mergheim, J. 2021. Numerical and experimental investigation of the isothermal assumption in selective laser sintering of PA12. *Additive Manufacturing* Vol. 37, 101676.

Wudy, K. & Drummer, D. 2019. Aging effects of polyamide 12 in selective laser sintering: Molecular weight distribution and thermal properties. *Additive Manufacturing* Vol. 25, 1–9.

Yang, F., Jiang, T., Lalier, G., Bartolone, J. & Chen, X. 2020. A process control and interlayer heating approach to reuse polyamide 12 powders and create parts with improved mechanical properties in selective laser sintering. *Journal of Manufacturing Processes* Vol. 57, 828–846.

Zhao, M., Wudy, K. & Dietmar, D. 2018. Crystallization Kinetics of Polyamide 12 during Selective Laser Sintering. *Polymers* Vol. 10 No 2, 168.

APPENDICES

- Appendix 1. Overview of additive manufacturing processes
- Appendix 2. Sinterit Studio Tabs
- Appendix 3. Tensile-, and tolerance test specimen geometry
- Appendix 4. Sinterit LISA PRO recoater crash visuals
- Appendix 5. Print layout during tensile specimens manufacturing
- Appendix 6. Illustrations of fractured tensile specimens
- Appendix 7. Tensile specimens measurement data

Appendix 1.1(1) - Overview of additive manufacturing processes

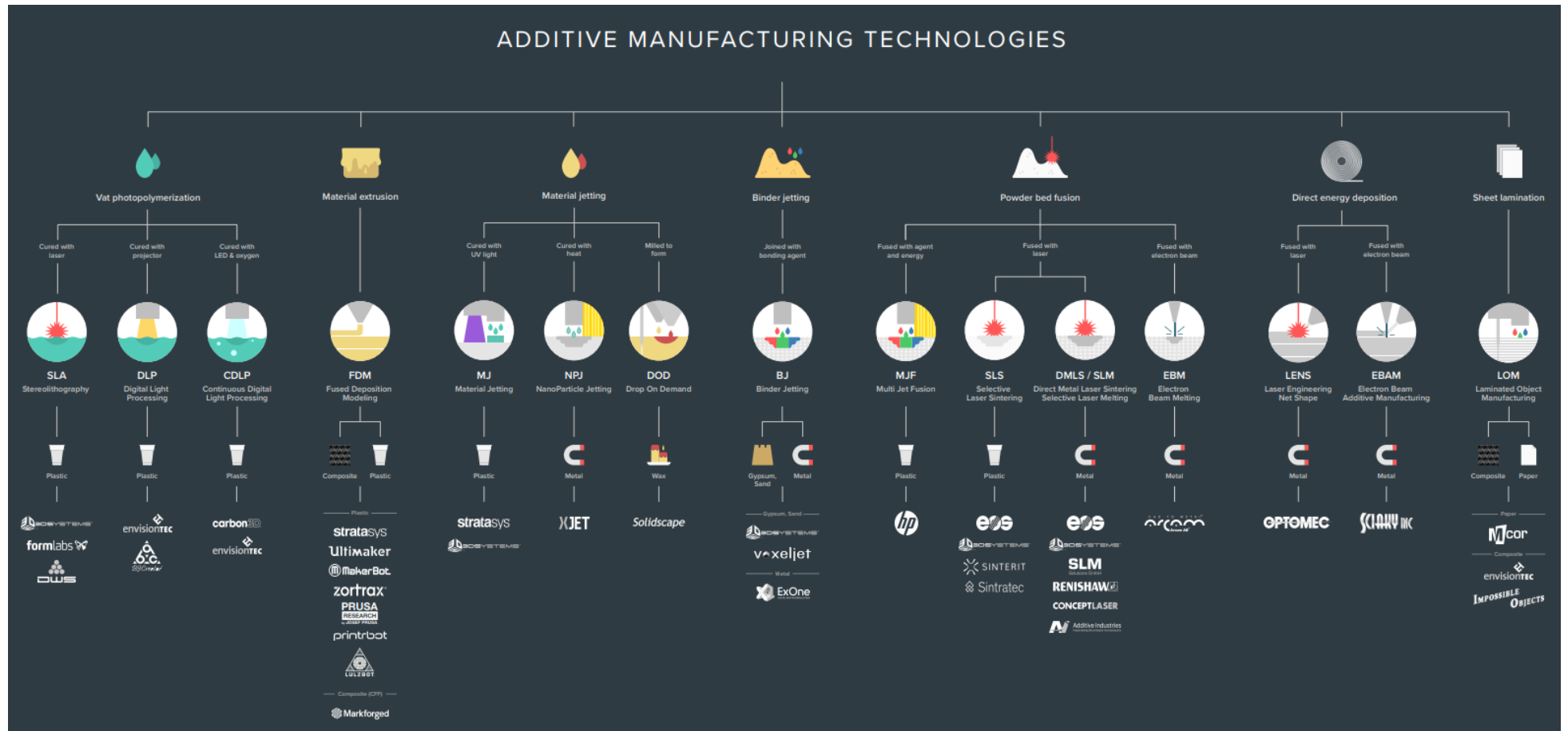


Figure 36. Overview of commercially available additive manufacturing technologies (3D Hubs 2021a)

Appendix 2. 1(3) - Sinterit Studio Tabs

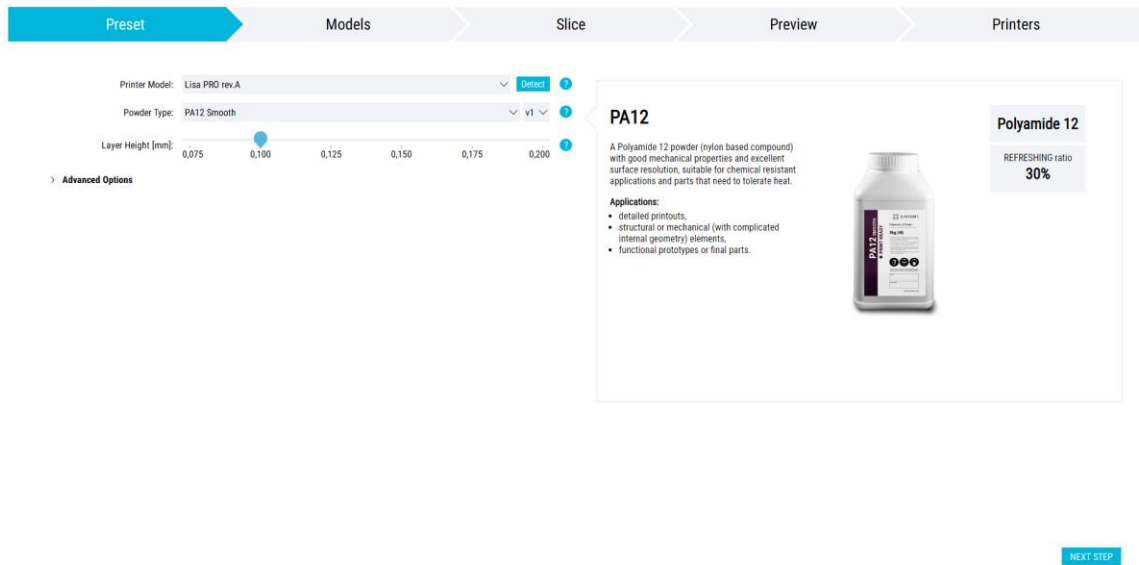


Figure 37. Sinterit Studio: Preset tab

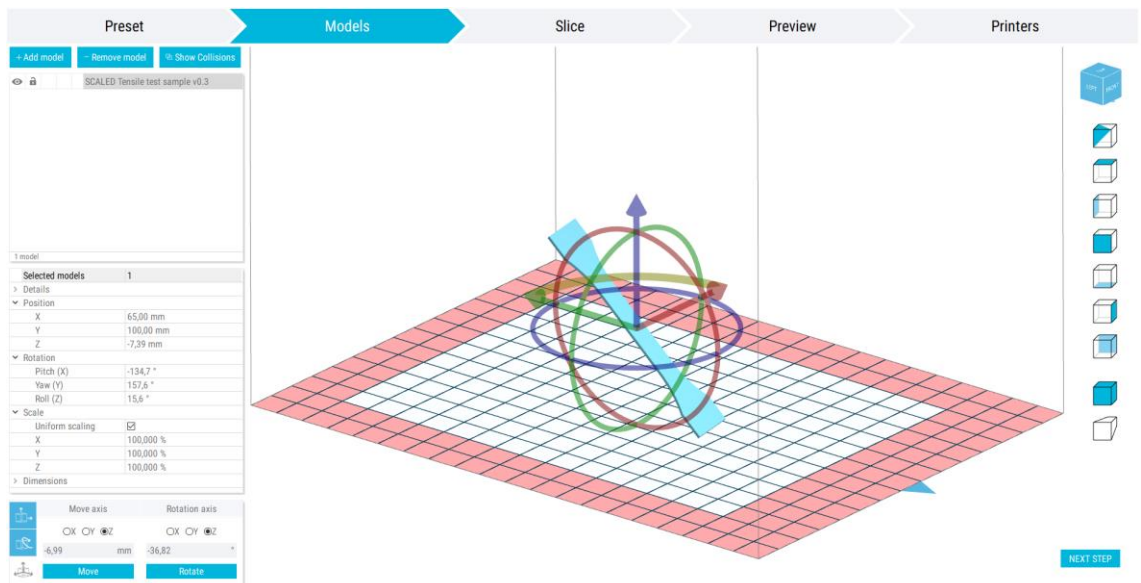


Figure 38. Sinterit Studio: Models tab

Appendix 2.2(3) - Sinterit Studio Tabs

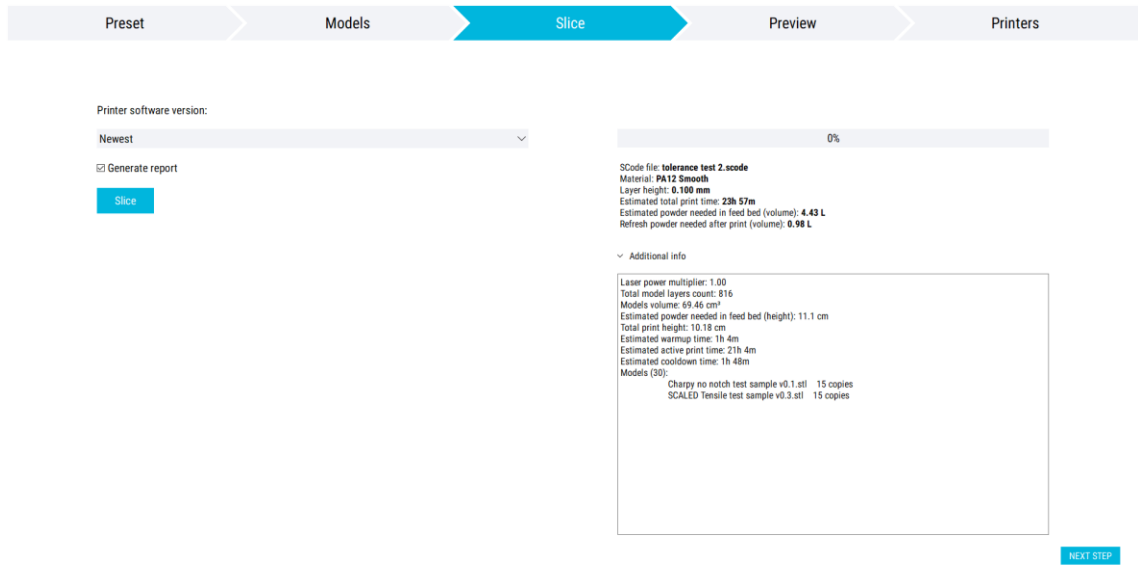


Figure 39. Sinterit Studio: Slice tab

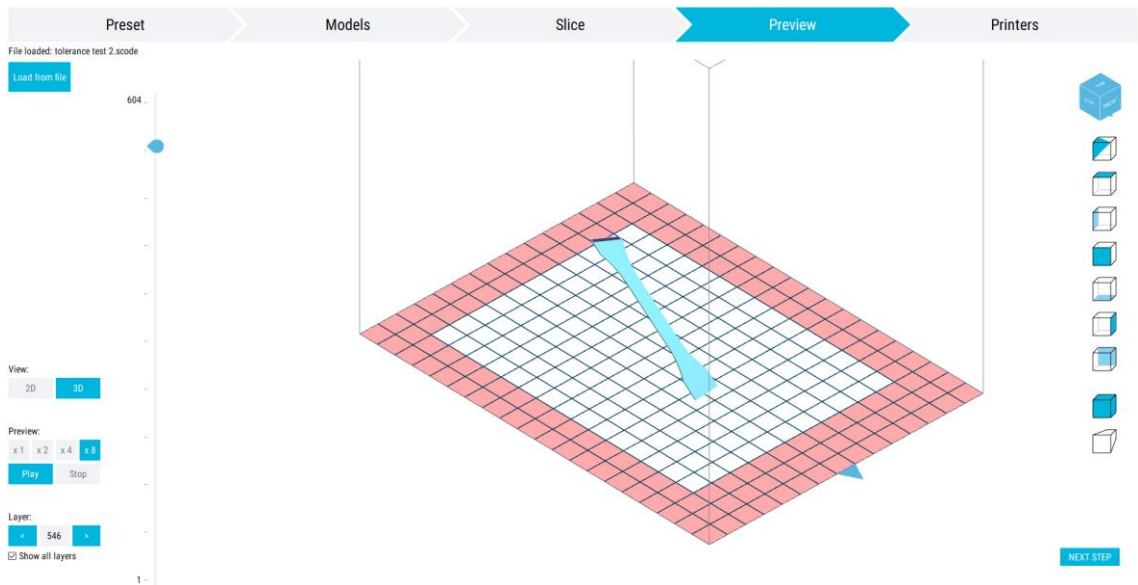


Figure 40. Sinterit Studio: Preview tab

Appendix 2. 3(3) - Sinterit Studio Tabs

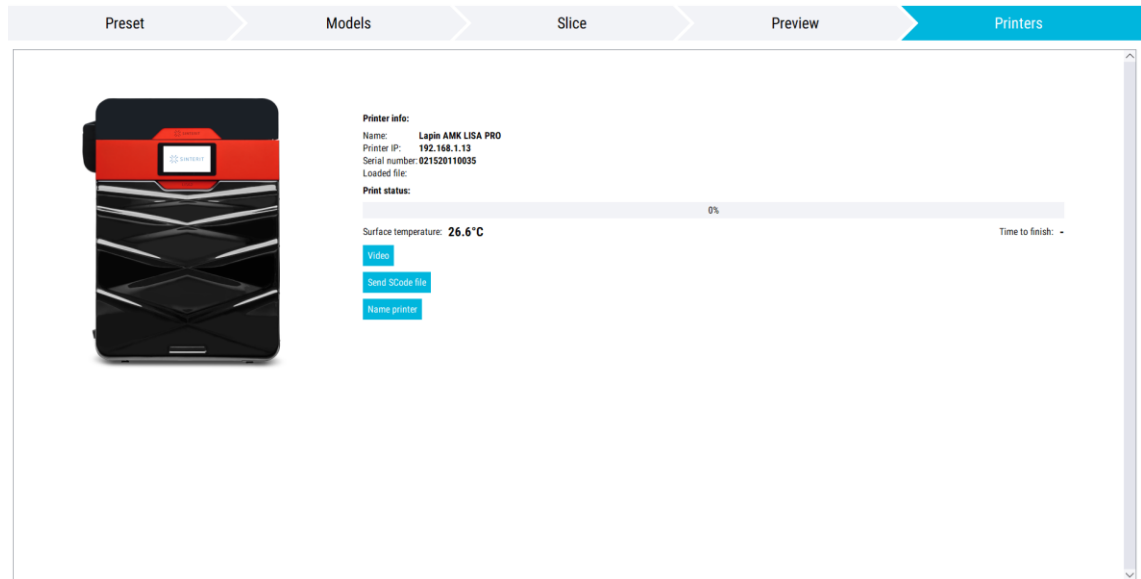


Figure 41. Sinterit Studio: Printers tab

Appendix 3. 1(2) - Tensile-, and tolerance test specimen geometry

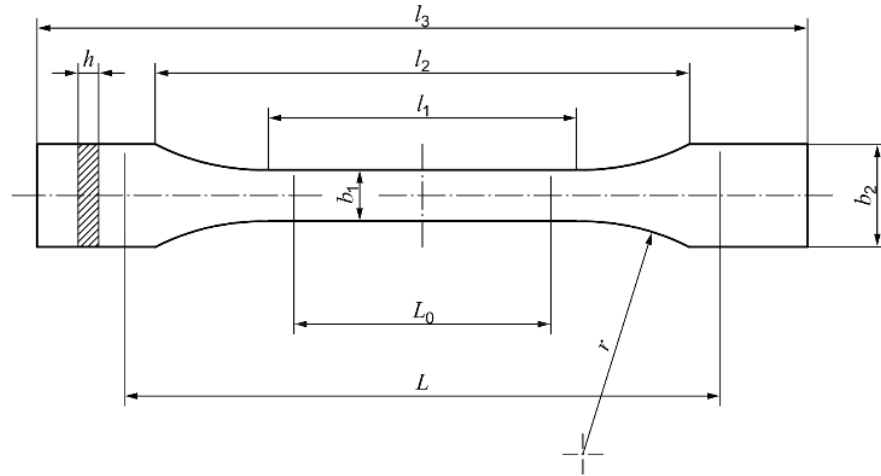


Figure 1 — Type 1A and 1B test specimens

Table 1 — Dimensions of type 1A and 1B test specimens

Dimensions in millimetres

	Specimen type	1A	1B
l_3	Overall length ^a	170	≥150
l_1	Length of narrow parallel-sided portion	80 ± 2	60,0 ± 0,5
r	Radius	24 ± 1	60 ± 0,5
l_2	Distance between broad parallel-sided portions ^b	109,3 ± 3,2	108 ± 1,6
b_2	Width at ends	20,0 ± 0,2	
b_1	Width at narrow portion	10,0 ± 0,2	
h	Preferred thickness	4,0 ± 0,2	
L_0	Gauge length (preferred)	75,0 ± 0,5	50,0 ± 0,5
	Gauge length (acceptable if required for quality control or when specified)	50,0 ± 0,5	
L	Initial distance between grips	115 ± 1	115 ± 1

^a The recommended overall length of 170 mm of the type 1A is consistent with ISO 294-1 and ISO 10724-1. For some materials, the length of the tabs may need to be extended (e.g. $l_3 = 200$ mm) to prevent breakage or slippage in the jaws of the testing machine.

^b $l_2 = l_1 + [4r(b_2 - b_1) - (b_2 - b_1)^2]^{1/2}$, resulting from l_1 , r , b_1 and b_2 , but within the indicated tolerances.

Figure 42. Tensile test specimen Type 1A geometry and dimensions (Austrian Standards Institute 2012, 4, 5)

Appendix 3. 2(2) - Tensile-, and tolerance test specimen geometry

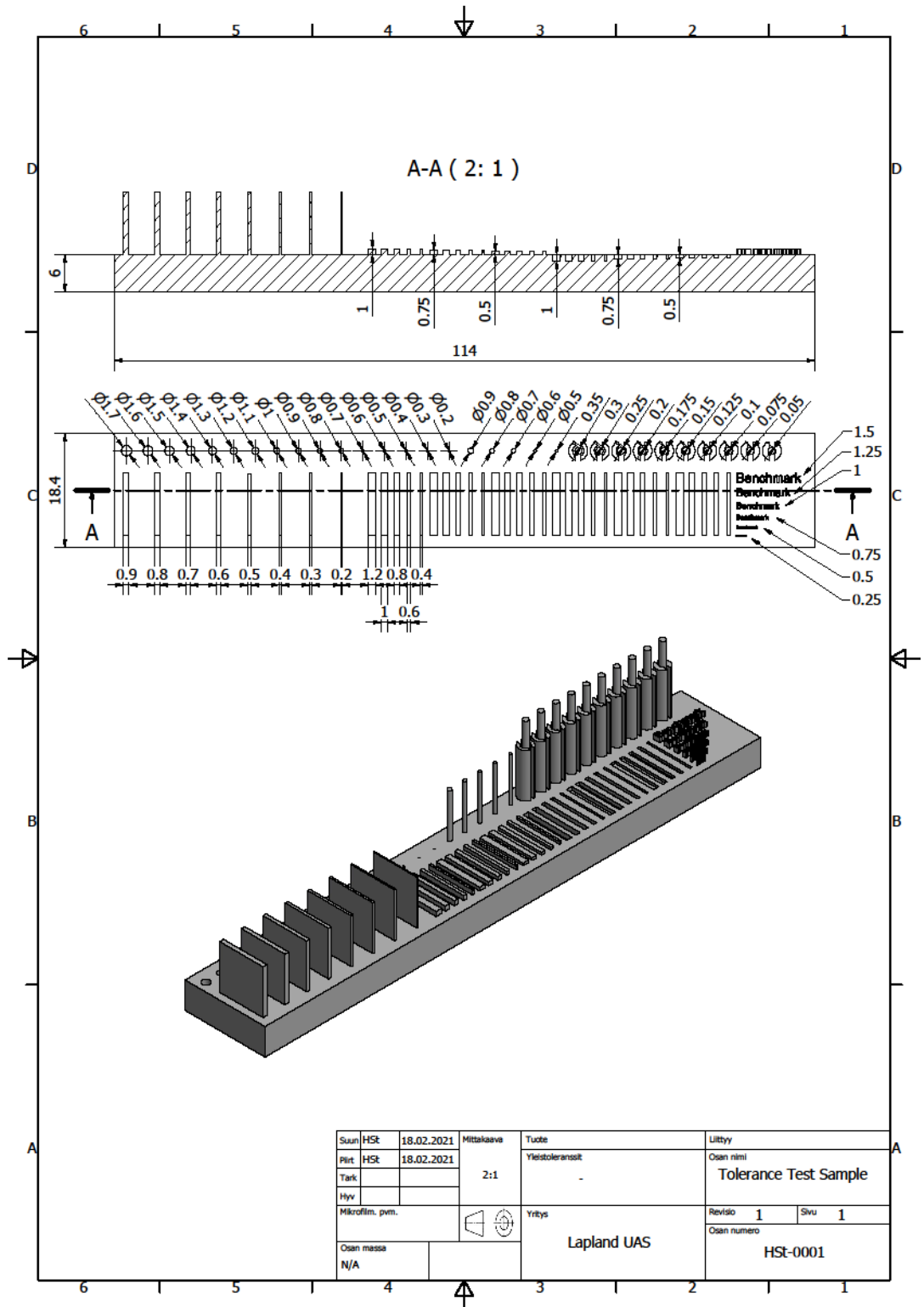


Figure 43. Drawing of tolerance test sample

Appendix 4. 1(2) - Sinterit LISA PRO recoater crash visuals

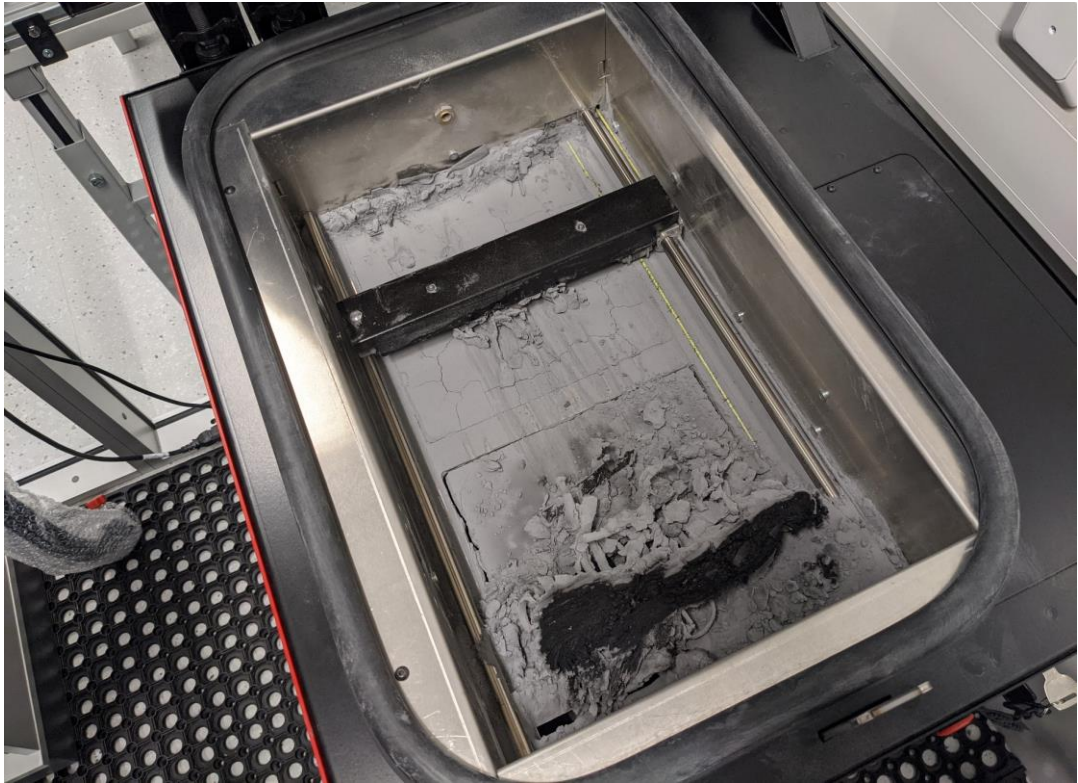


Figure 44. Recoater crash

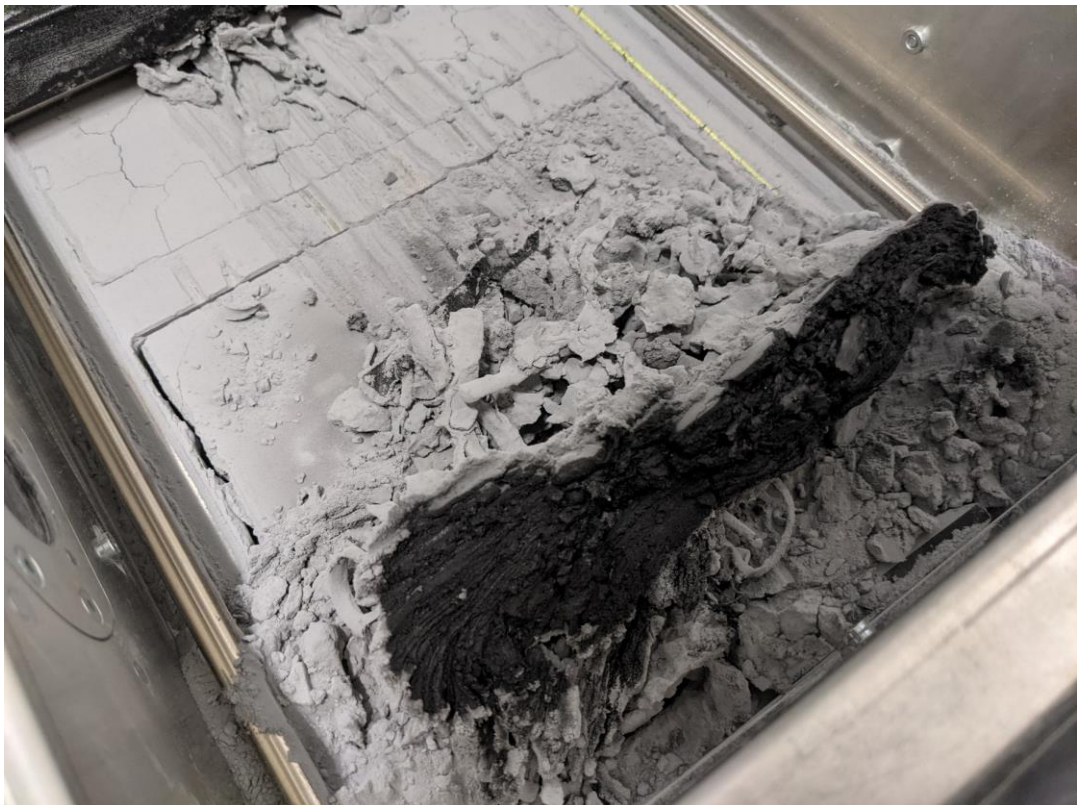


Figure 45. Recoater crash, detail shot of the build volume

Appendix 4. 2(2) - Sinterit LISA PRO recoater crash visuals



Figure 46. Recoater crash, detail shot of the recoater

Appendix 5. 1(2) - Print layout during tensile specimens manufacturing

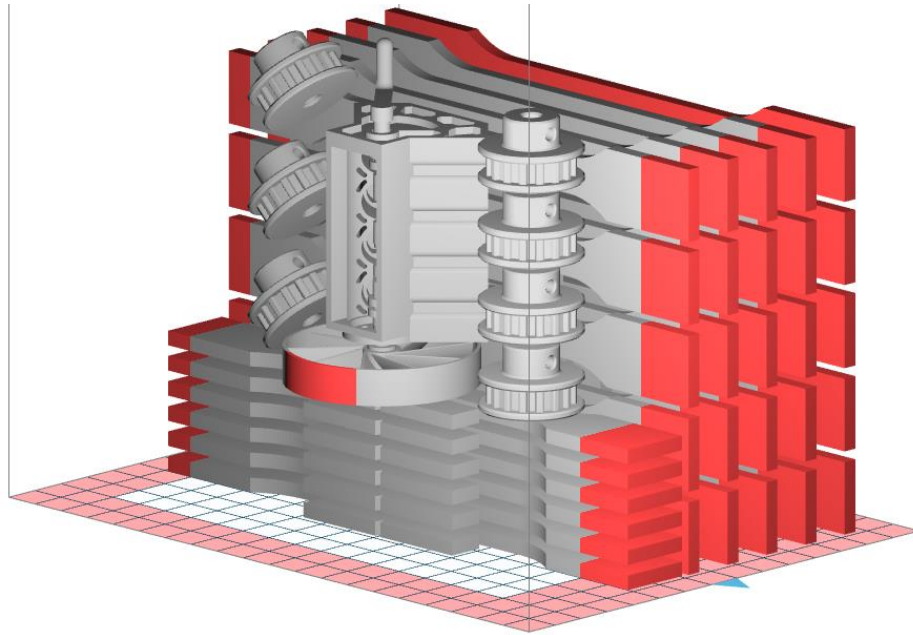


Figure 47. Isometric view of print layout of horizontal and horizontal-flat specimens manufacturing

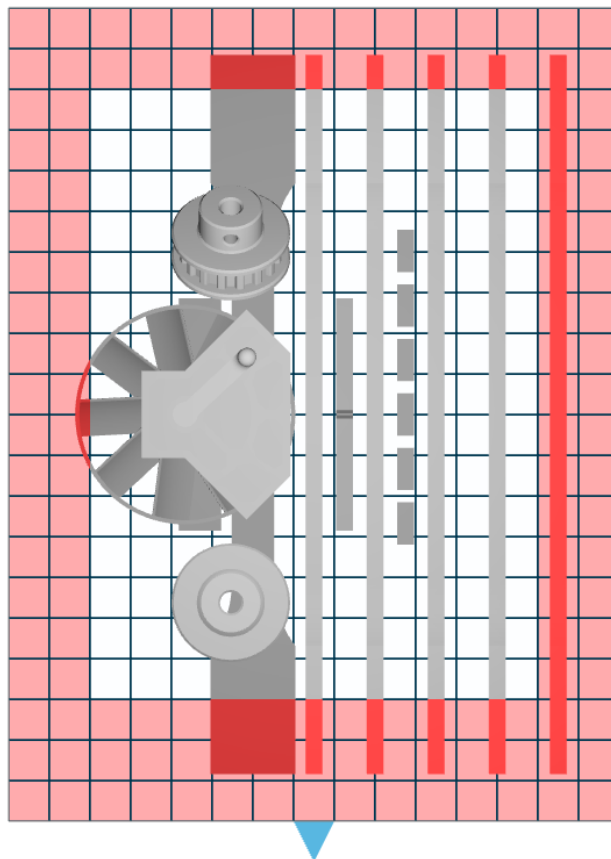


Figure 48. Top view of print layout of horizontal and horizontal-flat specimens manufacturing

Appendix 5. 2(2) - Print layout during tensile specimens manufacturing

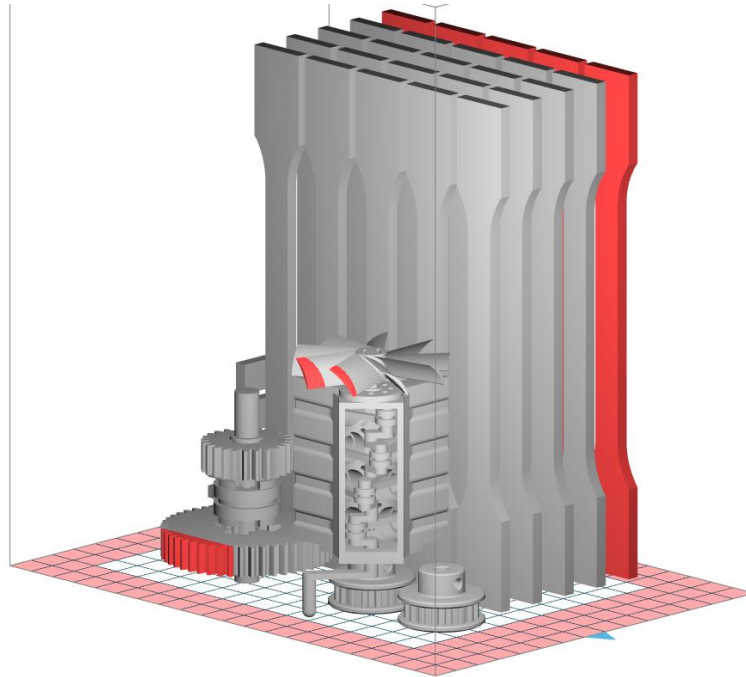


Figure 49. Isometric view of print layout of vertical specimens manufacturing

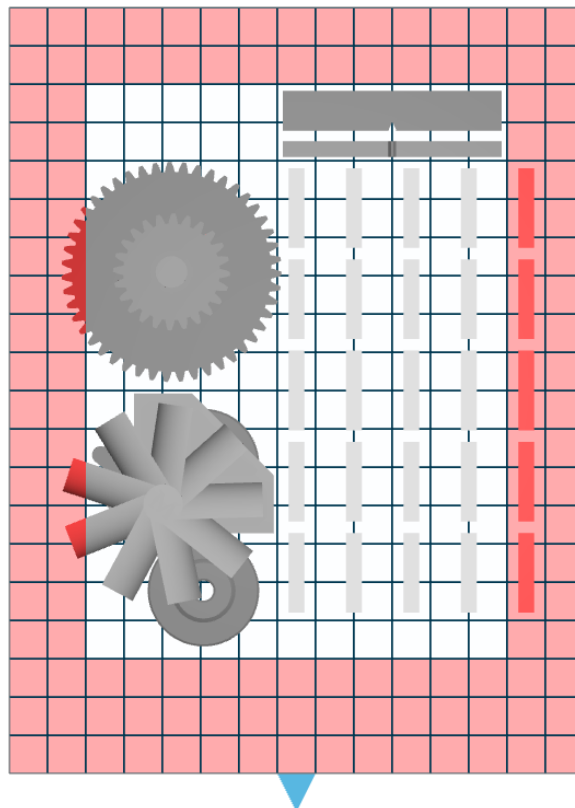


Figure 50. Top view of print layout of vertical specimens manufacturing

Appendix 6. 1(2) - Illustrations of fractured tensile specimens



Figure 51. Illustration of fractured vertical tensile specimens V-A1 - V-E5

Appendix 6.2(2) - Illustrations of fractured tensile specimens



Figure 52. Illustration of fractured horizontal tensile specimens H-A1 – H-E5 and horizontal-flat tensile specimens HF-1 - HF-5

Appendix 7. 1(3) - Tensile specimens measurement data

Table 2. Vertical tensile specimens V-A1 - V-E5 measurement data

Specimen identifier	E_t	E_{Sec}	σ_{x1}	σ_M	ϵ_M	$\epsilon_{M (Corr.)}$	σ_B	ϵ_B	$\epsilon_{B (Corr.)}$	h	b	A_0
	MPa	MPa	MPa	MPa	%	%	MPa	%	%	mm	mm	mm ²
VA1	1334.245479	1256.127659	14.89819334	23.37769699	2.527798116	2.535251163	23.37769699	2.527798116	2.535251163	4.11	10.1	41.511
VA2	1390.398506	1311.142912	16.53180055	29.74089175	3.510595262	3.529773643	29.74089175	3.510595262	3.529773643	4.15	10.1	41.915
VA3	1338.128637	1239.423128	13.83976663	23.48233379	2.650202513	2.661071721	23.48233379	2.650202513	2.661071721	4.1	10.1	41.41
VA4	1297.232633	1220.404582	14.20898732	23.7431666	2.931600511	2.947055391	23.7431666	2.931600511	2.947055391	4.1	10.1	41.41
VA5	1316.033096	1194.18629	12.4916856	20.96575157	2.25119397	2.261484738	20.96575157	2.25119397	2.261484738	4.1	10.1	41.41
VA	1335.20767	1244.256914	14.39408669	24.26196814	2.774278075	2.786927331	24.26196814	2.774278075	2.786927331	4.112	10.1	41.5312
σ	31.19376213	39.27853863	1.325489076	2.916935645	0.428176936	0.431910196	2.916935645	0.428176936	0.431910196	0.019390719	0	0.195846266
VB1	1312.639536	1210.459616	13.24981241	21.17425208	2.234400958	2.246553659	21.17425208	2.234400958	2.246553659	4.08	10	40.8
VB2	1303.404974	1220.21373	13.83571504	20.70721035	2.110196948	2.120716528	20.70721035	2.110196948	2.120716528	4.11	10	41.1
VB3	1338.440904	1234.330061	13.36866359	18.98345539	1.754392236	1.771297493	18.98345539	1.754392236	1.771297493	4.11	10.1	41.511
VB4	1305.078302	1209.728072	13.27409558	21.67390825	2.376596928	2.391653797	21.67390825	2.376596928	2.391653797	4.1	10.1	41.41
VB5	1327.314688	1238.372062	13.68827746	23.96330602	3.027596474	3.041998571	23.96330602	3.027596474	3.041998571	4.12	10	41.2
VB	1317.375681	1222.620708	13.48331281	21.30042642	2.300636709	2.31444401	21.30042642	2.300636709	2.31444401	4.104	10.04	41.2042
σ	13.5008499	11.87535141	0.235642344	1.610378617	0.417918163	0.417718701	1.610378617	0.417918163	0.417718701	0.01356466	0.048989795	0.249292118
VC1	1339.334665	1230.893222	13.32458142	22.77498823	2.614192069	2.631468067	22.77498823	2.614192069	2.631468067	4.11	10.1	41.511
VC2	1338.005488	1229.285613	13.34697639	22.57184118	2.50079751	2.517399625	22.57184118	2.50079751	2.517399625	4.16	10.1	42.016
VC3	1345.316804	1231.765673	13.08993927	23.46004752	2.875801623	2.894400867	23.46004752	2.875801623	2.894400867	4.08	10.1	41.208
VC4	1281.446311	1203.518601	13.85555227	22.92583246	2.832597494	2.852577938	22.92583246	2.832597494	2.852577938	4.09	10.1	41.309
VC5	1311.501112	1221.277948	13.5389889	22.19767253	2.475592345	2.49353855	22.19767253	2.475592345	2.49353855	4.08	10	40.8
VC	1323.120876	1223.348211	13.43120765	22.78607638	2.659796208	2.677877009	22.78607638	2.659796208	2.677877009	4.104	10.08	41.3688
σ	23.87000688	10.58804044	0.25558299	0.416174872	0.166018078	0.166907426	0.416174872	0.166018078	0.166907426	0.030066593	0.04	0.398008744
VD1	1281.582064	1212.241399	14.31866709	22.08917221	2.397602201	2.415697131	22.08917221	2.397602201	2.415697131	4.09	10	40.9
VD2	1345.145704	1240.163293	13.60457619	22.21668055	2.362801284	2.380843541	22.21668055	2.362801284	2.380843541	4.04	10	40.4
VD3	1360.506525	1244.99137	13.35588261	22.51913783	2.360400259	2.373961074	22.51913783	2.360400259	2.373961074	4.19	10.2	42.738
VD4	1360.769263	1256.302546	13.51303897	23.12356247	2.569793463	2.589791122	23.12356247	2.569793463	2.589791122	4.17	10.1	42.117
VD5	1340.339629	1236.197594	13.5041099	22.81069765	2.585996687	2.604587796	22.81069765	2.585996687	2.604587796	4.04	10	40.4
VD	1337.668637	1237.97924	13.65925495	22.55185014	2.455318779	2.472976133	22.55185014	2.455318779	2.472976133	4.106	10.06	41.311
σ	29.202577	14.52786511	0.339204367	0.379825391	0.1010756	0.102509172	0.379825391	0.1010756	0.102509172	0.063435006	0.08	0.950234497
VE2	1291.791708	1208.186646	13.89476361	19.74737661	1.914602071	1.93496756	19.74737661	1.914602071	1.93496756	4.06	10.1	41.006
VE3	1397.35673	1275.410098	13.42808137	21.19080606	2.016603202	2.035316556	21.19080606	2.016603202	2.035316556	4.09	10	41.511
VE4	1253.407943	1174.385671	13.52101834	20.52432145	2.191195935	2.213016701	20.52432145	2.191195935	2.213016701	3.96	9.9	39.204
VE5	1335.924354	1244.396421	14.19889457	22.87697321	2.488195449	2.500989978	22.87697321	2.488195449	2.500989978	3.98	9.9	39.402
VE	1319.620184	1225.594709	13.76068947	21.08486933	2.152649164	2.171072698	21.08486933	2.152649164	2.171072698	4.0225	9.975	40.28075
σ	53.54269678	37.94892483	0.307436977	1.153902034	0.217515566	0.214930266	1.153902034	0.217515566	0.214930266	0.054025457	0.08291562	0.996380293

Appendix 7. 2(3) - Tensile specimens measurement data

Table 3. Horizontal tensile specimens H-A1 - H-E5 measurement data

Specimen identifier	E_t	E_{Sec}	σ_{x1}	σ_M	ϵ_M	ϵ_M (Corr.)	σ_B	ϵ_B	ϵ_B (Corr.)	h	b	A_0
	MPa	MPa	MPa	MPa	%	%	MPa	%	%	mm	mm	mm ²
HA1	1447.543969	1348.753376	15.16570576	32.2696626	6.737396121	6.746686604	32.2696626	6.737396121	6.746686604	3.98	10.3	40.994
HA2	1455.961174	1359.999904	15.63363745	32.11675276	6.296396255	6.308296943	32.11675276	6.296396255	6.308296943	3.94	10.3	40.582
HA3	1458.834077	1332.300283	14.24673565	30.67069402	5.621996522	5.638051583	30.67069402	5.621996522	5.638051583	3.96	10.1	39.996
HA4	1482.07868	1404.8466	16.66728777	30.11280097	3.911996782	3.923821926	30.11280097	3.911996782	3.923821926	3.95	10.2	40.29
HA5	1508.133046	1410.150284	16.20199387	30.47477452	4.239599407	4.255598872	30.47477452	4.239599407	4.255598872	4.06	10.2	41.412
HA	1470.510189	1371.21009	15.5830721	31.12893697	5.361477017	5.374491186	31.12893697	5.361477017	5.374491186	3.978	10.22	40.6548
σ	22.02163487	30.95706335	0.839182271	0.888536156	1.113076826	1.111821825	0.888536156	1.113076826	1.111821825	0.043081318	0.074833148	0.50215631
HB1	1465.076858	1375.094265	16.02568813	31.88380839	6.202799678	6.222159214	31.88380839	6.202799678	6.222159214	3.9	10.3	40.17
HB2	1469.520235	1357.324024	14.96819517	31.63013491	6.237601042	6.249771394	31.63013491	6.237601042	6.249771394	3.9	10.3	40.17
HB3	1447.615474	1337.980879	14.77812053	28.63145445	3.795596063	3.812732104	28.63145445	3.795596063	3.812732104	3.85	10.1	38.885
HB4	1560.40987	1442.3479	15.76279479	31.28155176	4.273201823	4.288337799	31.28155176	4.273201823	4.288337799	3.88	10.1	39.188
HB5	1554.212626	1444.000645	15.92002575	30.5841802	3.947400749	3.967339834	30.5841802	3.947400749	3.967339834	3.99	10.2	40.698
HB	1499.367013	1391.349542	15.49096487	30.80222594	4.891319871	4.908068069	30.80222594	4.891319871	4.908068069	3.904	10.2	39.8222
σ	47.91479595	43.91618194	0.514849283	1.170025632	1.0960033	1.095061591	1.170025632	1.0960033	1.095061591	0.046733286	0.089442719	0.676684387
HC1	1496.267511	1384.969836	15.48858103	31.83776566	5.323800445	5.336592657	31.83776566	5.323800445	5.336592657	3.83	10.3	39.449
HC2	1394.390962	1340.967179	17.3190728	31.24308653	5.758788586	5.779341781	31.24308653	5.758788586	5.779341781	3.82	10.4	39.728
HC3	1484.353784	1378.14684	15.66374851	29.55137746	4.069798589	4.084905632	29.55137746	4.069798589	4.084905632	3.82	10.1	38.582
HC4	1525.836098	1449.267002	17.73453398	32.08116588	4.459793568	4.477548453	32.08116588	4.459793568	4.477548453	3.9	10.1	39.39
HC5	1586.186312	1479.867731	16.47720781	30.68980097	3.697197735	3.715253442	30.68980097	3.697197735	3.715253442	4	10.3	41.2
HC	1497.406933	1406.643718	16.53662883	31.0806393	4.661875784	4.678728393	31.0806393	4.661875784	4.678728393	3.874	10.24	39.6698
σ	62.40828266	50.54451001	0.884426412	0.904663391	0.769851715	0.770132201	0.904663391	0.769851715	0.770132201	0.069742383	0.12	0.855014479
HD1	1478.046247	1407.896125	17.05586077	31.85882164	4.888795316	4.904881007	31.85882164	4.888795316	4.904881007	3.85	10.3	39.655
HD2	1517.944189	1372.56711	13.79364224	30.81922711	4.978801012	4.988449715	30.81922711	4.978801012	4.988449715	3.93	10.3	40.479
HD3	1458.521931	1372.02531	15.87282038	28.53763381	3.501001	3.510517172	28.53763381	3.501001	3.510517172	3.88	10.2	39.576
HD4	1585.475566	1473.654442	16.34594471	30.50872015	3.572999835	3.590214139	30.50872015	3.572999835	3.590214139	3.86	10.1	38.986
HD5	1506.020893	1421.660933	16.728446	30.38291265	3.729598224	3.743677184	30.38291265	3.729598224	3.743677184	4	10.3	41.2
HD	1509.201765	1409.560784	15.95934282	30.42146307	4.134239078	4.147547843	30.42146307	4.134239078	4.147547843	3.904	10.24	39.9792
σ	43.45883678	37.50900006	1.152482318	1.075372357	0.657625144	0.657299007	1.075372357	0.657625144	0.657299007	0.05535341	0.08	0.773857196
HE5	1543.791837	1498.724575	20.84693269	37.23080344	4.558796585	4.574981523	37.23080344	4.558796585	4.574981523	3.99	10.2	40.698
HE	1543.791837	1498.724575	20.84693269	37.23080344	4.558796585	4.574981523	37.23080344	4.558796585	4.574981523	3.99	10.2	40.698

Appendix 7. 3(3) - Tensile specimens measurement data

Table 4. Horizontal-flat tensile specimens HF-1 - HF-5 measurement data

Specimen identifier	E_t	E_{Sec}	σ_{x1}	σ_M	ϵ_M	$\epsilon_M (Corr.)$	σ_B	ϵ_B	$\epsilon_B (Corr.)$	h	b	A_0
	MPa	MPa	MPa	MPa	%	%	MPa	%	%	mm	mm	mm ²
HF1	1426.495184	1299.752843	13.89127946	30.14853426	4.817399383	4.828408223	30.14853426	4.817399383	4.828408223	4.325	10.09	43.63925
HF2	1383.107163	1268.877221	13.69582807	30.18480548	5.199593306	5.2055551	30.18480548	5.199593306	5.2055551	4.365	10.16	44.3484
HF3	1362.738259	1263.398261	14.14665791	29.46467627	4.704592824	4.718202525	29.46467627	4.704592824	4.718202525	4.275	10.1	43.1775
HF4	1402.985884	1306.36497	14.86901027	30.11215091	4.572595954	4.58493201	30.11215091	4.572595954	4.58493201	4.25	10.03	42.6275
HF5	1406.41386	1285.691807	13.6817552	29.73824717	4.864803255	4.874760466	29.73824717	4.864803255	4.874760466	4.33	10.13	43.8629
HF	1396.34807	1284.81702	14.05690618	29.92968282	4.831796944	4.842371665	29.92968282	4.831796944	4.842371665	4.309	10.102	43.53111
σ	21.72174131	16.73916739	0.439571679	0.282544449	0.209731691	0.207286937	0.282544449	0.209731691	0.207286937	0.041158231	0.043543082	0.588437401

Table 5. Vertical specimens V-A1 - V-E5 detailed cross-sectional area measurement data

Cross-sectional area	A	B	C	D	E
1	81.78525	81.80648	80.99112	80.95566	77.56182
2	41.59856	41.83342	41.6953	41.80046	40.76988
3	41.28816	41.20722	41.47924	41.04654	40.10204
4	41.42058	40.69342	41.04108	40.77112	39.63902
5	81.5955	79.23756	79.7524	79.70164	77.90475